2019

Measurement and prediction of mass concrete parameters and thermal conductivity

Yogiraj Sargam
Iowa State University

Measurement and prediction of mass concrete parameters and thermal conductivity

by

Yogiraj Sargam

A thesis submitted to the graduate faculty

in partial fulfillment of the requirements for the degree of

MASTER OF SCIENCE

Major: Civil Engineering (Civil Engineering Materials)

Program of Study Committee:
Kejin Wang, Major Professor
Charles Jahren
Ashley Buss

The student author, whose presentation of the scholarship herein was approved by the program of study committee, is solely responsible for the content of this thesis. The Graduate College will ensure this thesis is globally accessible and will not permit alterations after a degree is conferred.

Iowa State University

Ames, Iowa

2019

DEDICATION

Dedicated to my family.....

TABLE OF CONTENTS

ACKNOWLEDGMENTS

I owe my sincere gratitude to my major advisor Dr. Kejin Wang for her support and guidance throughout the course of my master's program. Right from making a decision of hiring me to providing valuable financial and technical assistance, her contribution in shaping my career as a researcher has been immense. This research work involved a lot of meticulous planning and I unequivocally state that it would not have been possible without her.

I am also grateful to my committee members Dr. Charles Jahren and Dr. Ashley Buss for agreeing to serve on my committee. Their suggestions and comments from time to time helped me in the gradual development of my research plan and in achieving the goals. This thesis consists of journal articles for which I would like to thank the co-authors, namely, Mahmoud Faytarouni, Dr. Kyle Riding, Dr. Jay Shen, Dr. James Alleman, and Dr. In Ho Cho. The credit goes to all of my fellow lab mates, graduate students, lab managers, and visiting scholars at Iowa State as well who not only helped me with my lab experiments but also engaged in fruitful discussions on my research. They include, but not limited to, Robert Steffes (retired now), Paul McIntyre, Bharath MS, Siraj Al Qunaynah, Nikhil Padhye, Yifeng Ling, and Dr. Chuanqing Fu.

The list would be incomplete without the mention of my constant source of strength and motivation i.e., my family. I would especially dedicate this work to my late mother whom I miss every second of my life. The sacrifices made, and emotional support and motivation provided by my father are highly commendable. The inspirations given by my highly-educated siblings and sister-in-laws are also greatly appreciated. Last but not least, I would like to express my heartfelt gratitude to my long-time companion, best friend, and now wife also for believing in me and motivating me for higher studies. She has been there through thick and thin of my life and makes it wonderful every day. Along with my mother, I dedicate this piece of writing to her as well.

ABSTRACT

Mass concrete is a type of concrete used for structures with large dimensions that require precautionary measures to be taken in order to control the heat. The heat generated in the core of such a structure, due to hydration of cementitious materials, is dissipated at a slow rate leading to the formation of high temperature differential. This increases the risk of temperature-induced stresses and cracking that is dependent on many factors such as the materials and proportion of concrete mix, environmental and construction conditions, etc. In order to prevent cracking, a thermal control plan is essential before the placement of concrete that in turn requires prior knowledge of the temperature development in the mass concrete member. In this context, this study presents the analysis of a case in which the construction of a mass concrete bridge foundation was investigated and a computer program, ConcreteWorks (CW), was used to predict its overall thermal performance. Predictions of temperature development profile, temperature differential, maturity, and compressive strength were made using CW and were also validated with the measured data. The results suggest CW to be a useful tool for developing a thermal control plan and for the prevention of thermal cracking.

From the perspective of the rate of heat dissipation in a mass concrete element, thermal conductivity of concrete is an important parameter. Keeping other parameters the same, a concrete mix of high thermal conductivity can reduce the risk of temperature-induced cracking by increasing the rate of dissipation of heat. Therefore, in this study, the effects of various concrete materials, such as supplementary cementitious materials (SCMs), normal-weight, lightweight, and recycled aggregates, and steel and polypropylene (PP) fibers, on the thermal conductivity of concrete were experimentally determined. SCMs, lightweight, and recycled aggregates reduced conductivity of concrete while steel fiber was observed to improve it. In addition to the

experimental measurements, a prediction model for thermal conductivity was also developed. For this purpose, a database was developed from published articles and various machine learning (ML) algorithms were evaluated for their prediction accuracies. Performance metrics indicated an artificial neural network to be the best ML algorithm for the developed dataset and a 14-6-1 model architecture was finally adopted. The robustness of this model was also evaluated on an unseen/independent dataset that furnished satisfactory results with good performance ($R^2 \sim 0.80$).

CHAPTER 1. GENERAL INTRODUCTION

Background and Motivation

Concrete, a cement-based composite, is the most widely used construction material (Mehta and Monteiro 2006). Portland cement, aggregates, and water are the principal constituents of concrete and its structure also consist of voids. The hydration reaction of Portland cement, that provides strength, progresses with time and hence the mechanical properties and durability of concrete also change with time. It shows different properties in fresh and hardened states. A freshly-mixed concrete is of plastic consistency that provides it the ability to flow into formworks while in its hardened state, concrete is usually considered to be a three-phase composite consisting of aggregate particles, hydrated cement paste, and interfacial transition zone (ITZ) (Mehta and Monteiro 2006; Neville and Brooks 2010). With the progress of hydration, the pore structure of concrete also evolves with the time that makes it denser. This minimizes the probability of attack by harmful chemicals thereby making concrete more durable.

Nowadays, various materials are used as an additive or replacement to constituents of concrete with objectives of performance enhancement, sustainable construction, and economy. This has led to the design of special types of concrete e.g., high-strength and high-performance, lightweight, self-consolidating concrete and others. Mass concrete is also one of such types. ACI 116R defines mass concrete as “any volume of concrete with dimensions large enough to require that measures be taken to cope with generation of heat from the hydration of cement and attendant volume change to minimize cracking” (ACI (American Concrete Institute) 2000). Due to the large dimension of a mass concrete structure, the heat generated in its core is dissipated at a very slow rate or not dissipated at all leading to the formation of temperature differential. This increases the risk of thermal cracking. To minimize the risk of cracking, various preventive measures are taken

that includes (but not limited to) appropriate mix proportioning, control of pre-construction parameters, and post-construction measures (Juenger and Siddique 2015; Lothenbach et al. 2011; Scrivener et al. 2015; Shanahan et al. 2016). In this context, a knowledge of the temperature development in a mass concrete member is helpful in developing a thermal control plan prior to the placement of concrete. Finite element based computer programs (for example, ConcreteWorks and 4C Temp&Stress) are generally used for this purpose. Although a good number of published articles discuss various aspects of mass concrete construction (Lv and Qiao 2011; Yin et al. 2013; Zhang et al. 2012; Zheng et al. 2017; Zhu et al. 2004, 2014), not many studies have been performed on the tools available for prediction of temperature development and their validation on a real-time project. One of the motivations of this study is to address this research gap.

Another important aspect related to the rate of heat dissipation and temperature development in mass concrete is the thermal properties of concrete. Thermal conductivity, coefficient of thermal expansion, specific heat, etc. are some of these properties with thermal conductivity (hereafter denoted as '*k*') being the most important one. Studies suggest that increasing conductivity of concrete can reduce the probability of early-age thermal cracking in a mass concrete member (Poole et al. 2006; Riding et al. 2013; Sargam et al. 2019). This can be explained by the fact that an increase in *k* of concrete increases the rate of dissipation of heat generated in the core of the member. This results in a reduced temperature differential that further reduces the cracking probability. The constituents of mass concrete used nowadays comprise of various materials (such as supplementary cementitious materials, lightweight aggregates, recycled aggregates, fibers, etc.) that can affect its *k* and consequently the cracking probability. For example, due to their porous structure, the use of lightweight aggregates reduce the overall *k* of concrete whereas steel fiber has an opposite effect. In this context, a knowledge of the effect of

these constituent materials on *k* of concrete can aid in the design of mass concrete mixes and consequently in the development of thermal control plan. Although this knowledge is helpful, experimentally determined value of *k* is desired for the prediction of temperature development in mass concrete structures. However, due to the requirement of sophisticated test procedures, experimental measurement of *k* of concrete for every such structure is impractical. Hence, a model for prediction of *k* is demanded. A few mathematical (Campbell-Allen and Thorne 1963) and neural network (Lee et al. 2012) based models have been developed for this purpose. However, these models are not updated to the data corresponding to modern concrete materials, which often contain various supplementary cementitious materials (SCMs), different types of aggregates, and additives (e. g., fibers). This led to another motivation of this study to first experimentally determine the effect of various constituents of concrete on its thermal conductivity and then develop a prediction model for the same.

Objectives

In light of the above discussions, the overall goal of this study is the experimental measurement and predictive analysis of mass concrete parameters and concrete thermal conductivity. The specific objectives are as follows:

(1) To use a computer program called ConcreteWorks for the prediction of temperature development profile of a mass concrete bridge foundation and validate these predictions with the measured data

(2) To perform a sensitivity analysis (using ConcreteWorks) on the effect of various mass concrete parameters on temperature development

(3) To determine the effect of various modern constituent materials and age of concrete on its thermal conductivity using a simple test procedure

(4) To develop a prediction model for thermal conductivity of concrete using machine learning algorithms

Thesis Organization

This thesis is organized into five chapters.

Chapter 1 presents the background, motivation, and objectives of this study.

Chapter 2 to 4 each comprises of a journal article in modified form. These articles are ordered as follows:

- Chapter 2

  Predicting thermal performance of a mass concrete foundation – A field monitoring case study by Yogiraj Sargam, Mahmoud Faytarouni, Kyle Riding, Kejin Wang, Charles Jahren, and Jay Shen

  This chapter presents a case study in which the construction of a mass concrete bridge foundation in Iowa, USA was investigated and a computer program, ConcreteWorks (CW), was used to predict its overall thermal performance with an aim to prevent thermal cracking.

- Chapter 3

  Effects of modern concrete materials on thermal conductivity by Yogiraj Sargam, Kejin Wang, and James Alleman

  This chapter presents the results from an experimental study on the effects of various modern materials viz. SCMs, fibers, lightweight and recycled aggregates, etc., on the thermal conductivity of concrete.

- Chapter 4

  Predicting thermal conductivity of concrete using machine learning algorithms by Yogiraj Sargam, Kejin Wang, and In Ho Cho

  This chapter presents a machine learning-based prediction model for thermal conductivity of concrete. Various machine learning algorithms were evaluated and the parameters of the best-performing algorithm were tuned to improve the prediction accuracy.

Chapter 5 discusses the overall conclusions of this study.

References

ACI (American Concrete Institute). (2000). "Cement and Concrete Terminology." *ACI 116R*, Farmington Hills, MI.

Campbell-Allen, D., and Thorne, C. P. (1963). "The thermal conductivity of concrete." *Magazine of Concrete Research*, 15(43).

Juenger, M. C. G., and Siddique, R. (2015). "Recent advances in understanding the role of supplementary cementitious materials in concrete." *Cement and Concrete Research*, 78, 71–80.

Lee, J.-H., Lee, J.-J., and Cho, B.-S. (2012). "Effective Prediction of Thermal Conductivity of Concrete Using Neural Network Method." *International Journal of Concrete Structures and Materials*, 6(3), 177–186.

Lothenbach, B., Scrivener, K., and Hooton, R. D. (2011). "Supplementary cementitious materials." *Cement and Concrete Research*, 41, 1244–1256.

Lv, C., and Qiao, C. (2011). "Mass concrete construction technology of high-rise building foundation platform." *2011 International Conference on Electric Technology and Civil Engineering, ICETCE 2011 - Proceedings*, IEEE Computer Society, 442–445.

Mehta, P. K., and Monteiro, P. J. M. (2006). *Concrete: microstructure, properties, and materials*. *3rd ed.*, McGraw Hill.

Neville, A. M., and Brooks, J. J. (2010). "Concrete Technology." *Building and Environment*.

Poole, J., Riding, K., Browne, R. A., and Schindler, A. (2006). "Temperature management of mass concrete structures." *Concrete Construction - World of Concrete*, Hanley Wood LLC, 51(11), 47–53.

Riding, K. A., Poole, J. L., Schindler, A. K., Juenger, M. C. G., and Folliard, K. J. (2013). "Statistical Determination of Cracking Probability for Mass Concrete." *Journal of Materials in Civil Engineering*, 26(9), 04014058.

Sargam, Y., Wang, K., and Alleman, J. E. (2019). "Effect of Modern Concrete Materials on Thermal Conductivity." *Journal of Materials in Civil Engineering*, In Press.

Scrivener, K. L., Lothenbach, B., De Belie, N., Gruyaert, E., Skibsted, J., Snellings, R., and Vollpracht, A. (2015). "TC 238-SCM: hydration and microstructure of concrete with SCMs State of the art on methods to determine degree of reaction of SCMs." *Materials and Structures/Materiaux et Constructions*, 48, 835–862.

Shanahan, N., Tran, V., and Zayed, A. (2016). "Heat of hydration prediction for blended cements." *Journal of Thermal Analysis and Calorimetry*, 128, 1279–1291.

Yin, S. U., Huang, Y., and Yuan, Y. H. (2013). "Research on mass concrete construction techonogy of raft foundation of hongyun building." *Advanced Materials Research*, Trans Tech Publications Ltd, 690 693, 709–713.

Zhang, G., Li, H., and Shi, C. (2012). "Study on mass concrete slab construction technology of dalian world finance center." *Applied Mechanics and Materials*, Trans Tech Publications, 137, 175–180.

Zheng, S., Sun, Z., and Zhu, H. (2017). "Mass concrete construction technology of the Three Gorges Project." *Zhongguo Kexue Jishu Kexue/Scientia Sinica Technologica*, Chinese Academy of Sciences, 47(8), 796–804.

Zhu, H., Song, H., and Kuang, Q. (2004). "Application of Seamless Construction Technique to Mass Concrete Structures." *Huazhong Keji Daxue Xuebao (Ziran Kexue Ban)/Journal of Huazhong University of Science and Technology (Natural Science Edition)*, Huazhong University of Science and Technology, 32(11), 100–102.

Zhu, J., Zhang, Y. Bin, Du, X. F., and Jiang, Y. (2014). "Study on mass concrete construction technology of raft foundation in Yantai Ocean development center." *Advanced Materials Research*, Trans Tech Publications, 919–921, 1421–1425.

CHAPTER 2. PREDICTING THERMAL PERFORMANCE OF A MASS CONCRETE FOUNDATION – A FIELD MONITORING CASE STUDY

Modified from a manuscript published in *Case Studies in Construction Materials*

Yogiraj Sargam[1], Mahmoud Faytarouni[2], Kyle Riding[3], Kejin Wang[4], Charles Jahren[5], Jay Shen[6]

Abstract

High-temperature differentials in a mass concrete structure pose great risks of temperature-induced stresses and cracking. Prior knowledge of temperature development within such a structure is essential. In this context, this paper presents a case study in which the construction of a mass concrete bridge foundation in Iowa, USA was investigated and a computer program, ConcreteWorks (CW), was used to predict its overall thermal performance with an aim to prevent thermal cracking. The properties of mass concrete mixes, required as CW inputs, were measured through isothermal and semi-adiabatic calorimetry tests. The temperature development profile, temperature differential, maturity, and compressive strength of the mixes were predicted and compared with those measured through the real-time monitoring of the bridge foundation. It was observed that CW predictions match well with their corresponding measured values. Three

[1] Graduate Research Assistant; Iowa State University; Department of Civil, Construction, and Environmental Engineering; 813 Bissell Road , Ames, IA, USA, 50011; email: ysargam@iastate.edu
[2] Graduate Research Assistant; Iowa State University; Department of Civil, Construction, and Environmental Engineering; 813 Bissell Road , Ames, IA, USA, 50011; email: mfayt@iastate.edu
[3] Associate Professor; University of Florida; Engineering School of Sustainable Infrastructure and Environment; 265G Weil Hall, Gainesville, FL, USA, 116580; email: kyle.riding@essie.ufl.edu
[4] Professor (corresponding author); Iowa State University; Department of Civil, Construction, and Environmental Engineering; 813 Bissell Road , Ames, IA, USA, 50011; email: kejinw@iastate.edu
[5] Professor; Iowa State University; Department of Civil, Construction, and Environmental Engineering; 813 Bissell Road , Ames, IA, USA, 50011; email: cjahren@iastate.edu
[6] Associate Professor; Iowa State University; Department of Civil, Construction, and Environmental Engineering; 813 Bissell Road , Ames, IA, USA, 50011; email: jshen@iastate.edu

locations, centroid, top, and the face nearest to the centroid of the foundation, were found to be critical points for high temperature differentials. A sensitivity analysis, analyzing the effects of various mass concrete parameters, is also presented. The results provided clear insights into the temperature development of concrete with complex material compositions and environmental conditions. CW is a useful tool in developing thermal control plan for mass concrete projects.

Keywords: Case study – Mass concrete – Bridge foundation – Thermal cracking – ConcreteWorks – Sensitivity analysis

Introduction

ACI 116R defines mass concrete as "any volume of concrete with dimensions large enough to require that measures be taken to cope with generation of heat from the hydration of cement and attendant volume change to minimize cracking" (ACI (American Concrete Institute) 2000). Generally, structural members with a least dimension greater than 4 ft., fall into this category. The early-age temperature development in mass concrete structures has a significant impact on their durability. A high temperature differential in such structures can result in large temperature-induced stresses that can cause cracking, especially at early ages (Ballim 2004; Choktaweekarn and Tangtermsirikul 2010; Kolani et al. 2012; Nili and Salehi 2010). This can also cause durability problems such as delayed ettringite formation (DEF) and increased reinforcing steel corrosion risk from thermal cracking (Riding et al. 2006). The high temperature differential is primarily caused by a large amount of heat generated, due to hydration of cementitious materials, in the core of the structure that is dissipated at a very slow rate or is not dissipated locally, representing a true adiabatic condition (ACI (American Concrete Institute) 2006; Folliard et al. 2002; Riding et al. 2006, 2013). To minimize the risk of cracking, various preventive measures are taken that includes (but not limited to) the use of SCMs to replace parts of cement, precooling aggregates and water

before concrete mixing, the use of icy water or liquid nitrogen, cooling pipes, insulation blankets and others (Juenger and Siddique 2015; Lothenbach et al. 2011; Scrivener et al. 2015; Shanahan et al. 2016). Often a combination of these methods is necessary and is employed in relevant projects.

Nowadays, a very common procedure in mass concrete projects is to develop a thermal control plan (TCP) before the placement of concrete. Many studies have been carried out and a few finite element-based analysis computer programs (e.g., 4C Temp&Stress and ConcreteWorks) have been developed that help in predicting this temperature development. ConcreteWorks (CW) has specific capabilities to predict the early age thermal development and cracking potential of mass concrete and can assist in devising a TCP (Riding 2007). It contains modules for several structural concrete applications, including bridge deck types, precast concrete beams, and concrete pavements (Folliard et al. 2017). CW input data include: (a) concrete material properties (cementitious properties, mix proportions, etc.); (b) structural parameters (shape, dimension, subgrade condition etc.); (c) construction parameters (concrete placement temperature, casting rate, curing/insulation methods, formwork removal time etc.); and (d) environmental parameters (ambient temperature variation, relative humidity, wind speed etc.). The prediction of maximum absolute temperature, maximum temperature differential, maturity and compressive strength development with time, and cracking potential are furnished as outputs. The temperature development profile at any specified point in a mass concrete structure can also be obtained for analysis.

Based on experiences and observations from individual mass concrete projects, comprising mostly of dams and mat foundations, researchers have suggested the mix designs, construction technologies (Lv and Qiao 2011; Yin et al. 2013; Zhang et al. 2012; Zheng et al. 2017; Zhu et al.

2004, 2014) and ways to reduce heat, the probability of cracking, and cost of such projects (Abdun-Nur et al. 1990; Dunstan and Mitchell 1976; Lawrence et al. 2014; Poole et al. 2006; Wang et al. 2005; Xu et al. 2012). A few case studies could be found in the literature related to mass concrete construction. For example, Luther et al. (Luther et al. 2008) presented 30 case studies about various mass concrete projects in North America that included dams, mat foundations, bridge pier foundations and stems, reservoir foundations, and caissons. These case studies focused mainly on the concrete mixes (containing slag cement) used and the resulting temperature development. The details about the thermal control measures, adopted in the projects, were not discussed. Dilek (Dilek 2011) discussed the planning aspect of a critical mass concrete placement. A complete investigation of the construction process, with a focus on the adopted insulation regime, was presented. However, extensive validation of the predicted data was not discussed. To summarize, although a good amount of literature is available that discusses various aspects of a mass concrete project, studies related to aids available for developing a TCP and the validation of their application are scarce.

This paper presents a case study where CW was used for prediction of temperature development in a mass concrete bridge foundation and it was validated with actual/measured data. A rectangular footing of a bridge pier in Iowa, USA was selected for the investigation. The properties of concrete and its constituent materials were determined through various lab and field tests. The measured material properties, foundation temperature development profiles, and the results of the thermal analysis performed using CW are presented along with brief sensitivity analysis on the effect of various mass concrete parameters on temperature development. The observations from this case study will reinforce the importance of a TCP in a mass concrete project and can also provide experimental validation for the use of CW for future similar projects.

Investigation of a Mass Concrete Foundation

Real-time monitoring of the construction and heat development of a bridge foundation was carried out. A rectangular footing of a bridge pier, which was a mass concrete member as per ACI-207 (ACI (American Concrete Institute) 2006), was investigated. The project chosen for the investigation was I-35 NB to US 30 WB (Ramp H) bridge in Ames, Iowa. This was a 7-span continuous welded steel girder bridge constructed on 6 concrete piers with a total length of 1690 feet and a width of 36 feet. Fig. 1(a) shows a cross-section of the bridge along with all the piers and the location map of the bridge is shown in Fig. 1(b). The dimensions of the six pier footings are presented in Table 1. The footings of all of the six piers had a rectangular cross-section except one, the footing of pier 3 that had a cross-section of a rectangle with cuts at the two opposite corners. The rectangular footing of pier 4 was selected for this investigation as it was the largest amongst all footings with the dimensions of 33 ft. x 27 ft. x 7 ft. which. The depth of the footing (7 ft.) was the critical dimension that qualified it as a mass concrete member as per IA DOT specification (Iowa DOT 2009) and, therefore, its construction and early-age temperature profile were analyzed.

The temperature development in a mass concrete structure is dependent on a range of factors such as the subsurface profile, boundary and environmental conditions, concrete mix proportion, cooling method, and others. For this reason, the construction of pier 4 footing was studied in three stages – before, during, and after the placement of concrete. Some of the important information is presented and discussed in the sections below.

Subsurface Profile

The bridge site was located in an area of Iowa that has been formed by extensive Wisconsin age glacial activity. During the initial stage of project finalization, a soil investigation at the job

site was carried out by HDR Inc. The primary geologic strata encountered in this investigation included topsoil, existing fill soils, cohesive alluvium, alluvial sand, glacial till, and bedrock. Topsoil depths ranged from 5 to 8 inches along the project alignment. Bedrock was encountered at depths ranging from 34 to 83 feet. The bedrock units appeared to include siltstone, sandstone, and shale based on examination of split-barrel samples, with varying degrees of weathering.

Footing Support, Subbase, and Formwork

The load transfer mechanism for the footing was a total of 30 HP 14 x 117 steel bearing H-piles driven 55 feet below the ground surface and the steel reinforcement footing cage was placed over these piles. Based on the outcomes of the soil investigation, a layer of crushed limestone aggregate was placed on the subbase to provide a firm and dry casting surface.

Fig. 2 (a) shows the driven H-piles and the crushed rock casting surface. In central Iowa, usually, wood and steel formwork materials are used to form footing placements. The choice of formwork material depends on the nature of construction as well as the availability and cost of the material. Wood formwork was used in the construction of the footing. This formwork consisted of plywood attached to galvanized cold-rolled steel supporting members with nails. These, in turn, were supported by vertical cold-rolled steel members of the longer cross-section.

Insulation Method

The footing was constructed in the month of June when the average daily ambient temperature was 79 °F (26 °C). The temperature at the outer faces of footing was expected to be close to the ambient temperature while that in the core was expected to be higher due to cement hydration. This might have caused a large temperature differential. In order to keep the differential within the acceptable limits, the footing was insulated 10 hours after the placement of concrete. The exterior of the wood formwork and the top face of the footing were wrapped with a 2-inch

thick black insulation blanket with a specified R-value rating of 5 [Fig. 2(b)]. The decision regarding the removal of insulation and formwork should be made based on the monitoring of temperature development and environmental conditions. The environmental conditions such as the ambient temperature and relative humidity have a significant impact on the temperature development in a mass concrete member as well as on the hydration process of cementitious materials. Therefore, these parameters were also monitored, and the formwork was removed on the 5^{th} day after the placement of concrete while the footing was kept covered with insulation blankets up until the 10^{th} day. After removal of blankets, the footing surface was visually examined, and no cracking was observed.

Installation of Temperature Sensors

To monitor the temperature development of the concrete placement in footing, the temperature data were recorded in one-hour intervals and were monitored remotely as well at 4-hours intervals for a period of 10 days from the day of the concrete placement. A total of 7 sets of temperature sensors were installed. Each set included a primary and a backup temperature sensor. After installation, the exact location of the sensors was measured as shown in Fig. 3 (S1-S7). The locations are also explained as follows:

S1 – at the center of the concrete footing, installed 2.75 ft. below the top surface

S2 – in the middle of the length and width, near the top and lateral surfaces of the footing, installed at 6 inches below the top surface

S3 – in the middle of the length and height, installed at 3 inches inside the long lateral surface, 2.9 ft. from the top surface and 2.5 ft. from the bottom surface

S4 – installed outside the formwork, to measure the ambient air temperature

S5 – 1.08 ft. below S2, to monitor the temperature change along the vertical direction

S6 – installed at the middle of the height and width, 3 inches inside the short lateral surface, 3 ft. from the top surface and 2.5’ from the bottom surface, to monitor the temperature in another cross-section,

S7 – installed in the center, 1 ft. above the bottom surface of the footing, to investigate the effect of the subgrade temperature

Experimental Program

Materials and Mix Proportion

Ready-mixed concrete was used for the placement of footing. The concrete mix proportion is shown in Table 2. Materials used in the concrete were Type I/II cement, class C fly ash, 1-inch nominal maximum size limestone coarse aggregate, and river sand as fine aggregate. Total cementitious content of the mix was replaced with 20% of fly ash (by weight). The chemical composition of cementitious materials is presented in Table 3. Coarse and fine aggregates were tested for their properties such as specific gravity, absorption, dry – rodded unit weight (DRUW), and fineness modulus. The specific gravity, absorption, and DRUW of coarse aggregate were measured to be 2.68, 0.82%, and 100.44 lbs./ft.^{3}, respectively. The specific gravity, absorption, and fineness modulus of fine aggregate were measured to be 2.65, 0.98%, and 2.85, respectively.

Test Methods

Tests for measuring fresh properties of concrete were performed as per relevant ASTM standard test procedures. Slump (ASTM C143), air content (ASTM C173), and unit weight (ASTM C138) of the concrete mix were measured at the construction site during placement of concrete. Cylindrical specimens (4 in. x 8 in.) were cast and cured in site conditions for various hardened properties tests such as maturity (ASTM C1074) and compressive strength (ASTM C39). Nurse-Saul maturity method was employed in this study to monitor the development of

compressive strength of concrete based on its temperature history. Maturity was calculated in terms of temperature-time factor (TTF). The compressive strength-maturity relationship was then developed by performing a regression analysis to determine a best-fit equation to the measured data. The best-fit equation was found to be of the form where compressive strength is a linear function of the logarithm of TTF as given in Eqn. (1).

$$S = a + b \log (M) \quad (1)$$

Where S is the compressive strength (in psi), M is the TTF (in °F –hours), and 'a' and 'b' are coefficients.

Isothermal and semi-adiabatic calorimetry tests were performed to analyze the heat development due to the hydration of cementitious materials. In this study, an eight-channel PTC isothermal calorimeter was used to measure the heat generation of cement pastes following ASTM C1702. The semi-adiabatic calorimetry test method is explained in the following section.

Semi-adiabatic Calorimetry

The characterization of the temperature rise in a mass concrete structure requires an estimate of the adiabatic temperature rise of the concrete mixture (Poole 2007). Adiabatic calorimetry requires a process in which no heat is gained or lost to the system's surroundings. However, due to its high set-up cost and the requirement of a large sample size, it is less practical than a semi-adiabatic calorimeter. Therefore, in general, semi-adiabatic calorimetry is performed in which the heat loss is also measured and the measured temperature values of the concrete are corrected to account for this loss. Even though the semi-adiabatic calorimetry method is a common test, there is no standard test method for this. This study followed the guidelines outlined by Poole et al. based on which a semi-adiabatic calorimeter was developed in the laboratory (Poole 2007). A schematic diagram showing the details of the calorimeter is shown in Fig. 4.

24 inches by 34 inches cylindrical drum was used for building the semi-adiabatic calorimeter. Aeromarine insulation foam was poured inside the drum which solidifies and acts as the insulation. Top insulation lid was also prepared using the same insulation foam. For installing the 7 in. x 14 in. steel chamber in the middle of the drum, galvanized steel sheet was used. Fresh concrete collected from the construction site during concrete placement (into a 6 in. x 12 in. cylinder) was immediately transported to the laboratory (to minimize the heat loss) and was placed inside the steel chamber. The temperature was measured using Type T thermocouples (TC) at three locations – one at the center of the concrete specimen (MID), one at the surface of the steel chamber (EXT1) and one at an inch away from the chamber surface in the insulation (EXT2). EXT1 and EXT2 TCs were installed to measure the heat loss through the calorimeter. MID TC was placed 6 inches into the center of the fresh concrete specimen. A plug-in for this thermocouple was installed at the edge of the steel chamber opening. For connecting thermocouple wires to the data logger, a hole was drilled in the middle of the drum surface through which the wires were taken out. The test set up was kept in a closed room where temperature variations were limited. The temperature data were recorded using Pico Technology USB TC-08 data logger for 160 hours at 15-minute intervals. The calorimeter was calibrated before the test to determine the calibration factors. The values of the calibration factors 1 and 2 were 0.0197 and 0.3970 W/°C, respectively.

Results and Discussions

Material Properties

General properties of concrete mix

The ready-mixed concrete at the construction site was tested for its fresh properties following relevant ASTM standards as mentioned earlier. The values of the slump, air content, unit weight, and temperature were measured to be 2.75 in., 7.50%, 149.12 lbs./ft.^{3}, and 63.6 °F, respectively. The compressive strength development was monitored by the Nurse-Saul maturity

method as shown in Fig. 5(a). Compressive strength is plotted as a function of the temperature-time factor (TTF) in Fig. 5(b). The values of the coefficients ‘a’ and ‘b’ of the best-fit linear equation [Eq. (1)] were calculated to be -5610.1 and 1089.7, respectively.

Activation energy

It is well-known in cement chemistry that like other chemical reactions, the hydration of cementitious materials is also sensitive to temperature. The apparent activation energy is a useful measure of the early-age temperature sensitivity of a concrete mixture and various calculation methods have been proposed for its calculation. A single linear approximation of reaction rate was used in this study for activation energy calculation (L Poole et al. 2007). The paste (cement + fly ash) samples were tested in the isothermal calorimeter at four constant temperatures: 10, 20, 30, and 40 °C. The reaction rate was calculated using a single, best-fit least-squares line of the linear, acceleration phase of the isothermal rate of heat curve. The slope of the best-fit line determined the reaction rate k at a particular temperature. ln (k) was then plotted versus the inverse of absolute temperature to determine E_a. The plot obtained in this study is shown in Fig. 6. The E_a of this mix was calculated to be 34,173 J/mol. This value was then used as an input in CW for predictions of the temperature profile of mass concrete foundation.

Hydration curve parameters

The fresh concrete sample collected from the pier 4 footing placement was brought to the lab for the semi-adiabatic calorimetry test. The test was run for 160 hours which recorded the temperature development under semi-adiabatic conditions along with the temperature change due to heat loss from the calorimeter. However, since the conditions in a mass concrete structure are truly adiabatic, the temperature development under these conditions needed to be known. The apparent activation energy (calculated from isothermal calorimetry), total heat of hydration

(estimated from the chemical composition of cementitious materials), and the measured data from semi-adiabatic calorimetry were used to calculate a theoretical adiabatic hydration curve following the procedure outlined by Poole et al. (Poole 2007). The measured and calculated semi-adiabatic and calculated adiabatic curves are shown in Fig. 7. Three curve-fit parameters (α_u, β, and τ) were obtained by fitting a theoretical curve to the measured semi-adiabatic curve as presented in Table 4. α_u (= 0.748) is the ultimate degree of hydration (DOH), β (= 0.840) is the hydration shape parameter, and τ (= 20 hours) is the hydration time parameter. A larger α_u indicates the higher magnitude of ultimate DOH, larger β indicates a higher hydration rate at the linear portion of hydration curve, and a larger τ means a larger delay of hydration (Xu et al. 2010). These parameters of the concrete mix were then used as inputs in CW for temperature prediction for the mass concrete foundation.

Results from Foundation Investigation

As discussed in section 2, sensors were installed in the mass concrete foundation to monitor the temperature development after the placement of concrete. The monitoring was done until the insulation was removed. The measured values of temperature by all the sensors are plotted in Fig. 8. The differential temperatures along with the Iowa DOT specified limits in early-age mass concrete are shown in Fig. 9. Analyzing the measured data and the plots presented in Figs. 8-9, the following observations, can be made:

- The concrete temperature at the time of placement was 66.2 °F which was within the Iowa DOT specified limits of 40 °F and 70 °F.
- The maximum concrete temperature of 149 °F was recorded at the core (sensor S1) that occurred after 40.35 hours of concrete placement (Fig. 8). The conditions in the core of a mass concrete member, a rectangular footing, in this case, can be almost fully adiabatic for

a few days. The heat generated, due to the exothermic hydration reaction of cementitious materials and water, is not dissipated easily. It is due to this reason that the temperature at the core of the member was found to be maximum. The Iowa DOT specification requires the concrete temperature in mass concrete structures to be less than 160 °F.

- The temperature differential (TD) between the core and the north as well as the long side sensors (Fig. 9) was found to be well within the specified limits whereas that between the core and top sensors was observed to cross the specified limit only for a short duration from 44 to 48 hours. Barring this, TD was well within the specified limits. The maximum value of TD was observed to be 39.6 °F that occurred around 73.5 hours after the placement of concrete.
- The maximum value of the temperature recorded at the top of the footing (S2) was 120 °F while that at the bottom of the footing was 134.6 °F.
- No significant difference was observed in the recorded temperatures in the centers of the North and West side faces (S3 and S6).

Thermal Analysis using ConcreteWorks

ConcreteWorks computer program was used for thermal analysis of the rectangular footing investigated in this study. With structural, material, construction, and environmental parameters as inputs, CW predicts the maximum temperature (T_{max}), maximum temperature differential (ΔT_{max}), maturity and strength development, and cracking potential of a mass concrete member. In this analysis, the measured properties of the concrete mix, as presented in section 4.1, were used as inputs. For all other inputs, CW default values were used. Baseline values of all the inputs, used for the analysis of footing, are presented in Table 5.

Usually, in rectangular footings that qualify as mass concrete, only three locations are critical from the perspective of thermal cracking. These locations are core, top, and the center of the face at the smallest distance from the core of the footing (the short side in this case; sensor S3 in Fig. 3). Therefore, the temperature profile at these three locations of the footing was analyzed using CW and compared with the measured values as shown in Fig. 10. Following observations can be made:

- CW predicted T_{max} to be 149.16 °F at the core of the footing, which was only slightly more than the measured value of 149 °F. The complete temperature development profile at the core predicted by CW simulates the measured profile really well as shown in Fig. 10(a). CW prediction of the time to reach T_{max} (52 hours) was also close to that of the field-measured value (50 hours). If the approximate time to reach T_{max} is known in addition to the value of T_{max}, an appropriate TCP can be developed in advance to control thermal cracking.
- The T_{max} prediction at the top of the footing by CW was 121.2 °F against a measured value of 120.2 °F. Also, CW simulation of the complete temperature development profile at the top was quite close to the measured profile except for an underestimation after around 125 hours [Fig. 10(b)].
- CW underestimated the temperature profile at the short side by approximately 3.5 °F on an average. T_{max} prediction was 136.3 °F while the measured value was 143.6 °F. It can be seen from Fig. 10(c) that the overall temperature profile was underestimated by CW.

Large temperature differences in a mass concrete member can be very detrimental from the perspective of thermal cracking/shock. The temperature difference causes a volume change due to expansion/contraction when the member is restrained by adjacent parts of the mass foundation

which might result in cracking (Riding et al. 2006). It is for this reason that most of the specifications restrict ΔT_{max} that a mass concrete member can experience during early age and therefore various preventive measures are employed in this age to meet the specifications and to prevent cracking.

It is very helpful in developing a preventive TCP if the TD between the critical points within a mass concrete member can be predicted in advance. CW predicts T_{max} as one of the outputs. The differential between two points could also be predicted and analyzed. In this study, the differentials between the core and other critical locations top, and the short side of the rectangular footing were predicted using CW and compared with the measured values. The differential temperature charts are shown in Fig. 11. The time series for maximum TD specified by Iowa DOT is also plotted in these charts. The observations from Fig. 11 are as follows:

- CW prediction of the core and top TD profile very well simulated the measured profile, as shown in Fig. 11 (a). Since this is the most critical TD, its prediction close to the actual value, (especially in the initial 100 hours), can be very helpful in preparing the TCP. CW, however, overestimated the core and top TD after around 125 hours of the placement of concrete that can be said to be conservative from the perspective of the factor of safety.

The TD profile between the core and the center of the face at the shortest distance from the core (short side) was overestimated by CW for the entire duration of analysis, as can be seen in Fig. 11 (b). On average, CW overestimated the TD between the core and short side by 9.5 °F. Similar to the core and top TD prediction, this is also conservative.

ConcreteWorks Sensitivity Analysis

A brief sensitivity analysis was performed, using ConcreteWorks, to investigate the effects of various parameters on the temperature development in mass concrete. Critical variables in three

major groups (Mix proportion, concrete material properties, and construction parameters) were analyzed for their effects on the maximum temperature and temperature differential in the rectangular footing. The analyzed inputs, baseline values, and their input and output ranges (and trends) are shown in Table 6. The baseline values were kept the same as those used in the thermal analysis presented in section 4.3. The trends observed in maximum temperature (T_{max}) and maximum TD (ΔT_{max}) corresponding to the changes in input types are plotted as bar charts in Fig. 12 and are discussed in following sub-sections.

Mix proportion parameters

The mix proportion parameters evaluated were cement content, class C fly ash, class F fly ash, slag, and silica fume. It can be observed from Fig. 12(a) that increasing cement content from 414 lbs. /yd^3 to 594 lbs. /yd^3 increased T_{max} as well as ΔT_{max}. This can be attributed to the increase in heat of hydration with an increase in cement content in the concrete mix. Replacing cement with supplementary cementitious materials (SCMs) is an effective way of reducing heat and this is confirmed with the trends shown in Fig. 12(a). Increasing the replacement percentage of C fly ash, F fly ash, and silica fume reduced T_{max} and $\Delta T_{max.}$ A similar reducing trend was also observed in the case of slag replacement from 0% to 50%. However, an increase in both T_{max} and ΔT_{max} can be seen from 50% to 70%. This is contrary to earlier belief but some of the recent experimental adiabatic studies on concrete mixes containing slag confirm this observation (Moon et al. 2018). The effect of pozzolanic as well as the latent hydraulic activity of slag on the cement hydration might be the reasons for an increase in the generated heat. This needs to be investigated further. However, the observations from this sensitivity study can be used to optimize the concrete mix proportion for minimum heat generation.

Material properties

Cement type, coefficient of thermal expansion (CTE), concrete thermal conductivity (*k*), and combined aggregate specific heat capacity (C_p) were the concrete material properties investigated in this study (Fig. 12). The order of T_{max} and ΔT_{max} in case of cement types were I > I/II > II > V. This is expected as the heat generation due to cement hydration depends predominantly on the C_3A content of cement. The typical C_3A contents of these cement types reduce in that order (I > I/II > II > V) thereby reducing T_{max} and ΔT_{max}. Changing CTE did not have any effect whereas increasing *k* and C_p reduced T_{max} and ΔT_{max}. Thermal conductivity is defined as the rate of heat conduction and as it increases, the heat generated in the core of a mass concrete member is dissipated at a faster rate thereby reducing T_{max} and ΔT_{max}.

Construction parameters

The parameters related to mass concrete construction are also important factors affecting the temperature development. Placement temperature, formwork type, insulation blanket R-value, curing method, and subbase type were construction parameters evaluated in this study (Fig. 12). Mass concrete placement temperature was observed to have a great impact on T_{max} and ΔT_{max}. A 30 °F increase in placement temperature caused a corresponding 30 °F and 11.45 °F increase in T_{max} and $\Delta T_{max,}$ respectively. Various formwork types (steel, wood, and insulated steel) and curing methods (curing compound, blanket, and white/black plastic) were evaluated separately but no change was observed in the temperature development. However, their combinations along with changes in other properties might result in an increase/decrease of T_{max} and $\Delta T_{max.}$ R-value is a quantification of the thermal insulation property of a material (insulation barrier such as a blanket) and is defined as the ratio of material thickness and its thermal conductivity. A greater R-value represents better insulation power of the material. Increasing R-value of the insulation blanket

from 0.51 to 1.41 hr-ft^2-F/BTU increased T_{max} and ΔT_{max} by 1.15 °F and 0.63 °F, respectively which can be said to be a minimal change. Type of subbase, on the other hand, was found to affect heat dissipation considerably. Changing topsoil to concrete subbase, T_{max} increased only by approximately 1.8 °F while an increase of 9.5 °F occurred in ΔT_{max}. A similar change of subbase type from limestone to sand resulted in a 1.2 °F and 15.1 °F increase in T_{max} and ΔT, respectively.

Conclusions

In this study, ConcreteWorks (CW) computer program was used to perform a brief sensitivity study and to predict the temperature profile of a mass concrete structure. The predictions were validated for their accuracies with the results and observations from the investigation of a mass concrete bridge footing. Specific conclusions from this study are as follows:

(1) The apparent activation energy (E_a) and hydration curve parameters (α_u, β, and τ), obtained respectively from isothermal and semi-adiabatic calorimetry measurements, are two significant material properties for temperature development predictions in a mass concrete member.

(2) The temperature differentials, between the centroid (core) and the midpoints of the top surface and the surface nearest to the centroid of a rectangular mass concrete footing, are critical for thermal cracking. The temperature development at these three locations is necessary to be monitored.

(3) CW predictions of absolute maximum temperature, maximum temperature differential, maturity, and compressive strength development for the rectangular footing were all very precise in their comparisons with the measured data.

(4) The temperature differentials (core-top and core-short side) were slightly overestimated by CW, especially after 125 hours. However, this can be said to be conservative from the perspective of the factor of safety.

(5) Sensitivity study revealed a considerable impact of concrete mix proportion, cement type, concrete thermal properties, placement temperature, insulation R-value, and foundation subbase on temperature development in the footing.

Acknowledgments

This study was a part of a research project "Evaluate, Modify, and Adapt the ConcreteWorks Software for Iowa's Use", sponsored by the Iowa Highway Research Board (IHRB). The authors would like to acknowledge the sponsorship.

References

Abdun-Nur, E. A., Anderson, F. A., Boggs, H. L., Bonikowsky, D. A., Bradshaw Jr., R. A., Bush, E. G. W., Diaz, L. H., Dolen, T. P., Hansen, K. D., Mass, G. R., McCarthy, A. T., Oliverson, J. E., Oury, R. F., Raphael, J. M., Schrader, E. K., and Tatro, S. B. (1990). "Effect of restraint, volume change, and reinforcement on cracking of mass concrete." *ACI Materials Journal*, 87(3), 271–295.

ACI (American Concrete Institute). (2000). "Cement and Concrete Terminology." *ACI 116R*, Farmington Hills, MI.

ACI (American Concrete Institute). (2006). "Guide to Mass Concrete." *ACI 207-06*, Farmington Hills, MI.

ASTM C39. (2016). "Standard Test Method for Compressive Strength of Cylindrical Concrete Specimens." *ASTM*, West Conshohocken, PA.

Ballim, Y. (2004). "A numerical model and associated calorimeter for predicting temperature profiles in mass concrete." *Cement and Concrete Composites*, 26(6), 695–703.

Choktaweekarn, P., and Tangtermsirikul, S. (2010). "Effect of aggregate type, casting, thickness and curing condition on restrained strain of mass concrete." *Songklanakarin Journal of Science and Technology*, 32(4), 391–402.

Dilek, U. (2011). "Planning and execution of a mass concrete placement utilizing insulation regimen." *American Concrete Institute, ACI Special Publication*, American Concrete Institute, 2011-Octob(SP 325), 1–12.

Dunstan, M. R. H., and Mitchell, P. D. (1976). "Results of a Thermocouple Study in Mass Concrete in the Upper Tamar Dam." *Proceedings of the Institution of Civil Engineers (London). Part 1 - Design & Construction*, 60(pt 1), 27–52.

Folliard, K. J., Juenger, M., Schindler, A., Riding, K., Poole, J., Kallivokas, L. F., Slatnick, S., Whigham, J., and Meadows, J. L. (2002). "Prediction Model for Concrete Behavior: Final Report." *Texas Department of Transportation*, Austin,TX.

Folliard, K., Schindler, A., and Pesek, P. (2017). "ConcreteWorks V3 Training / User Manual ConcreteWorks Software (P2)." Concrete Durability Center, Texas, USA.

Iowa DOT. (2009). *Developmental Specifications for Mass Concrete -Control of Heat of Hydration*.

Juenger, M. C. G., and Siddique, R. (2015). "Recent advances in understanding the role of supplementary cementitious materials in concrete." *Cement and Concrete Research*, 78, 71–80.

Kolani, B., Buffo-Lacarrière, L., Sellier, A., Escadeillas, G., Boutillon, L., and Linger, L. (2012). "Hydration of slag-blended cements." *Cement and Concrete Composites*, 34, 1009–1018.

L Poole, J., A Riding, K., J Folliard, K., C G Juenger, M., and K Schindler, A. (2007). "Methods for Calculating Activation Energy for Portland Cement." *ACI Materials Journal*, 104(1), 303.

Lawrence, A. M., Tia, M., and Bergin, M. (2014). "Considerations for handling of mass concrete: Control of internal restraint." *ACI Materials Journal*, American Concrete Institute, 111(1), 3–11.

Lothenbach, B., Scrivener, K., and Hooton, R. D. (2011). "Supplementary cementitious materials." *Cement and Concrete Research*, 41, 1244–1256.

Luther, M. ., Bohme, P., and Wilson, W. (2008). "Case studies-North American mass concrete projects featuring ASTM C989 slag cement." *ACI Special Publication:ACI Fall 2008 Convention*, American Concrete Institute, Farmington Hills, MI, 13–30.

Lv, C., and Qiao, C. (2011). "Mass concrete construction technology of high-rise building foundation platform." *2011 International Conference on Electric Technology and Civil Engineering, ICETCE 2011 - Proceedings*, IEEE Computer Society, 442–445.

Moon, H., Ramanathan, S., Suraneni, P., Shon, C. S., Lee, C. J., and Chung, C. W. (2018). "Revisiting the effect of slag in reducing heat of hydration in concrete in comparison to other supplementary cementitious materials." *Materials*, 11(10).

Nili, M., and Salehi, A. M. (2010). "Assessing the effectiveness of pozzolans in massive high-strength concrete." *Construction and Building Materials*, 24(11), 2108–2116.

Poole, J. (2007). "Hydration Study of Cementitious Materials Using Semi-adiabatic Calorimetry." *PhD Dissertation*, The University of Texas at Austin, Austin, TX.

Poole, J., Riding, K., Browne, R. A., and Schindler, A. (2006). "Temperature management of mass concrete structures." *Concrete Construction - World of Concrete*, Hanley Wood LLC, 51(11), 47–53.

Riding, K. A. (2007). “Early Age Concrete Thermal Stress Measurement and Modeling.” *PhD Dissertation*, The University of Texas at Austin, Austin, TX.

Riding, K. A., Poole, J. L., Schindler, A. K., Juenger, M. C. G., and Folliard, K. J. (2006). “Evaluation of Temperature Prediction Methods for Mass Concrete Members.” *ACI Materials Journal*, 103(5).

Riding, K. A., Poole, J. L., Schindler, A. K., Juenger, M. C. G., and Folliard, K. J. (2013). “Statistical Determination of Cracking Probability for Mass Concrete.” *Journal of Materials in Civil Engineering*, 26(9), 04014058.

Scrivener, K. L., Lothenbach, B., De Belie, N., Gruyaert, E., Skibsted, J., Snellings, R., and Vollpracht, A. (2015). “TC 238-SCM: hydration and microstructure of concrete with SCMs State of the art on methods to determine degree of reaction of SCMs.” *Materials and Structures/Materiaux et Constructions*, 48, 835–862.

Shanahan, N., Tran, V., and Zayed, A. (2016). “Heat of hydration prediction for blended cements.” *Journal of Thermal Analysis and Calorimetry*, 128, 1279–1291.

Wang, C., Zhou, Z., Hu, Q., and Ou, J. (2005). “Construction control of mass concrete of Nanjing 3rd Yangtze Bridge using FRP-packaged FBG sensors.” *Proceedings of SPIE - The International Society for Optical Engineering*, SPIE, 5855 PART II, 1012–1015.

Xu, Q., Hu, J., Ruiz, J. M., Wang, K., and Ge, Z. (2010). “Isothermal calorimetry tests and modeling of cement hydration parameters.” *Thermochimica Acta*, 499(1–2), 91–99.

Xu, Z., Ding, Y., Zhai, C., and Li, Q. (2012). “Cracking and temperature control in mass concrete construction.” *Advanced Materials Research*, Trans Tech Publications, 446–449, 841–845.

Yin, S. U., Huang, Y., and Yuan, Y. H. (2013). “Research on mass concrete construction techonogy of raft foundation of hongyun building.” *Advanced Materials Research*, Trans Tech Publications Ltd, 690 693, 709–713.

Zhang, G., Li, H., and Shi, C. (2012). “Study on mass concrete slab construction technology of dalian world finance center.” *Applied Mechanics and Materials*, Trans Tech Publications, 137, 175–180.

Zheng, S., Sun, Z., and Zhu, H. (2017). “Mass concrete construction technology of the Three Gorges Project.” *Zhongguo Kexue Jishu Kexue/Scientia Sinica Technologica*, Chinese Academy of Sciences, 47(8), 796–804.

Zhu, H., Song, H., and Kuang, Q. (2004). “Application of Seamless Construction Technique to Mass Concrete Structures.” *Huazhong Keji Daxue Xuebao (Ziran Kexue Ban)/Journal of Huazhong University of Science and Technology (Natural Science Edition)*, Huazhong University of Science and Technology, 32(11), 100–102.

Zhu, J., Zhang, Y. Bin, Du, X. F., and Jiang, Y. (2014). “Study on mass concrete construction technology of raft foundation in Yantai Ocean development center.” *Advanced Materials Research*, Trans Tech Publications, 919–921, 1421–1425.

Figures

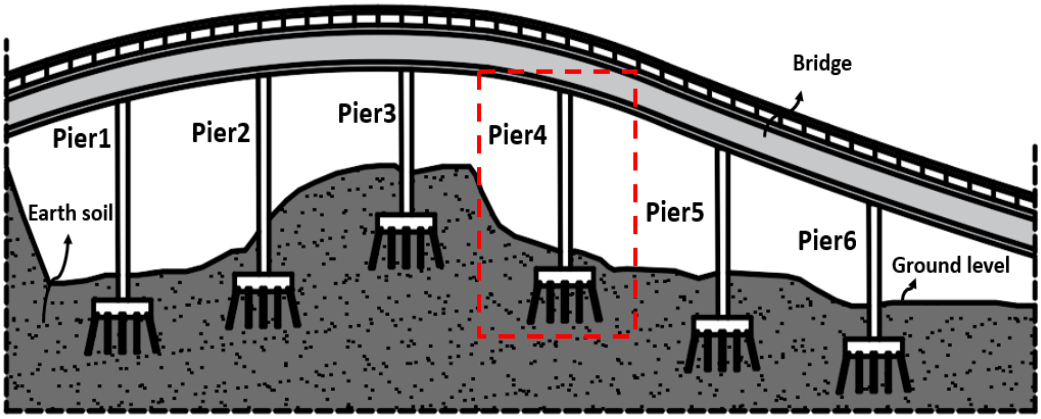

(a) cross-section

(b) Location (Map data © 2019 Google)

Fig. 1. US30-I35 Bridge in Iowa, USA

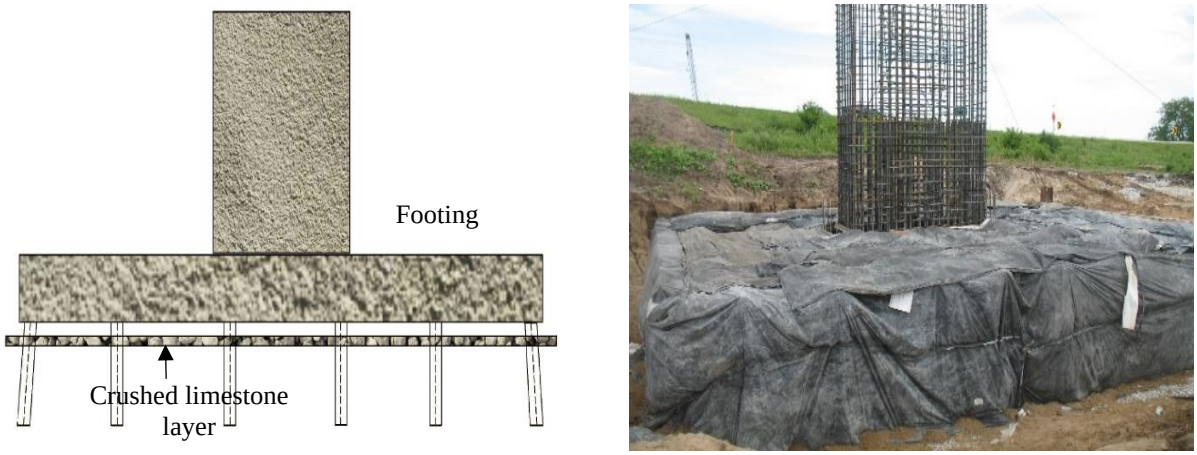

(a) Diagram of footing support and subbase (b) Footing covered with insulation blanket

Fig. 2. Pier 4 footing and insulation

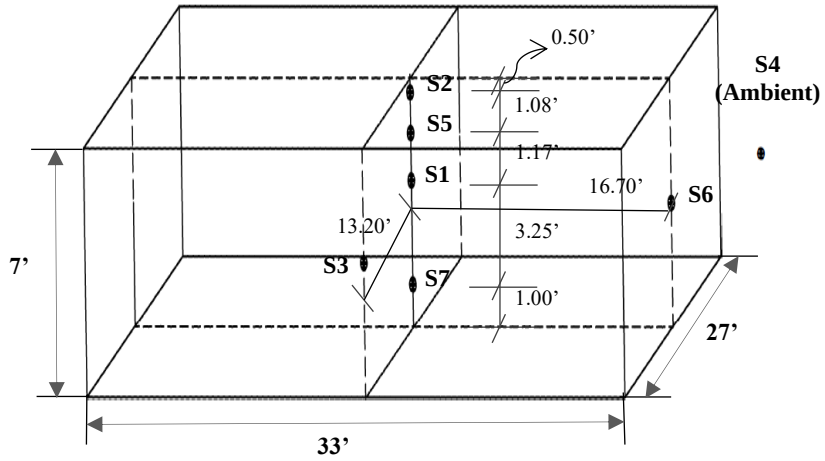

Fig. 3. Location of temperature sensors installed in the footing (not in scale)

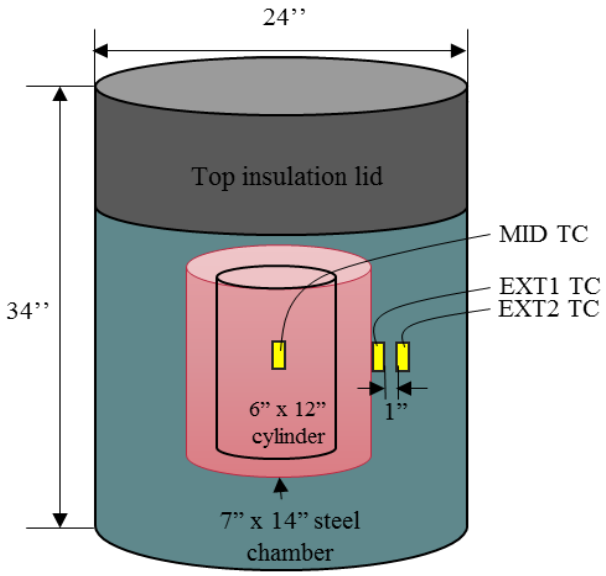

Fig. 4. Schematic diagram of the semi-adiabatic calorimeter

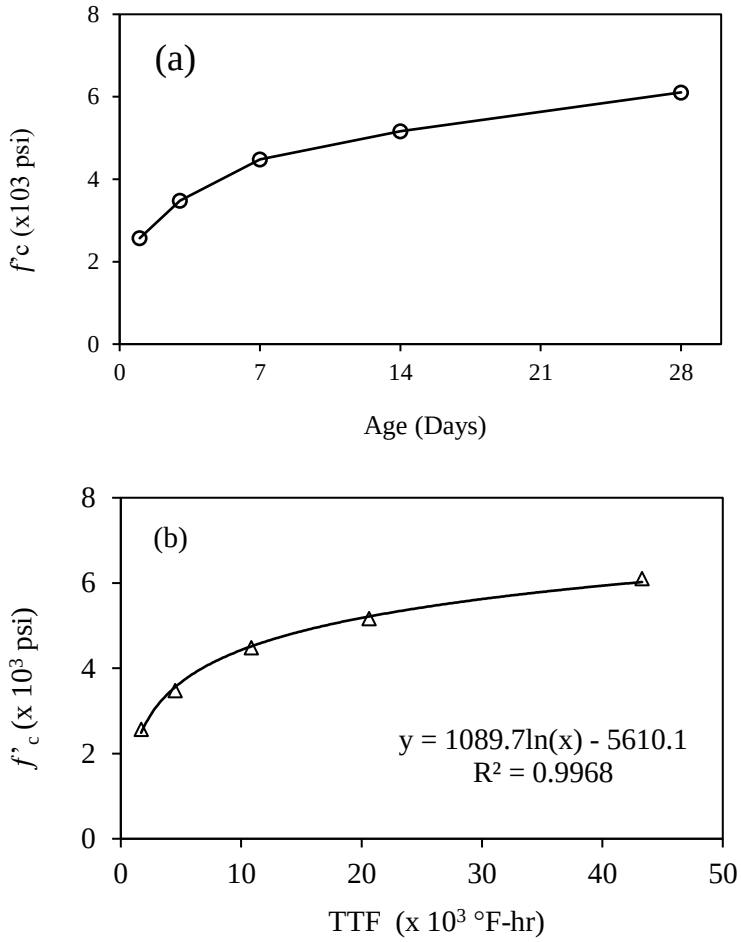

Fig. 5. (a) Compressive strength development; and (b) strength-maturity relationship

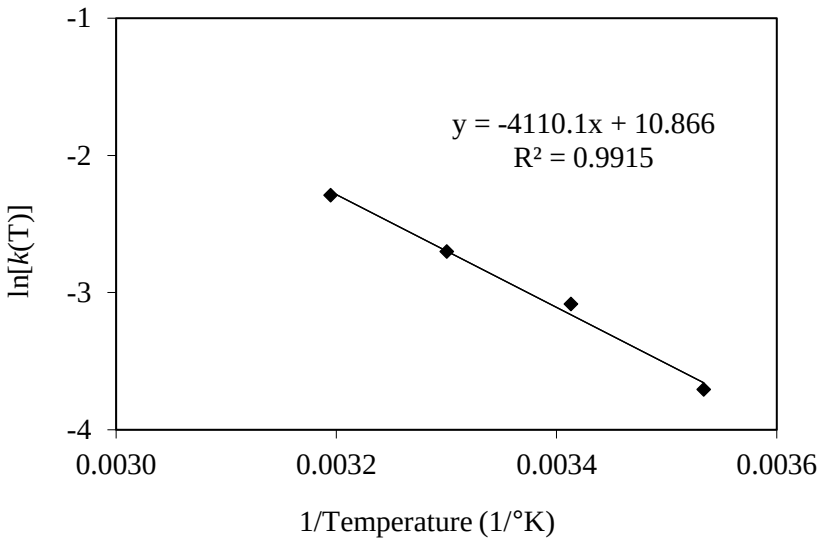

Fig. 6. Arrhenius plot for activation energy calculation

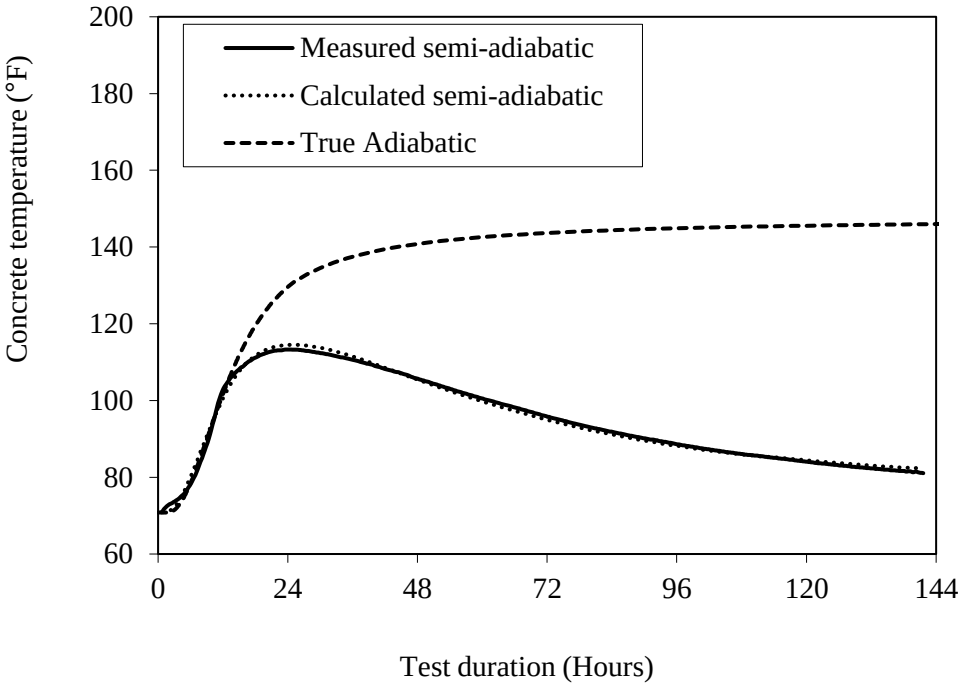

Fig. 7. Semi-adiabatic and true adiabatic curves

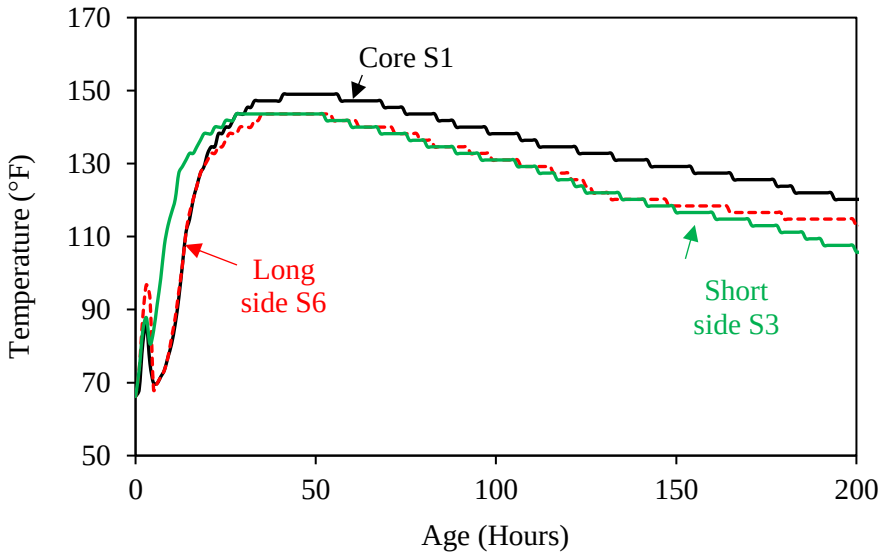

(a) Core and side sensors

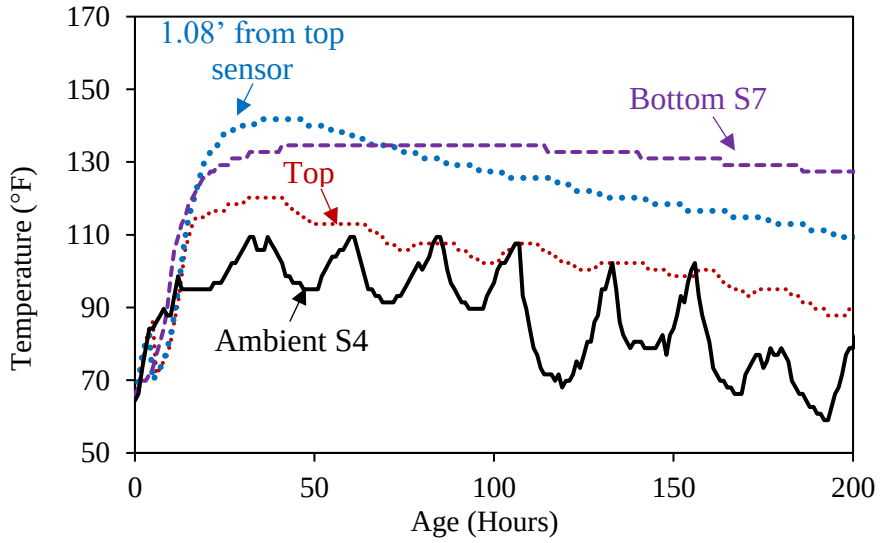

(b) Top, 1.08’ from top, ambient, and bottom sensors

Fig. 8. Temperature measured by installed sensors

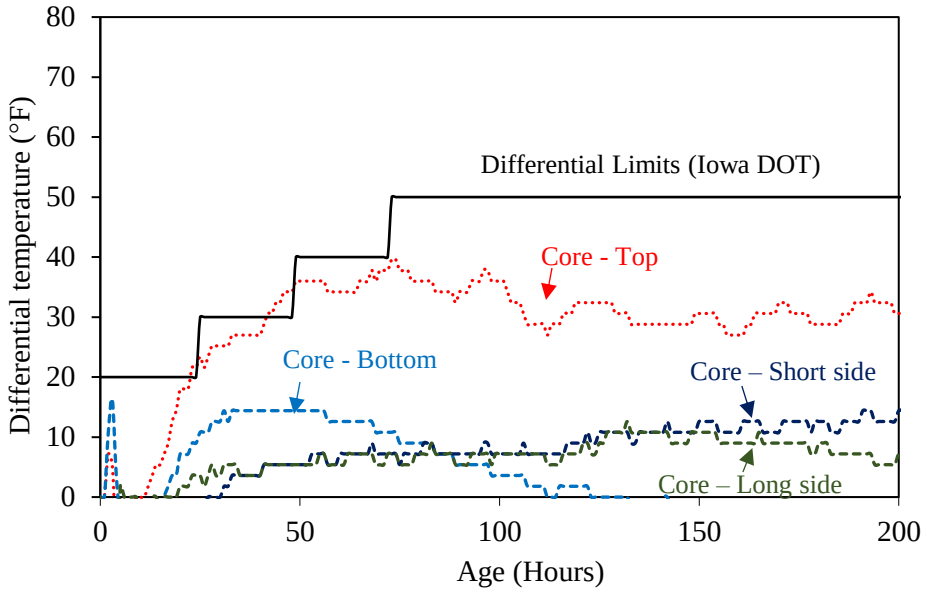

Fig. 9. Measured differential temperature in footing

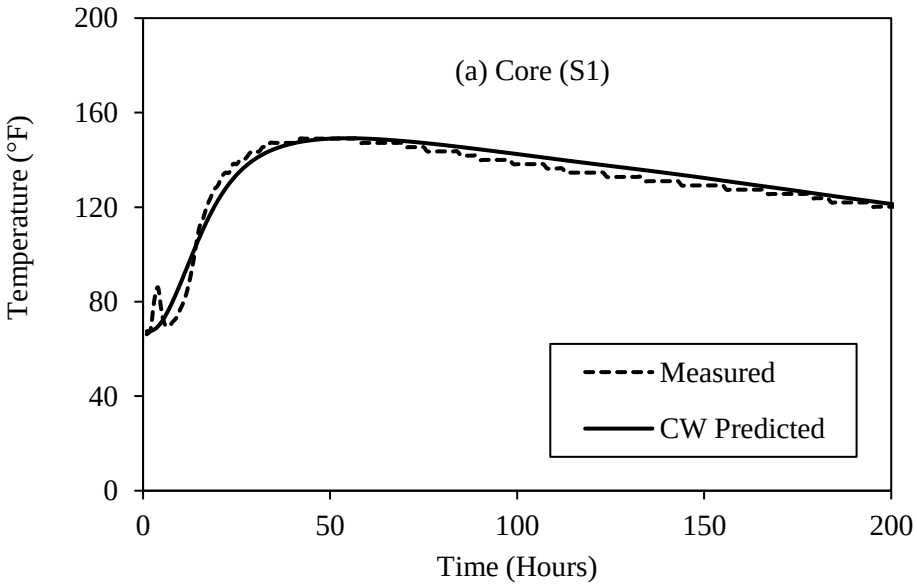

Fig. 10. Measured and CW predicted temperature profiles at (a) core of the footing

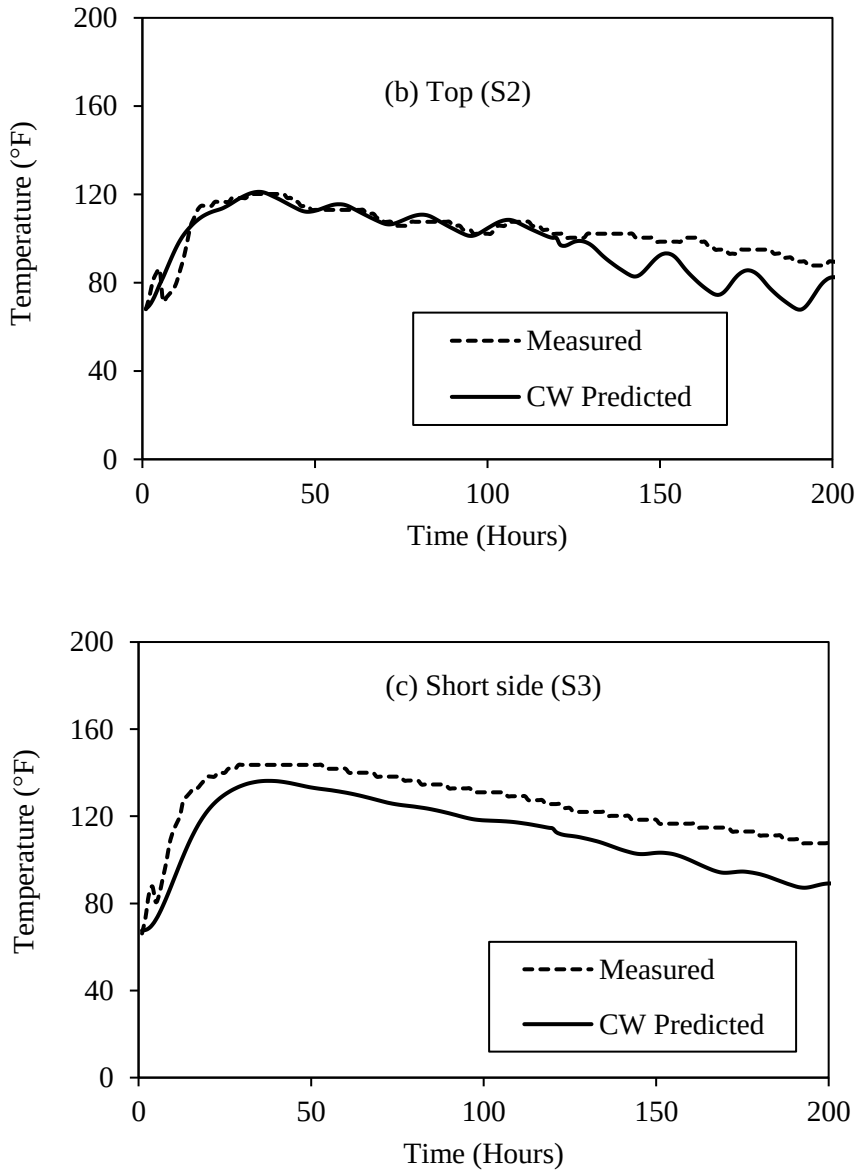

Fig. 10. (continued) Measured and CW predicted temperature profiles at (b) top; and (c) short side of the footing

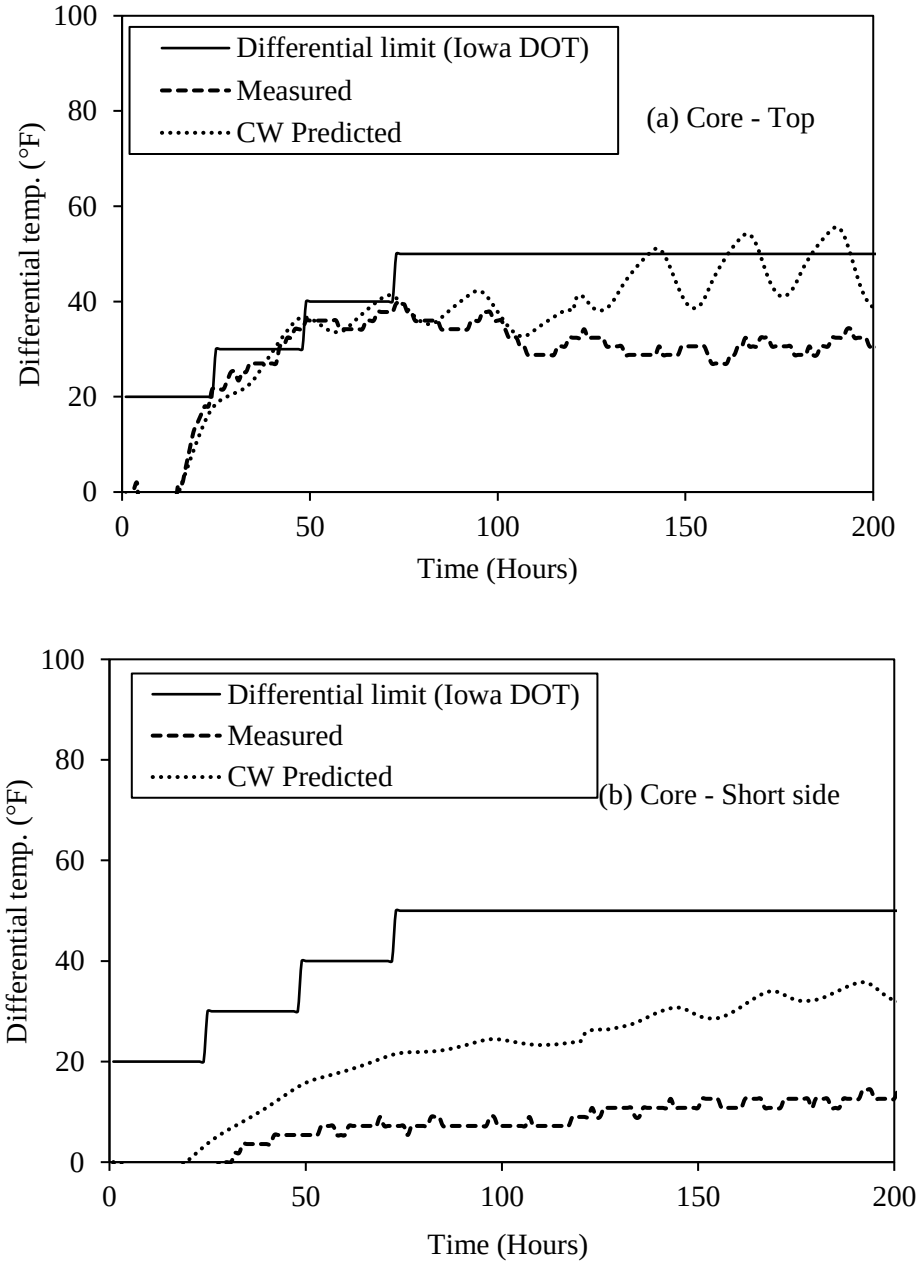

Fig. 11. CW predicted and measured temperature differentials

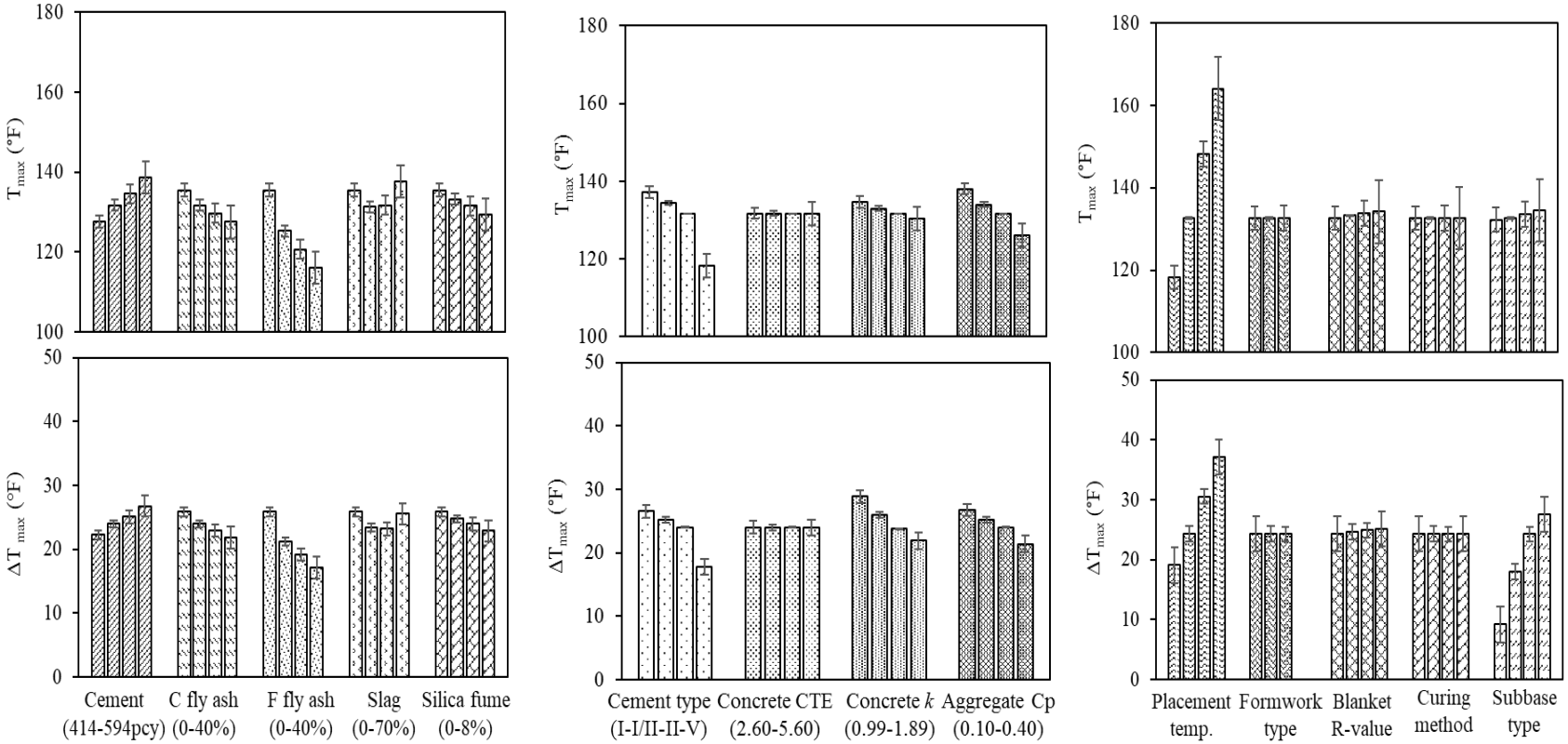

(a) Mix proportion parameters (b) Material properties parameters (c) Construction parameters

Fig. 12. Effect of mass concrete parameters on maximum temperature (T_{max}) and temperature differential (ΔT_{max})

Tables

Table 1. Dimensions of all pier footings

Footing of pier #	Dimension of footing (length x width x depth)
Pier 1	33'x 21'x 6'
Pier 2	33'x 21'x 6'
Pier 3	33'x 27'x 6'
Pier 4	**33'x 27'x 7'**
Pier 5	30.5'x 21'x 6'
Pier 6	33'x 21'x 6'

Table 2. Mass concrete mix proportion

Mixture Constituents	Quantity ($lb./yd^3$)
Cement (Type I/II)	474
Fly Ash (Class C)	119
Fine Agg.	1500
Coarse Agg.	1517
Water	255
Water-to-Binder ratio	0.43

Table 3. Chemical composition of cementitious materials

Oxides	Type I/II cement (%)	Class C fly ash (%)
SiO_2	20.44	33.76
Al_2O_3	5.11	15.23
Fe_2O_3	3.27	6.30
CaO	60.95	31.17
MgO	3.59	4.98
SO_3	3.03	2.25
Na_2O	0.18	1.35
K_2O	0.61	0.60
Others	1.52	4.93
LOI	1.96	0.57

Table 4. Estimated total heat, activation energy, and hydration curve parameters

Mixture	Hu, J/Kg	E_a, J/mol	α_u	β	τ, hours	R^2
Concrete	472,296	34,173	0.748	0.840	20.006	0.994

Table 5. ConcreteWorks inputs for thermal analysis of bridge footing

Parameter	Value	Units	Parameter	Value	Units
General Inputs			Member Inputs		
Project location	Ames, IA		Shape choice	Rectangular Footing	
Unit system	English		Member width	27	Ft.
Analysis duration	14	days	Member length	33	Ft.
Concrete placement time	8	AM	Member depth	7	Ft.
Mixture Proportions			Material Properties		
Cement content	474	lb/yd^3	Cement type	I/II	
C Fly ash	119	lb/yd^3	Cement chemistry values	Measured (from Table 3)	
Water content	255	lb/yd^3	Hydration parameter values	α_u=0.748; β=0.840; τ=20	
Coarse agg. Content	1517	lb/yd^3	Thermal conductivity	1.56	BTU/hr-ft-°F
Fine agg. content	1500	lb/yd^3	CTE	4.6	10^{-6}/°F
Air content	7.5	%	Coarse agg. type	Limestone	
Chemical admixture	Type A, NRWR		Fine agg. type	Siliceous river sand	
Construction Inputs			Environmental Inputs		
Concrete fresh temp	66.2	°F	Ave. daily max temp.	81.5	°F
Blanket R-value	0.5	$hr\text{-}ft^2$-°F/BTU	Ave. daily min temp.	58	°F
Form type	Wood		Ave. daily max solar radiation	731.1	W/m^2
Soil temperature	80	°F	Ave. daily max wind speed	24.1	m/s
Footing subbase	Limestone		Ave. daily max RH	95.1	%
Side cure method	Black plastic		Ave. daily min RH	45	%

Table 6. ConcreteWorks sensitivity analysis

Group	Input type	Baseline values	Input range	Unit	Range of Outputs (°F)	
					T_{max} (trend)	ΔT_{max} (trend)
Mix proportion inputs	Cement content	474	414,474,534,594	pcy	127-138 (→)	22-26 (→)
	C fly ash replacement	20	0,20,30,40	%	135-127 (←)	26-21 (←)
	F fly ash replacement	0	0,20,30,40	%	135-116 (←)	26-17 (←)
	Slag replacement	0	0,30,50,70	%	135-137 (←)	26-25 (←)
	Silica fume replacement	0	0, 3, 5, 8	%	135-129 (←)	26-23 (←)
Material Properties inputs	Cement type	I/II	I,II, I/II, V	Type	137-118 (←)	26-18 (←)
	CTE	4.6	2.6,3.6,4.6,5.6	10^{-6}/F	131-131 (--)	24-24 (--)
	Concrete k	1.59	0.99, 1.29, 1.59, 1.89	BTU/hr.-ft-F	134-130 (←)	29-22 (←)
	Combined aggregate Cp	0.2	0.18, 0.19, 0.20, 0.22	BTU/lb.-F	138-126 (←)	27-21 (←)
Construction inputs	Placement temperature	66	51, 66, 81, 96	°F	114-164 (→)	19-37 (→)
	Formwork type	Steel	Steel, wood, insulated steel	Type	132-132 (--)	24-24 (--)
	Blanket R-value	0.51	0.51, 0.81, 1.11, 1.41	$hr.-ft^2$-F/BTU	132-134 (→)	24-25 (→)
	Curing method	Black plastic	White curing compound, black plastic, wet curing blanket, white or clear plastic	method	132-132 (--)	24-24 (--)
	Type of subbase	Limestone	Limestone, topsoil, concrete, sand	type	132-134 (→)	09-24 (→)

CHAPTER 3. EFFECTS OF MODERN CONCRETE MATERIALS ON THERMAL CONDUCTIVITY

Modified from a manuscript published in *Journal of Materials in Civil Engineering*

Yogiraj Sargam[7], Kejin Wang[8], James E. Alleman[9]

Abstract

Thermal conductivity, *k*, is one of the key factors that control heat transfer in concrete. This paper presents the results of an experimental study conducted to analyze the effects of modern concrete materials, such as supplementary cementitious materials (SCMs), normal-weight, lightweight, and recycled aggregates, and steel and polypropylene (PP) fibers, on the thermal conductivity of concrete. The thermal conductivity tests were performed on cylindrical specimens of concrete mixes containing various amounts of these materials. The results indicate that *k* values of concrete reduced with the amount of SCM (slag and fly ash) replacement for cement. The mineralogy and absorption of normal weight aggregate considerably affect *k* value of concrete. Replacing normal weight coarse aggregate by lightweight or recycled aggregate reduced the *k* value of concrete. Addition of steel fiber at a dosage higher than 0.25% (by volume) increased *k* value of concrete noticeably, while the addition of up to 2% PP fiber showed little effect.

Keywords: Concrete – Thermal Conductivity – SCMs – Lightweight Aggregate – Recycled Aggregate - Fiber

[7] Graduate Research Assistant; Iowa State University; Department of Civil, Construction, and Environmental Engineering; 813 Bissell Road , Ames, IA, USA, 50011; email: ysargam@iastate.edu

[8] Professor; Iowa State University; Department of Civil, Construction, and Environmental Engineering; 412 Town Engineering Building, Ames, IA, 50011 (corresponding author); email: kejinw@iastate.edu

[9] Professor; Iowa State University; Department of Civil, Construction, and Environmental Engineering; 420 Town Engineering Building, Ames, IA, 50011; email: jea@iastate.edu

Introduction

Thermal properties of concrete materials are attracting increasing attention, not only because of their effects on building energy efficiency but also on structural performance and serviceability. Thermal conductivity, *k*, defined as the constant of proportionality between heat flux and temperature gradient, is one of the major factors governing heat transfer. Materials with low *k* values are generally desired for structures that require thermal insulation, such as buildings and radiation shielding in nuclear power stations (Campbell-Allen and Thorne 1963; Khan 2002). Many countries, including the United States (US), have adopted energy-conservation building codes and standards. ACI Committee 122 (2002) states that *"the design of energy-conserving buildings now requires an expanded understanding of the thermal properties of the building envelope and the materials comprising the envelope system"*. On the other hand, materials with high *k* levels are desired for floors and driveways with embedded heaters (Marshall 1972). Thermal conductivity is also a very important parameter in the design and control of thermal cracking of concrete pavements, large foundations, and dam structures (Gui et al. 2007; Schindler 2002). Gui et al. (2007) studied the impact of pavement thermophysical properties on surface temperatures, and they suggested that among other effects, *k* could also contribute to Urban Heat Island (UHI) impacts.

Modern concrete materials, such as various supplementary cementitious materials (SCMs), different types of aggregates (lightweight and recycled aggregates), and fibers, have been increasingly used in transportation structures, such as pavements and bridge decks, as well as large foundations (mass concrete), where thermal behavior is important and sensitive for the structure performance. Using a computer program, ConcreteWorks (Folliard et al. 2017; Riding 2007), the authors of this paper have recently evaluated the effect of thermal conductivity of concrete materials on the early-age temperature development of a bridge foundation. Thermal analyses were performed on a 33 ft. x 27 ft. x 7 ft. (8.23 m x 10.06 m x 2.13 m) rectangular footing of a bridge pier, which is considered as a mass concrete member according to ACI Committee 207 (2006). In the analyses, all input

parameters were kept the same and only *k* value of concrete was changed. Fig. 1 shows the temperature development in the footing as predicted by ConcreteWorks for different values of *k.* According to the figure, as *k* was increased from 0.4 W/m-K to 1.6 W/m-K, the maximum temperature developed in the core of rectangular footing decreases from 68 °C to 63 °C at the age of 3 days, and the temperature decrease become faster at later ages. Such a reduction in the maximum temperature can bring about a reduction in the maximum differential temperature and can subsequently reduce the early-age thermal cracking probability of the structural element. Therefore, understanding the thermal behavior of construction materials is essential for the design of the thermal control plan for placing concrete in extreme weather (hot and cold) conditions and for mass replacement.

Research has revealed that the factors affecting thermal conductivity of concrete include: mineralogical characteristics of aggregate, mix proportion, density, moisture, and degree of hydration of concrete (Breugel 1998; Campbell-Allen and Thorne 1963; Khan 2002; Marshall 1972; Schindler 2002). Since approximately 50-70% volume of concrete is often occupied by aggregates, the type and volume of aggregates in a concrete mix have the most influence on its conductivity. Aggregates with lower *k* values produce less conductive concrete and vice-versa (Campbell-Allen and Thorne 1963; Neville 2011). Quartzite and sandstone aggregates have the highest *k*; limestone and dolomite have intermediate effects, whilst basalt and dolerite have the lowest *k* values (Marshall 1972). Several researchers have shown that there is a direct relationship between density and *k* of concrete (Ganjian 1990), while others (ACI (American Concrete Institute) 2002; Valore 1980) displayed an exponential relationship between dry density and *k* of concrete. ACI Committee 122 also suggests an increase of 6% in *k* value of concrete for each 1% of moisture by weight (ACI (American Concrete Institute) 2002). Ganjian (1990) performed extensive research to study the effect of porosity, pore-volume, and pore structure on the *k* of concrete. He also developed a mathematical model relating *k* of concrete to its dry density, total porosity, and median pore diameter. However, other influencing factors, such as supplementary cementitious materials (SCMs), fiber addition, etc., were not considered in his model.

Recently, more researches have been conducted to determine *k* of concrete containing various waste materials, some of which were summarized by Misri et al. (2018). However, in spite of the vast range and extent of waste materials used in concrete, prior study of thermal conductivities within waste-amended and/or additive-supplemented concrete remains limited.

This paper presents the results and discussions from a simple thermal conductivity experiment, performed on concrete containing different types of aggregate (e.g., normal-weight aggregates with different absorption values, lightweight, and recycled aggregate), SCMs (e. g., fly ash and ground granulated blast furnace slag (GGBFS)), and fibers (steel and polypropylene fiber). The effects of these concrete materials on thermal conductivity are analyzed. The analysis of the experimental dataset is also presented wherein trend lines of the variation in thermal conductivity of concrete are shown as functions of its dry-density and compressive strength.

Experimental Program

Materials and Mix Proportions

One type of Portland cement and two types of blended cement were used in this study, and they are Type I/II cement meeting ASTM C150 criteria, Type IP(25) cement containing 25% class F fly ash, and Type IS(20) cement containing 20% grade 100 GGBFS satisfying ASTM C595 criteria. The SCMs used included Class C fly ash under ASTM C618 and Grade 100 slag under ASTM C989. Table 1 shows the chemical composition, Blaine's fineness, and specific gravity (SpG) of these types of cement and SCMs.

One fine aggregate was used in all concrete mixes studied, which was river sand. This sand had a specific gravity of 2.68, absorption of 1.39%, and fineness modulus of 2.75. Three different types of coarse aggregates were used, including normal-weight aggregate, lightweight aggregate, and recycled concrete aggregate. The lightweight aggregate was expanded shale. The recycled aggregate was obtained from a concrete pavement in Minnesota, USA. Table 2 provides the specific gravity and absorption of the coarse aggregates, and Fig. 2 provides the gradation of the aggregates.

Two types of fibers were used, and they are steel fiber and polypropylene (PP) fiber. The length and diameter of both types of fiber were 12.7 mm and 0.2 mm. The aspect ratios of these two fibers were accordingly the same (63.5). Two types of admixtures were also evaluated, including the air-entraining agent (AEA) and medium-range water-reducer (MRWR). The AEA was synthetic and the MRWR was a lignosulfonates-based material.

Different concrete mixes were studied; all of the mixes had different types of cementitious materials and aggregates. The effect of the water-to-binder ratio (w/b) on thermal conductivity was evaluated using concrete mixes containing recycled concrete as coarse aggregate. Table 3 presents the mix proportions of all concrete mixes based on the volume fraction of constituent materials. The lightweight and recycled aggregate replacements were prepared in relation to the volume of coarse aggregate in the mix. Therefore, the mix proportions of concrete mixes shown here are presented in terms of the volume fraction of constituents.

Experiments

Sample preparation

Following the designed mix proportion as presented in Table 3, concrete mixes were prepared as per the standard operating procedure ASTM C192 (ASTM 2016) using a pan mixer. After testing fresh properties of a concrete mix, cylindrical specimens (4” X8”) were prepared for various tests such as compressive strength and dry density. The specimen preparation for thermal conductivity test was a bit different (shown in Fig. 3). At first, two iron disks of 1-inch thickness and a ½ inch diameter rod were prepared [Fig. 3 (a)]. One disk was kept at the bottom of the 4-inch diameter by 8-inch length cylindrical mold and the iron rod was inserted through it [Fig. 3 (b)]. The disk was made to hold the rod. The concrete was then cast into the cylinder, compacted, and the other disk was then kept on the top. After 24 hours, the rod was pulled out, the disks were removed, and the set concrete sample was demoulded [Fig. 3 (c)]. After demolding, all cylindrical specimens were then cured in

limewater curing baths (ASTM C192) for the desired time. Prior to testing, the specimens for thermal conductivity tests were dried in the oven at 105 °C for 48 hours and then cooled to room temperature.

Test methods

Tests for measuring fresh properties of concrete were performed as per relevant ASTM standard test procedures. Slump (ASTM C143), air content (ASTM C173), and unit weight (ASTM C138) of all concrete mixes were measured. After 28 days of curing, the cylindrical specimens were tested for compressive strength and oven-dry density in accordance with ASTM C39 (ASTM 2016) and ASTM C127 (ASTM 2015) test procedures respectively.

Several steady and transient methods can be used to measure the thermal conductivity of concrete, and different methods may furnish different values (Asadi et al. 2018; Gomes et al. 2017). The most widely used procedure for measuring thermal conductivity is that of ASTM C177-13 (i.e., "*Standard test method for steady-state heat flux measurements and thermal transmission properties by means of guarded hot plate apparatus*") (ASTM 2004). This method tracks specimen temperature at steady state to determine *k* and requires precise slab specimen geometries. Unfortunately, though, this method is not recommended for highly non-homogeneous materials such as concrete. The test method used in this project was the one proposed by Carlson et al. (2010), "*Determining thermal conductivity of paving materials using cylindrical sample geometry*". This experimental method allows thermal properties to be determined from commonly used cylindrical specimen geometries with minimal preparation. The complete test setup for measuring thermal conductivity is shown in Fig. 4 (a). Below are the detailed steps for the experiment:

(1) A silicone-based paste (k = 2.3 W/m-K), manufactured by Omega Engineering, Inc., was poured evenly into the central 0.5" diameter hole of the specimen, and a cartridge heater (0.375" diameter, 1000W, with a resistance of 57.9 Ω) was then inserted into the hole/core.

(2) Seven temperature sensors (Type K thermocouples) were installed at various locations as shown in Fig. 4 (b). One sensor was at one third from the top into the core of the specimen (Core top).

One sensor was at one third from the bottom into the core of the specimen (Core bottom). Five sensors were on the outer surface of the specimen (S1, S2, S3, S4, and S5). One sensor was used to measure the ambient temperature.

(3) Two ½ inch thick Styrofoam insulation sheets (Fig. 4) were placed at the top and bottom of the cylindrical specimen and the entire setup was held together using three bar clamps.

(4) The thermocouples were connected to a data logger, which recorded the temperature data of all the eight sensors at two minutes intervals.

(5) To start a test, the heater inserted in a test sample was connected to a voltage regulator, which was connected to a power source. Then, a voltage was gradually applied to the heater, which was measured by a multimeter.

It was noticed that as the applied voltage increased, the temperature in the core of the tested sample also increased. A very high testing temperature may have a significant effect on the concrete microstructure, thus affecting the test results. As a result, an attempt was made to control the core temperature to be around 50°C. Based on previous experiments (Bai 2013; Carlson et al. 2010), the input voltage was set to 21.7 V with an input power of 8.13 W in the present experiments. The testing temperature was recorded from this point. Fig. 4 (c) shows an example of the temperature profiles during the test, where the thermal conductivity was calculated every half an hour until the difference between two adjacent measurements became less than 2%, which was considered as the steady-state. It has been observed in the experiments that it took approximately two and a half hours for a concrete specimen to reach its steady-state.

An important factor in measuring *k* of materials is to establish a one-dimensional heat flow. In the present study, this was achieved by thermally isolating the top and bottom of the cylindrical specimen and using highly conductive paste in the core according to the research conducted by Carlson et al. (2010). Since the thermal conductivity of the Styrofoam insulating sheet (0.02 W/m-K) placed on the top of the tested specimen was significantly lower than that of Omega paste (2.3 W/m-

K) in the hole of the specimen, more heat was transferred horizontally through the specimen. Thus, heat loss could be neglected, and Equation (1) was used for the overall calculation of thermal conductivity.

$$\boldsymbol{k} = \frac{(\boldsymbol{VI})\cdot \boldsymbol{ln}\,(\boldsymbol{r_2}/\boldsymbol{r_1})}{\boldsymbol{2\pi L}\,(\boldsymbol{T_1}-\boldsymbol{T_2})} \quad (1)$$

Where *k* is the thermal conductivity (W/m-K), VI is the power input to the heater (W), r_2 and r_1 are outer and inner radii (m), L is the length of the specimen (m), T_1 is the average temperature in the core of the specimen (K), and T_2 is the average temperature on the surface of the specimen (K). The *k* value calculated using Equation (1) at the steady-state was then taken as the *k* of the tested concrete specimen. A minimum of three specimens was tested for each concrete mix and two separate tests were performed for each specimen. The mean value of six observations was thus considered as the final *k* of that mix.

Experimental Results and Discussion

General Properties of Concrete Mixes

All concrete mixes were tested for their fresh and hardened properties. The measured values of these properties are all presented in Table 4. Slump for most of the mixes were 76.2 ± 25.4 mm (3 ± 1 inch). For mixes containing steel fiber and recycled aggregate, the slump was adjusted using an additional dosage of medium-range water reducer. The air content of most of the mixes was measured to be 5-8%. The air-entrainment was not done in concrete mixes containing recycled aggregate and hence the air contents of such mixes were not measured. Unit weight was measured using a calibrated 0.007 m^3 (0.25 ft^3) cylinder.

Effect of w/b

Four concrete mixes with varying w/b and containing recycled coarse aggregate (Table 3) were prepared to evaluate the effect of w/b ratio on the conductivity of concrete. The measured values of *k* are plotted in Fig. 5. The table inserted in the figure also shows the dry density and the 95% confidence

intervals (CIs) for the measured mean *k* values of all the mixes. The confidence interval here means that there is 95% belief that if the test is performed several times, the mean *k* will lie in the specified interval.

The trend in Fig. 5 shows that with an increase in w/b ratio, there is a linear decrease in the concrete conductivity. This is because increasing w/b made the concrete more porous, which was evident by the reduction in the measured dry density of the concrete samples. The *k* of composite materials like concrete is directly related to dry density. Previous studies have demonstrated that reduction in dry density could cause a corresponding decrease in the conductivity of concrete (ACI (American Concrete Institute) 2002; Ganjian 1990; Gencel et al. 2013; Morabito 1989; Nagy et al. 2015; Tinker and Cabrera 1992; Zhu et al. 2015). Analyzing the measured data and trend, one can deduce that the thermal conductivity of a concrete mix with a 0.30 w/b is estimated to be 1.07 W/m-K with a 95% confidence interval of (1.06, 1.08). For a 0.05 increase in the w/b ratio, the *k* value decreases by 0.074 W/m-K with a 95% confidence interval (CI) of (0.070, 0.078) on average. The proportion of variability in conductivity described by w/b ratio is approximately 96%.

Effect of SCMs

Five different concrete mixes with varying percentages of cement replacement by fly ash and GGBFS were used to analyze the effect of commonly used supplementary cementitious materials (SCMs) on *k* of concrete. Fly ash has been very commonly used in almost all types of concrete mixes these days either co-blended with the Portland cement or separately blended while concrete mixing. In this study, Portland cement in all four mixes (containing SCMs) was replaced with 20% (by weight) of class C fly ash. The measured thermal conductivity values of these concrete mixes are plotted in Fig. 6. The table inserted in the figure presents the 95% CIs for the measured mean *k* values of all the mixes. From the analysis and visualization of measured data, it can be inferred that the thermal conductivity of a concrete mix with no SCM replacement is estimated to be 1.24 W/m-K with a 95% confidence interval of (1.20, 1.28). For a unit increase in the SCM replacement percentage by weight

of cement, the *k* value decreases by 0.003 W/m-K with a 95% CI of (0.002, 0.005) on average. The proportion of variability in conductivity described by percentage SCM replacement is 75%.

From Fig. 6 and the inferences presented above, it is evident that with an increase in the SCM replacement, there is a decrease in the *k* value of concrete. This can be explained by the fact that the *k* values of fly ash and slag pastes are lesser than that of cement paste and also the dry density of concrete mixes decreases with an increase in SCM replacement. As per the regression analysis performed by Choktaweekarn (2009) for developing a thermal conductivity model for concrete, the *k* of cement and fly ash was obtained to be 1.55 and 0.76 W/m-K, respectively. In a similar study on the effect of silica fume on paste conductivity, Fu and Chung (1999) concluded that silica fume was effective in decreasing conductivity of cement paste which can be due to its relatively low conductivity and low density of the paste containing silica fume. The trend of decrease in *k* in this study is also consistent with studies by other researchers (Choktaweekarn 2009; Demirboga and Gul 2003). Although the reduction in *k* value is not very substantial here, it can be significant in the case of concrete mixes containing very high amounts of SCMs.

Effect of Age of Concrete

In this research, the *k* of concrete was measured at curing ages of 3, 7, 14, 28, and 56 days. Since the conductivity measurement method adopted in this study required a dry concrete specimen, it was not possible to measure the *k* of fresh concrete. Fig. 7 presents the measured values of the four mixes (shown in Table 3) at various ages. It is observed from Fig. 7 that the *k* of concrete decreased from 3 to 7 days, then increased from 7 to 28 days and became almost constant after that. The increase in *k* could be explained by the fact that with the increase in the degree of hydration, as hydration products are being formed, the overall porosity of concrete decreases, concrete becomes denser and therefore an increase in *k* occurs. In his study on *k* of paste and mortar, Choktaweekarn (2009) also observed a decrease in *k* after the age of about 3 days and almost negligible change after that, similar to the observations found in this research. However, conflicting arguments are found in literature about

the change in thermal conductivity with the degree of hydration (DOH) and the age of concrete (Breugel 1998; Brown and Javaid 1970; Choktaweekarn 2009; Schindler 2002). Van Breugel (1998) suggested an increase in conductivity with increasing DOH, while Schindler (2002) recommends a linear decrease of k with the DOH from 1.33 times the ultimate k to the ultimate k [$k_c(\alpha) = k_{uc}\,(1.33 - 0.33\alpha)$, where k_c is the concrete thermal conductivity (W/m-K), α is the degree of hydration, and k_{uc} is the ultimate hardened concrete thermal conductivity]. Brown and Javaid (1970) measured k of fresh concrete starting at 6 hours up to 7 days and found a 30% decrease in k from its initial value during this period which remained constant after that. Further study is necessary to find out rational explanations for the effect of age on k of concrete.

Effect of Fiber

Fibers are primarily used in concrete to control cracking due to plastic and drying shrinkage (Mehta and Monteiro 2006; Neville 2011). However, depending on the type, content, geometry, orientation, and density, these also affect other properties of concrete. In this study, two types of fiber (steel and polypropylene) at four different volume fractions: 0.25, 0.5, 1, and 2% were used in concrete mixes as shown in Table 3. As the length-to-diameter ratio of fiber affects the properties of fresh as well as hardened concrete, this ratio was kept the same (l/d = 63.5) for both types of fiber. Fig. 8 shows the change in k of concrete with the addition of fiber. The table inserted in the figure also presents the 95% confidence intervals for the measured mean k values.

In the case of steel fiber, the k of concrete did not change at the fiber volume fraction (VF) of 0.25%. However, the increase in k was observed when VF increased from 0.50% to 2%. This is probably related to the degree of percolation of fiber particles in the matrix. In general, percolation is a physical phenomenon in composite materials in which the highly conducting particles distributed randomly in a matrix form at least one continuous chain connecting the opposing faces of the matrix (Devpura et al. 2001). In fiber-reinforced concrete, it refers to the connectivity of fiber particles in the cement matrix which results in a continuous conductive path (Javier Baeza et al. 2010; Sun et al. 1998).

Formation of such conductive path causes a steep increase in the thermal conductivity of concrete. The fiber volume fraction above which percolation occurs is known as the percolation threshold (Javier Baeza et al. 2010). In this study, the percolation threshold was 0.50% VF of steel fiber above which the degree of percolation increased resulting in a conductive network and a consequent increase in thermal conductivity of concrete.

Statistical analysis of experimental data revealed that the thermal conductivity of a concrete mix with no steel fiber is estimated to be 1.05 W/m-K with a 95% confidence interval of (1.03, 1.08). For a unit percentage increase in the fiber volume fraction, the *k* value increases by 0.065 W/m-K with a 95% CI of (0.05, 0.08) on average. The proportion of variability in conductivity described by steel fiber VF percentage is 83%. On the other hand, PP fiber did not show any substantial effect on the *k* of concrete, mainly because the fiber was not thermally conductive. These experimental observations can be explained by the fact that since the thermal conductivity of steel fiber is very high (approximately 45.0 W/m-K) as compared to other constituents of concrete, its addition increases the overall conductivity of concrete. Whereas the conductivity of polypropylene fiber being low, it does not increase the overall *k* of concrete. It is known that the use of fiber helps improve the post-cracking durability of concrete. However, the effectiveness of fiber depends also on how well-dispersed it is in the concrete. Therefore, in applications where conductive concrete is desired, such as mass concrete and heated pavement systems, the use of steel fiber could be explored.

Effect of Lightweight Aggregate

Use of lightweight aggregate in concrete is beneficial for a variety of reasons such as weight reduction, reduced early-age cracking, reduced permeability, and enhanced durability (ACI (American Concrete Institute) 2003; Cavalline et al. 2017; Newman and Owens 2003). Depending on the type of raw material (clay, shale or slate), and the process of thermal treatment, the porosity and other properties of lightweight aggregate are determined. In this study, expanded shale lightweight aggregates were used and three concrete mixes (shown in Table 3) were designed to analyze their

effect on the conductivity of concrete. These mix options included: (1) a control mix containing all normal weight limestone coarse aggregate (NW100), (2) a mix containing all lightweight expanded shale coarse aggregate (LW100), and (3) another mix containing 50% by volume of both (NW50+LW50). The bulk loose unit weights of limestone and expanded shale coarse aggregates used in the concrete mixes were 1570 kg/m^3 (98 lb/ft^3) and 877 kg/m^3 (54.8 lb/ft^3) respectively. The dry densities of the NW100, LW100, and NW50+LW50 concrete mixes were measured to be 2226 kg/m^3 (139 lb/ft^3), 1626 kg/m^3 (101 lb/ft^3), and 1892 kg/m^3 (118 lb/ft^3) respectively. Fig. 9 shows the change in *k* of concrete with an increase in lightweight aggregate percentage. The table inserted in the figure also presents the 95% confidence intervals for the measured mean *k* values. It is observed that thermal conductivity decreases with increasing content of lightweight aggregate. The conductivity of a concrete mix with no LWA replacement is estimated to be 1.07 W/m-K with a 95% confidence interval of (1.03, 1.12). For a unit percentage increase in the LWA replacement, the *k* value decreases by 0.002 W/m-K with a 95% CI of (0.001, 0.003) on average. The proportion of variability in conductivity described by steel fiber VF percentage is 88%.

The reduction in conductivity is expected since the expanded shale aggregates have a porous structure which is also evident from the reduced dry density of concrete. The air gets trapped in these pores thereby reducing the density, weight, and overall conductivity of concrete. In their study also, Cavalline et al. (2017) observed a strong inverse relationship between thermal conductivity and total void content of lightweight aggregate concrete ($R^2 = 0.875$). It shall be noted that the trend, shown in Fig. 9, is not linear. A reduction of approximately 30% in thermal conductivity is observed from that of NW100 to LW100, which is very significant. This property of lightweight aggregates could be used to enhance the insulation performance of concrete structures (i.e., especially buildings) thereby saving energy and cost.

Effect of Recycled Coarse Aggregate (RCA)

Replacing natural aggregates (NA) with recycled aggregates (RA) from construction and demolition waste (C&D) has many advantages such as the conservation of natural resources, landfill, cost, etc. Many studies have been conducted to evaluate the mechanical properties of concrete containing RA (Ajdukiewicz and Kliszczewicz 2002; Anderson et al. 2009; Dhar et al. 2018; Duan et al. 2013a; Faysal et al. 2019; Gómez-Soberón 2002; Knaack and Kurama 2013; Kou and Poon 2013; Mahedi et al. 2018; Medina et al. 2014; Dos Santos et al. 2004). However, limited data are available on the thermal properties especially thermal conductivity of such concrete (Zhu et al. 2015). Unlike virgin NA, mortar attached with RA is known to affect properties such as shrinkage and creep of recycled aggregate concrete (Kou and Poon 2013; Xiao et al. 2010) and therefore it might also affect the thermal properties. Four concrete mixes, containing normal coarse aggregate replaced by RA at replacement levels of 0, 30, 50, and 100%, were analyzed as part of this study. The details of the mixes are presented in Table 3. The conductivity of mixes was measured and is presented in Fig. 10. The table inserted in the figure shows the 95% confidence intervals for the measured mean *k* values. Similar to the trend observed in the case of lightweight aggregate, the replacement of normal aggregate with recycled aggregate was also found to decrease the conductivity of concrete. The conductivity of a concrete mix with no RCA replacement is estimated to be 1.20 W/m-K with a 95% confidence interval of (1.19, 1.21). For a unit percentage increase in the LWA replacement, the *k* value decreases by 0.0034 W/m-K with a 95% CI of (0.003, 0.004) on average. The proportion of variability in conductivity described by RCA replacement percentage is approximately 94%.

The high absorption (7%) of RA used in this study suggests that the aggregate is more porous than the NA (0.61% absorption). Relatively high porous nature of RA can be attributed to the presence of mortar attached to the aggregate surface which itself is porous and also creates a weaker bond with the new mortar. Therefore, the replacement of NA with RA increased the overall porosity of the concrete, thereby decreasing its density and thermal conductivity. This inference is also supported by

the experimentally measured dry densities of four concrete mixes. The dry densities of concrete mixes with 0, 30, 50, and 100% RCA replacement were measured to be 2279 kg/m^3 (142 lb/ft^3), 2251 kg/m^3 (141 lb/ft^3), 2153 kg/m^3 (134 lb/ft^3), and 2056 kg/m^3 (128 lb/ft^3) respectively. Hence, from the observations of this study, it can be inferred that even though by using recycled aggregates in concrete, the mechanical properties such as strength and elastic modulus are compromised, the thermal insulation potential of such a concrete mix is improved.

Effect of Absorption of Aggregate

Various agencies specify an upper limit on the absorption of aggregates to be used in concrete. At the same time, good quality aggregates (having less absorption) are depleting. This is increasing the need to explore even the use of aggregates having higher absorption values in concrete. This was one of the motivations to study the effect of absorption of aggregates on the thermal conductivity of concrete. To analyze this, five concrete mixes were prepared using limestone and dolomite aggregates with different absorption values. As the effect of absorption was desired, the same volume fractions of constituents of concrete were used for all five mixes. The mixes have been designated based on the type of aggregate and its percentage absorption (Table 3).

The *k* of concrete mixes was measured, the results of which are presented in Table 5. Column 3 in Table 5 shows the mean value of measured *k* and column 4 shows the 95% confidence interval for the mean. From the measured values of conductivity, it is observed that even the absorption of dolomite aggregates used in this research is high, the *k* value of concrete containing dolomite is not lower than that containing limestone. This can be expected as the thermal conductivity of dolomite stone is often higher than that of limestone (Campbell-Allen and Thorne 1963; Neville 2011; Robertson 1988). As far as the effect of absorption of aggregates on *k* of concrete is concerned, for limestone aggregates with absorption value up to 3.5%, no significant change in *k* of concrete is observed. However, for dolomite aggregates, the *k* of concrete reduces by approximately 21% when absorption of dolomite increased from 4.1 to 6.8%. Due to unavailability of dolomite aggregates with higher absorption

values, further tests could not be performed in the present study, and therefore, it would be premature to make a definite statement at this time based on only two observations. Further tests would need to be performed to reach a definitive conclusion.

General Discussion

Various parameters related to concrete were analyzed in this study for their effects on the thermal conductivity of concrete. The parameters included water-binder ratio, SCM replacement, age, PP and steel fiber, and lightweight, recycled, and normal weight absorptive aggregates. Table 6 presents the range of values of these parameters and *k* values of concrete mixes corresponding to them. These values are also plotted in Fig. 11 where the arrows represent the effect (increasing/decreasing) of parameters on conductivity. It can be observed that an increase in w/b, SCM, LWA, and RCA replacement reduced the *k* of concrete while the increase in steel fiber had the opposite effect. Thermal conductivity of concrete changed differently with age, as discussed earlier. It can also be said that amongst all the parameters, the effect of age (on *k*) appeared more pronounced probably because of changing cement hydration characteristics with age.

As dry density and strength are frequently and easily measured properties of concrete, their relationship with thermal conductivity can be a useful tool. The measured *k* values of various concrete mixes, corresponding to all the parameters presented earlier, were plotted against their oven-dry dry densities and 28-day compressive strengths as shown in Fig. 12 (a) and (b), respectively. The trendlines plotted in these figures show the statistical relationships between the dependent variable (*k*) and the independent variable (density and strength). The best-fit relationships to explain the variability in *k* as a function of dry density and compressive strength were found to be exponential and linear, respectively. Thermal conductivity, *k*, was found to increase exponentially with an increase in the dry density of concrete while a linear increase in *k* was observed with an increase in the compressive strength. Using higher-order polynomial functions can furnish a relationship with better performance on statistical evaluation parameters, however, physical justification of these

functions will be difficult. Therefore, linear and exponential relationships were adopted in this study. Considering all data points (70), the coefficient of determination (R^2) values of 0.6116 and 0.6005 were obtained respectively for the best-fit exponential and linear functions. However, the data points corresponding to the effect of w/b seemed outliers for both the functions and their removal from the model increased R^2 values to 0.7905 and 0.7155, respectively (Fig. 12). The reason for these data points being outliers might be the use of recycled coarse aggregate in concrete to analyze the effect of water-binder ratio. Although the obtained R^2 values are relatively low, since the data used for developing the relationships considered a wide range of concrete mixes designed by varying parameters such as water-binder ratio, SCMs, fiber, lightweight, recycled and absorptive aggregates, the presented relationships can be used for prediction of *k* of concrete mixes containing similar materials.

Conclusions

The experimental method employed in this study allows the test to be performed on a frequently used cylindrical concrete specimen with minimal preparation, and therefore it is a convenient test procedure to measure the thermal conductivity of concrete. Specific findings from this research were as follows:

(1) Thermal conductivity of the concrete decreases almost linearly with an increase in w/b.

(2) SCMs replacement for cement reduced the thermal conductivity of concrete, and the reduction is more at the early age (≤ 14 days) than at the later age (after 28 days).

(3) The thermal conductivity of concrete was found to decrease during the initial period of curing, from 3 to 7 days, but increased afterward as curing continued up to 28 days. After 28 days, thermal conductivity of concrete had little change.

(4) Addition of steel fiber (0.25 to 2% volume fraction) in concrete increased its thermal conductivity whereas the addition of PP fiber had little effect on concrete thermal conductivity.

(5) Properties of aggregate have a significant effect on concrete thermal conductivity. The conductivity of concrete reduced by approximately 20% as absorption of dolomite increased from 4.1 to 6.8%. A 100% substitution of normal weight limestone aggregates with expanded shale lightweight aggregates reduced the thermal conductivity of concrete by approximately 30%. Replacing normal coarse aggregate with recycled coarse aggregate also reduced the conductivity of concrete by approximately 33%.

(6) Thermal conductivity of concrete was found to increase exponentially and linearly with an increase in its dry density and compressive strength, respectively.

Acknowledgments

The present study is a part of a research project "Evaluate, Modify, and Adapt the ConcreteWorks Software for Iowa's Use", sponsored by the Iowa Highway Research Board (IHRB). The authors would like to acknowledge the sponsorship.

References

ACI (American Concrete Institute). (2002). "Guide to Thermal Properties of Concrete and Masonry Systems." *ACI 122-02*, Farmington Hills, MI.

ACI (American Concrete Institute). (2003). "ACI 213R-03:Guide for Structural Lightweight-Aggregate Concrete." *ACI 213-03*, Farmington Hills, MI.

ACI (American Concrete Institute). (2006). "Guide to Mass Concrete." *ACI 207-06*, Farmington Hills, MI.

Ajdukiewicz, A., and Kliszczewicz, A. (2002). "Influence of recycled aggregates on mechanical properties of HS/HPC." *Cement and Concrete Composites*, 24, 269–279.

Anderson, K. W., Uhlmeyer, J. S., Russell, M., and 726, W.-R. (2009). "Use of Recycled Concrete Aggregate in PCCP: Literature Search." *Washington DOT*.

Asadi, I., Shafigh, P., Abu Hassan, Z. F. Bin, and Mahyuddin, N. B. (2018). "Thermal conductivity of concrete – A review." *Journal of Building Engineering*, 20, 81–93.

ASTM. (2004). "Standard Test Method for Steady-State Heat Flux Measurements and Thermal Transmission Properties by Means of the Guarded-Hot-Plate Apparatus." *ASTM C177*, West Conshohocken, PA.

ASTM. (2015). "Standard Test Method for Relative Density (Specific Gravity) and Absorption of Coarse Aggregate." *ASTM C127*, West Conshohocken, PA.

ASTM. (2016). “Standard Practice for Making and Curing Concrete Test Specimens in the Laboratory.” *ASTM C192*, West Conshohocken, PA.

ASTM C39. (2016). “Standard Test Method for Compressive Strength of Cylindrical Concrete Specimens.” *ASTM*, West Conshohocken, PA.

Bai, H. (2013). “Validation of cylindrical pavement specimen thermal conductivity protocol.” *Graduate Theses and Dissertations*, 13525.

Breugel, K. Van. (1998). “Prediction of Temperature in Hardening Concrete.” *Prevention of Thermal Cracking in Concrete at Early Ages*, R. Springenschmid, ed., London, 51–74.

Brown, T. D., and Javaid, M. Y. (1970). “The thermal conductivity of fresh concrete.” *Materials and Structures/Materiaux et Constructions*, 3(18), 411–416.

Campbell-Allen, D., and Thorne, C. P. (1963). “The thermal conductivity of concrete.” *Magazine of Concrete Research*, 15(43).

Carlson, J. D., Bhardwaj, R., Phelan, P. E., Kaloush, K. E., and Golden, J. S. (2010). “Determining Thermal Conductivity of Paving Materials Using Cylindrical Sample Geometry.” *Journal of Materials in Civil Engineering*, 22(2), 186–195.

Cavalline, T. L., Castrodale, R. W., Freeman, C., and Wall, J. (2017). “Impact of Lightweight Aggregate on Concrete Thermal Properties.” *ACI Materials Journal*, 114, 945–956.

Choktaweekarn, P. (2009). “A model for predicting thermal conductivity of concrete.” *Magazine of Concrete Research*, 61(4), 271–280.

Demirboga, R., and Gul, R. (2003). “The effects of expanded perlite aggregate, silica fume and fly ash on the thermal conductivity of lightweight concrete.” *Cement and Concrete Research*, 33(5), 723–727.

Devpura, A., Phelan, P. E., and Prasher, R. S. (2001). “Size Effects on the Thermal Conductivity of Polymers Laden with Highly Conductive Filler Particles.” *Microscale Themophysical Engineering*, 5, 177–189.

Dhar, A., Rajasankar, J., and Anandavalli, N. (2018). “A mathematical formulation to find effective bulk and shear moduli of recycled aggregate concrete.” *Construction and Building Materials*, 168, 747–757.

Duan, Z. H., Kou, S. C., and Poon, C. S. (2013). “Prediction of compressive strength of recycled aggregate concrete using artificial neural networks.” *Construction and Building Materials*, 40, 1200–1206.

Faysal, M., Mahedi, M., Aramoon, A., Thian, B., Hossain M, S., Khan M, A., and Khan M, S. (2019). “Determination of the Structural Coefficient of Different Combinations of Cement-Treated/Untreated Recycled Base Materials.” *Geotechnical and Structural Engineering Congress 2016*, Proceedings.

Folliard, K., Schindler, A., and Pesek, P. (2017). "ConcreteWorks V3 Training / User Manual ConcreteWorks Software (P2)."

Fu, X., and Chung, D. D. L. (1999). "Effect of admixtures on thermal and thermomechanical behavior of cement paste." *ACI Materials Journal*, 96(4), 455–461.

Ganjian, E. (1990). "The Relationship between Porosity and Thermal Conductivity of concrete." *PhD Dissertation*, The University of Leeds.

Gencel, O., Koksal, F., Sahin, M., Durgun, M. Y., Hagg Lobland, H. E., and Brostow, W. (2013). "Modeling of thermal conductivity of concrete with vermiculite using by artificial neural networks approaches." *Experimental Heat Transfer: A Jornal of Thermal Energy Generation, Transport, Storage, and Conversion*, 26(4), 360–383.

Gomes, M. G., Flores-Colen, I., Manga, L. M., Soares, A., and de Brito, J. (2017). "The influence of moisture content on the thermal conductivity of external thermal mortars." *Construction and Building Materials*, 135, 279–286.

Gómez-Soberón, J. M. V. (2002). "Porosity of recycled concrete with substitution of recycled concrete aggregate: An experimental study." *Cement and Concrete Research*, 32(8), 1301–1311.

Gui, J., Phelan E., P., Kaloush, K. E., and Golden, J. S. (2007). "Impact of pavement thermophysical properties on surface temperatures." *Journal of Materials in Civil Engineering*, 19(8), 1–6.

Javier Baeza, F., Chung, D. D. L., Zornoza, E., Andión, L. G., and Garcés, P. (2010). "Triple percolation in concrete reinforced with carbon fiber." *ACI Materials Journal*, 107(4), 396–402.

Khan, M. . (2002). "Factors affecting the thermal properties of concrete and applicability of its prediction models." *Building and Environment*, 37(6), 607–614.

Knaack, A., and Kurama, Y. (2013). "Design of Concrete Mixtures with Recycled Concrete Aggregates." *ACI Materials Journal*, 110(5), 483–494.

Kou, S. C., and Poon, C. S. (2013). "Long-term mechanical and durability properties of recycled aggregate concrete prepared with the incorporation of fly ash." *Cement and Concrete Composites*, 37, 12–19.

Mahedi, M., Khan, M. S., Ahmed, A., and Hossain, M. (2018). "Prediction of Strength and Stiffness Properties of Recycled Pavement Base Materials Using Non-Destructive Impact Echo Test." *"International Congress and Exhibition" Sustainaible Civil Infrastructures:Innovative Infrastructure Geotechnology*, 121–136.

Marshall, A. L. (1972). "The Thermal Properties of Concrete." *Build. Sci*, Pergamon Press, 7, 167–174.

Medina, C., Zhu, W., Howind, T., Sánchez De Rojas, M. I., and Frías, M. (2014). "Influence of mixed recycled aggregate on the physical-mechanical properties of recycled concrete." *Journal of Cleaner Production*, 68, 216–225.

Mehta, P. K., and Monteiro, P. J. M. (2006). *Concrete: microstructure, properties, and materials*. *3rd ed.*, McGraw Hill.

Misri, Z., Ibrahim, M. H. W., Awal, A. S. M. A., Desa, S. M., and Ghadzali, N. S. (2018). "Review on factors influencing thermal conductivity of concrete incorporating various type of waste materials." *IOP Conf. Ser.: Earth Environ. Sci*, 140, 12141.

Morabito, P. (1989). "Measurement of the thermal properties of different concretes." *High Temperatures-High Pressures*, 21(1), 51–59.

Nagy, B., Nehme, S. G., and Szagri, D. (2015). "Thermal properties and modeling of fiber reinforced concretes." *Energy Procedia*, 78, 2742–2747.

Neville, A. . (2011). *Properties of Concrete*. Pearson, Essex.

Newman, J., and Owens, P. (2003). "Properties of lightweight concrete." *Advanced Concrete Technology*.

Robertson, E. C. (1988). *United States Department of the Interior Geological Survey:Thermal Properties of Rocks*.

Dos Santos, J. R., Branco, F., and De Brito, J. (2004). "Mechanical properties of concrete with coarse recycled aggregates." *Structural Engineering International: Journal of the International Association for Bridge and Structural Engineering (IABSE)*.

Schindler, A. K. (2002). "Concrete Hydration, Temperature Development, and Setting at Early-Ages." *PhD Dissertation*, The University of Texas at Austin.

Sun, M., Li, Z., Mao, Q., and Shen, D. (1998). "Thermoelectric Percolation Phenomena in Carbon Fiber-reinforced Concrete." *Cement and Concrete Research*, 28(12), 1702–1712.

Tinker, L., and Cabrera, J. G. (1992). "Modeling the Thermal Conductivity of Concrete Based on Its Measured Density and Porosity." *Buildings V. Conference Proceedings*, 91–95.

Valore, R. C. (1980). "Calculation of U-values of Hollow Concrete Masonary." *Concrete International*, 2(2), 40–63.

Xiao, J., Liu, Q., and Tam, V. W. Y. (2010). "Numerical Simulation of Damage and Failure of Recycled Aggregate Concrete with a Lattice Model." *Key Engineering Materials*, 417–418, 689–692.

Zhu, L., Dai, J., Bai, G., and Zhang, F. (2015). "Study on thermal properties of recycled aggregate concrete and recycled concrete blocks." *Construction and Building Materials*, 94, 620–628.

Figures

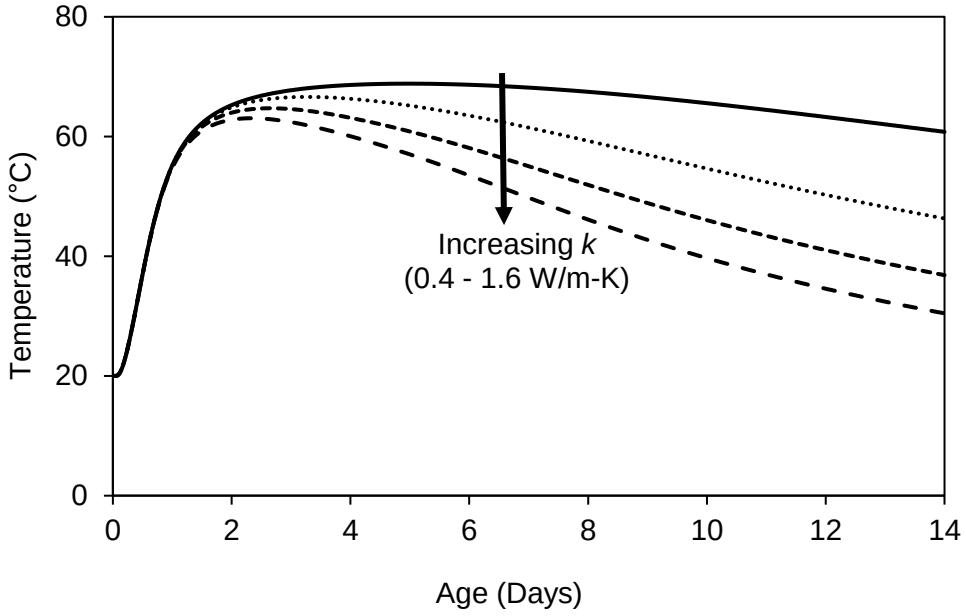

Fig. 1. Effect of *k* on temperature development in a mass concrete member

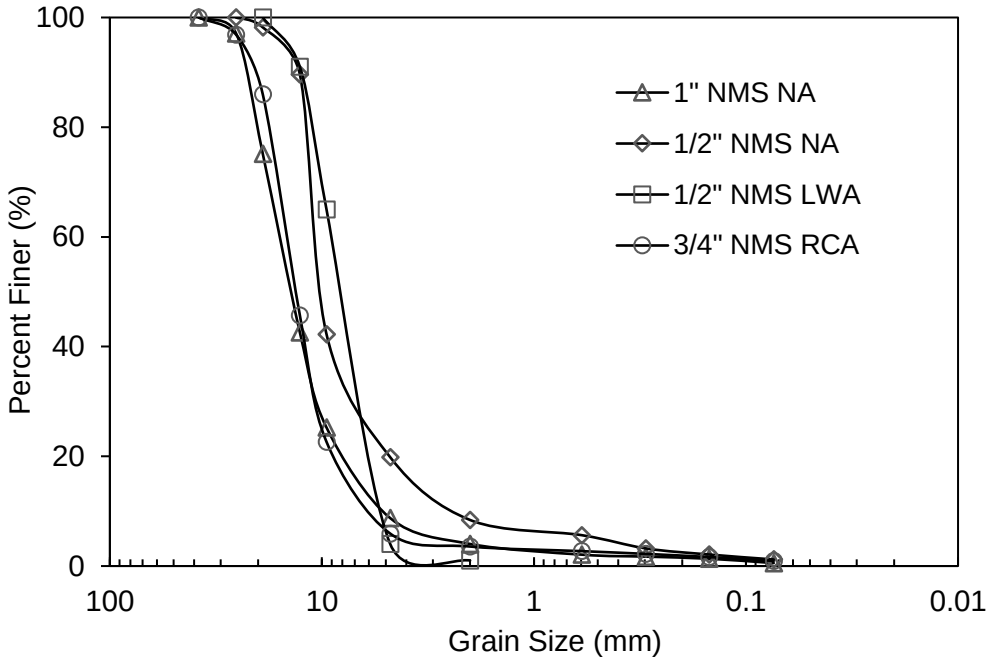

Fig. 2. Gradations of coarse aggregates used

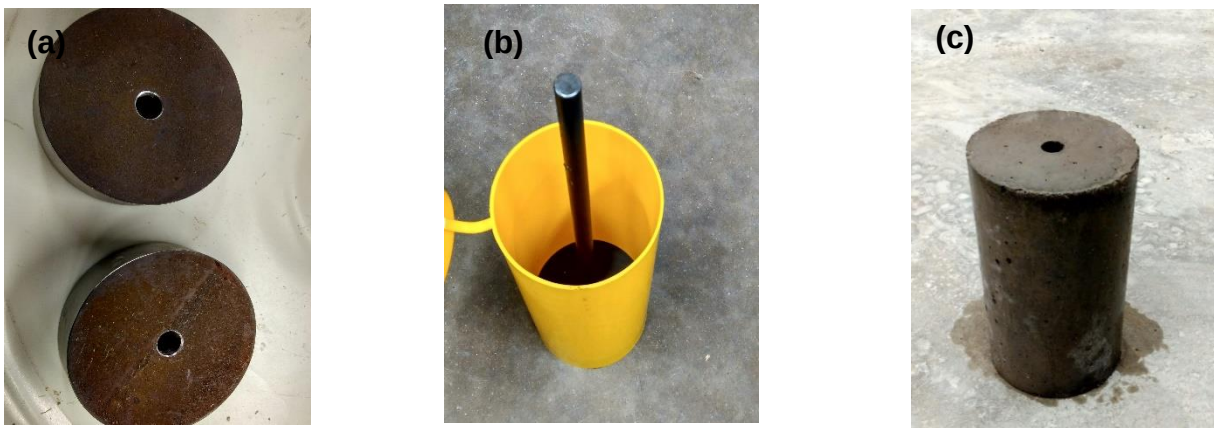

Fig. 3. Sample preparation for conductivity experiment: (a) 1" thick iron disks; (b) 0.5" diameter rod holding disks together; (c) sample after demoulding

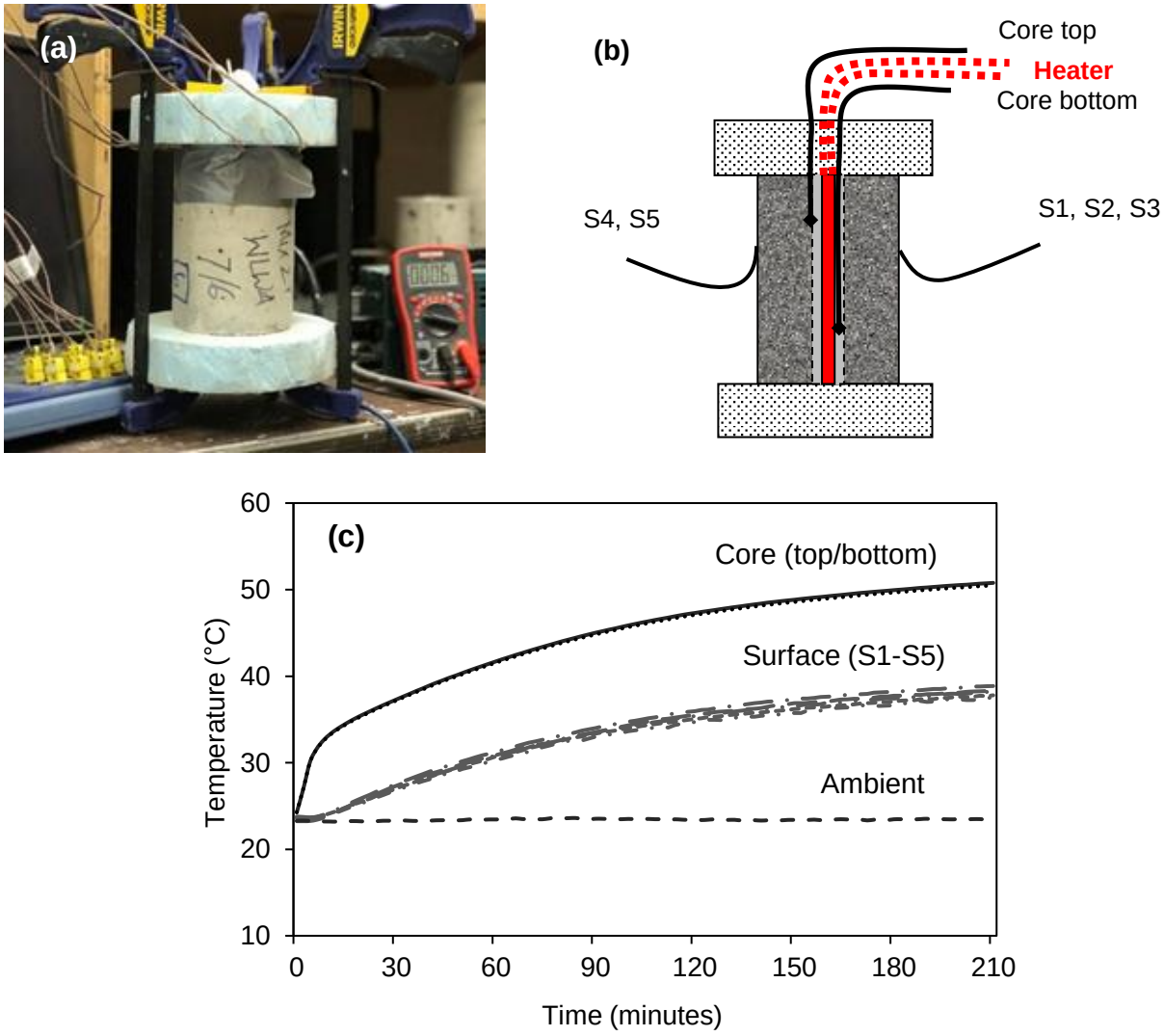

Fig. 4. Thermal conductivity test setup and typical test results
(a) test setup, (b) sensor locations, and (c) typical test results

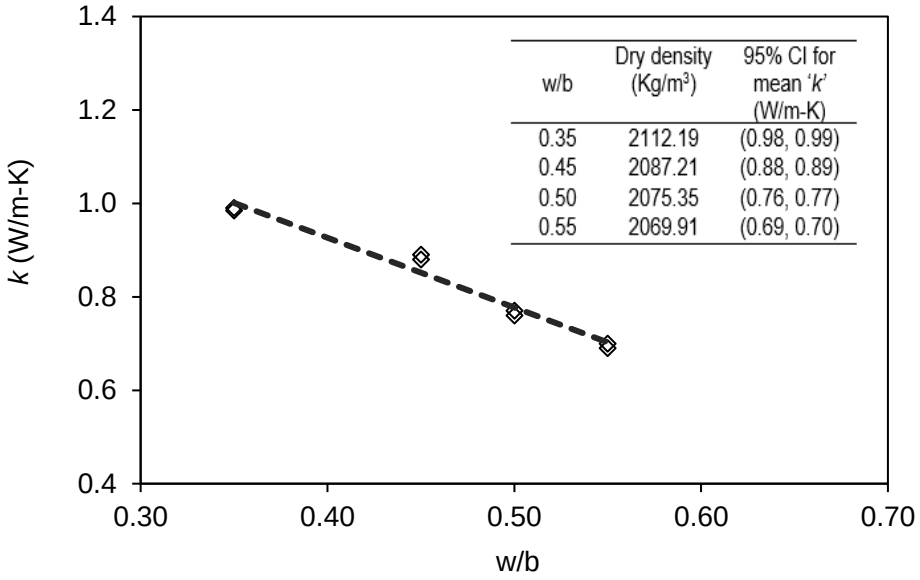

Fig. 5. Effect of water-binder ratio on *k* of concrete

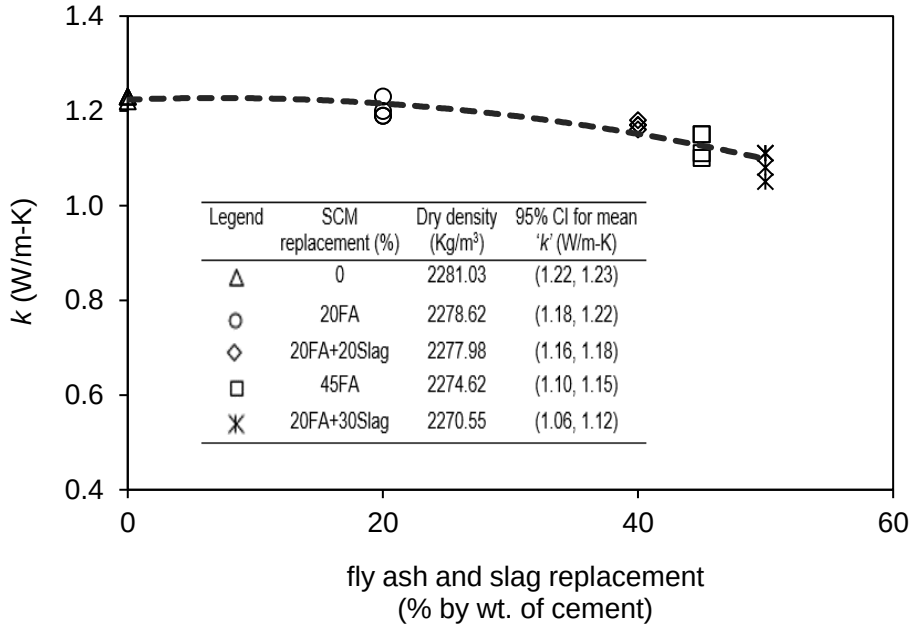

Fig. 6. Effect of SCMs on *k* of concrete

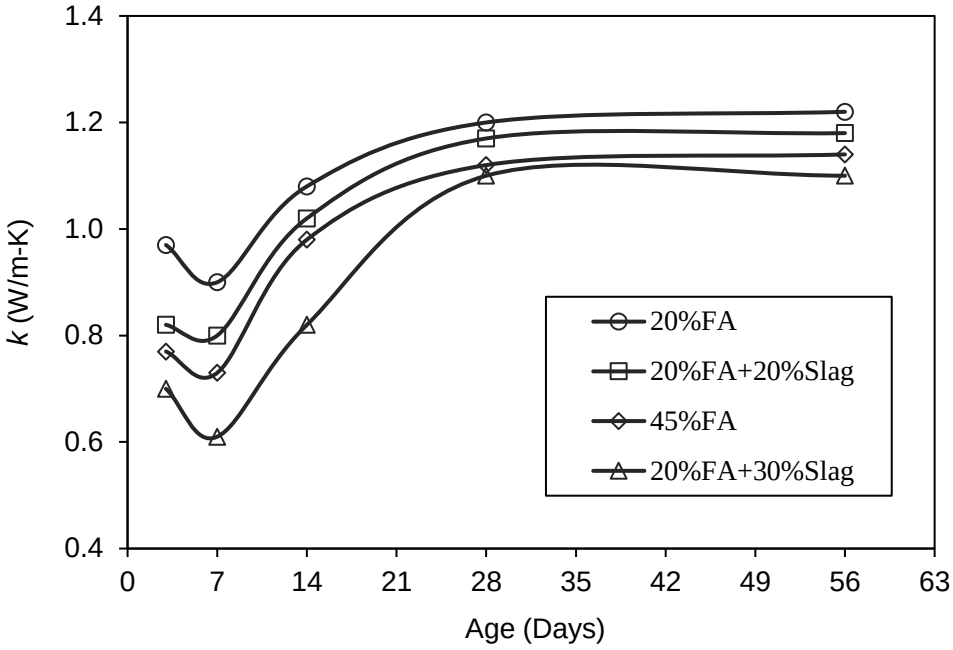

Fig. 7. Effect of age on *k* of concrete

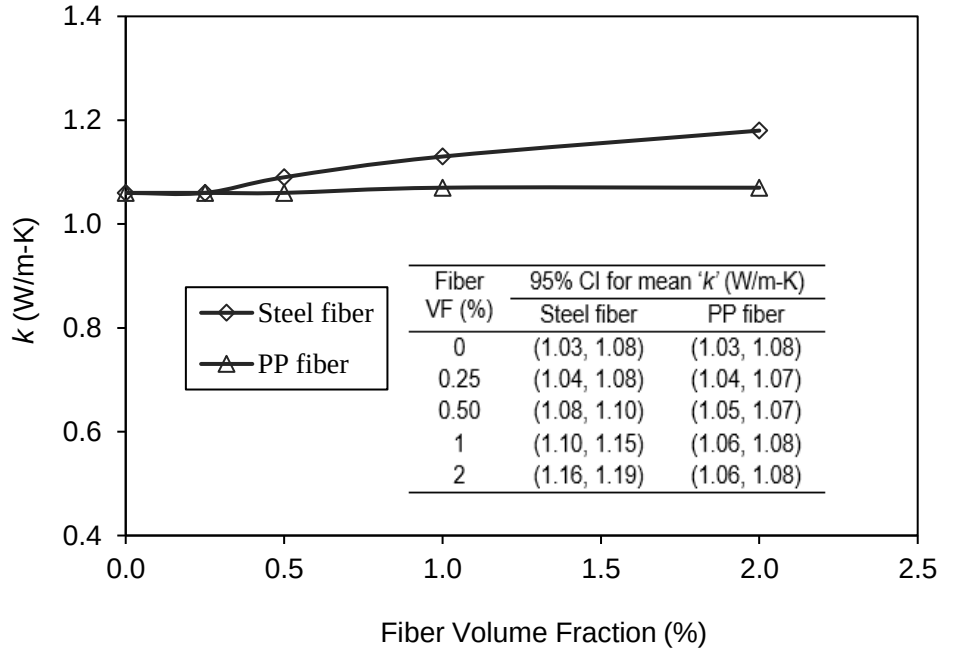

Fiber VF (%)	95% CI for mean '*k*' (W/m-K)	
	Steel fiber	PP fiber
0	(1.03, 1.08)	(1.03, 1.08)
0.25	(1.04, 1.08)	(1.04, 1.07)
0.50	(1.08, 1.10)	(1.05, 1.07)
1	(1.10, 1.15)	(1.06, 1.08)
2	(1.16, 1.19)	(1.06, 1.08)

Fig. 8. Effect of fiber on *k* of concrete

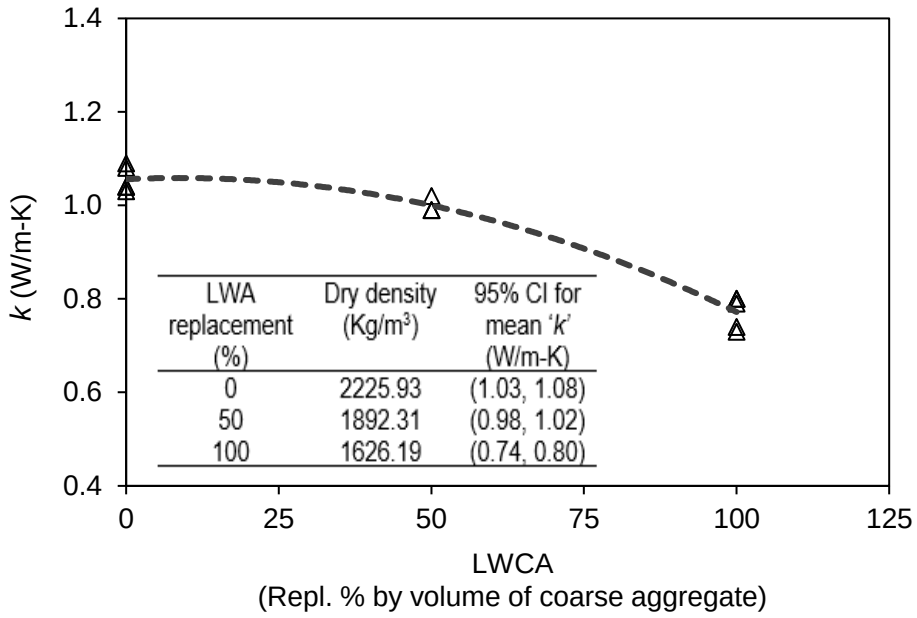

Fig. 9. Effect of lightweight aggregate on *k* of concrete

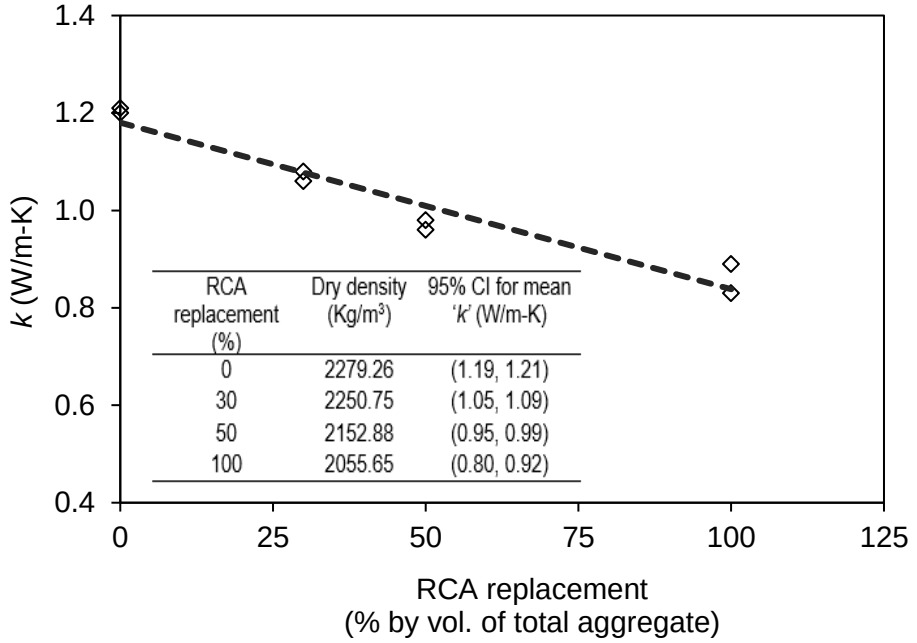

Fig. 10. Effect of recycled aggregate on *k* of concrete

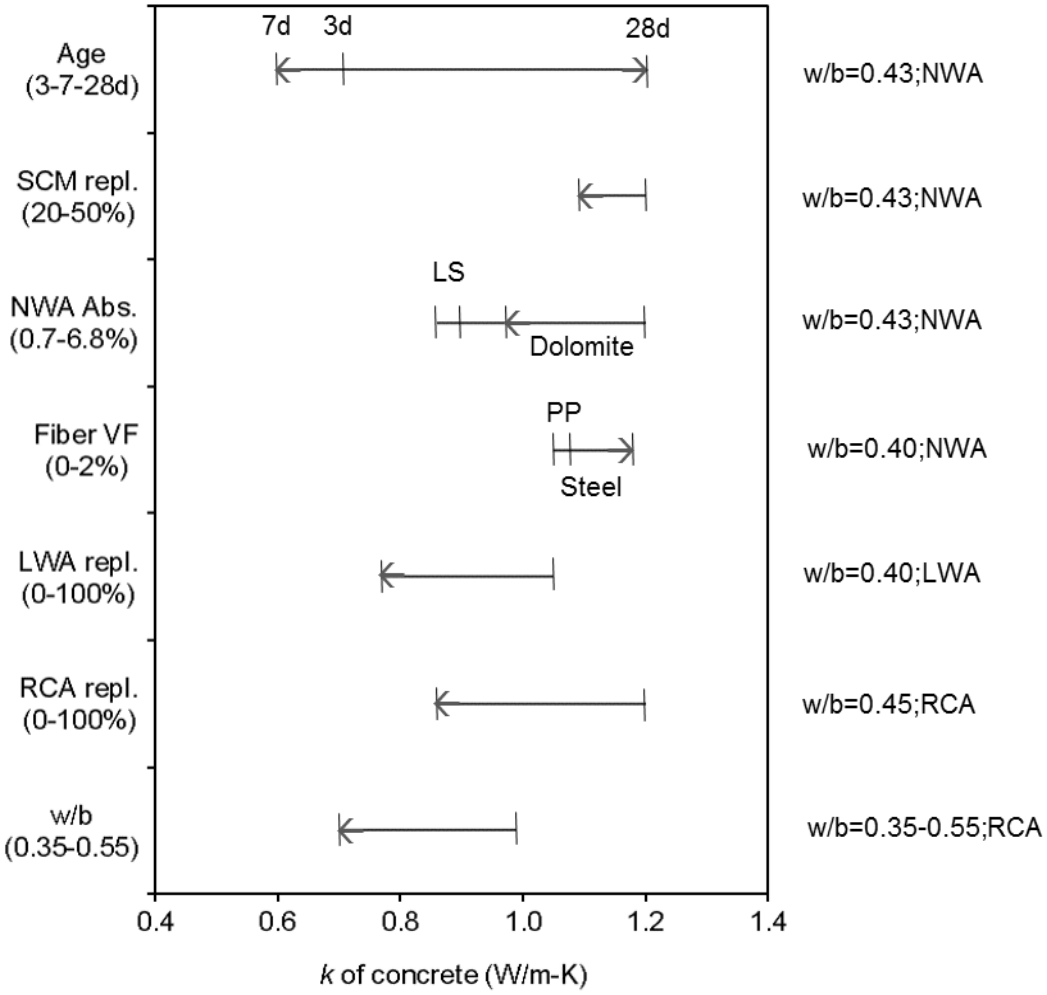

Fig. 11. Effect of all paramaters on conductivity of concrete

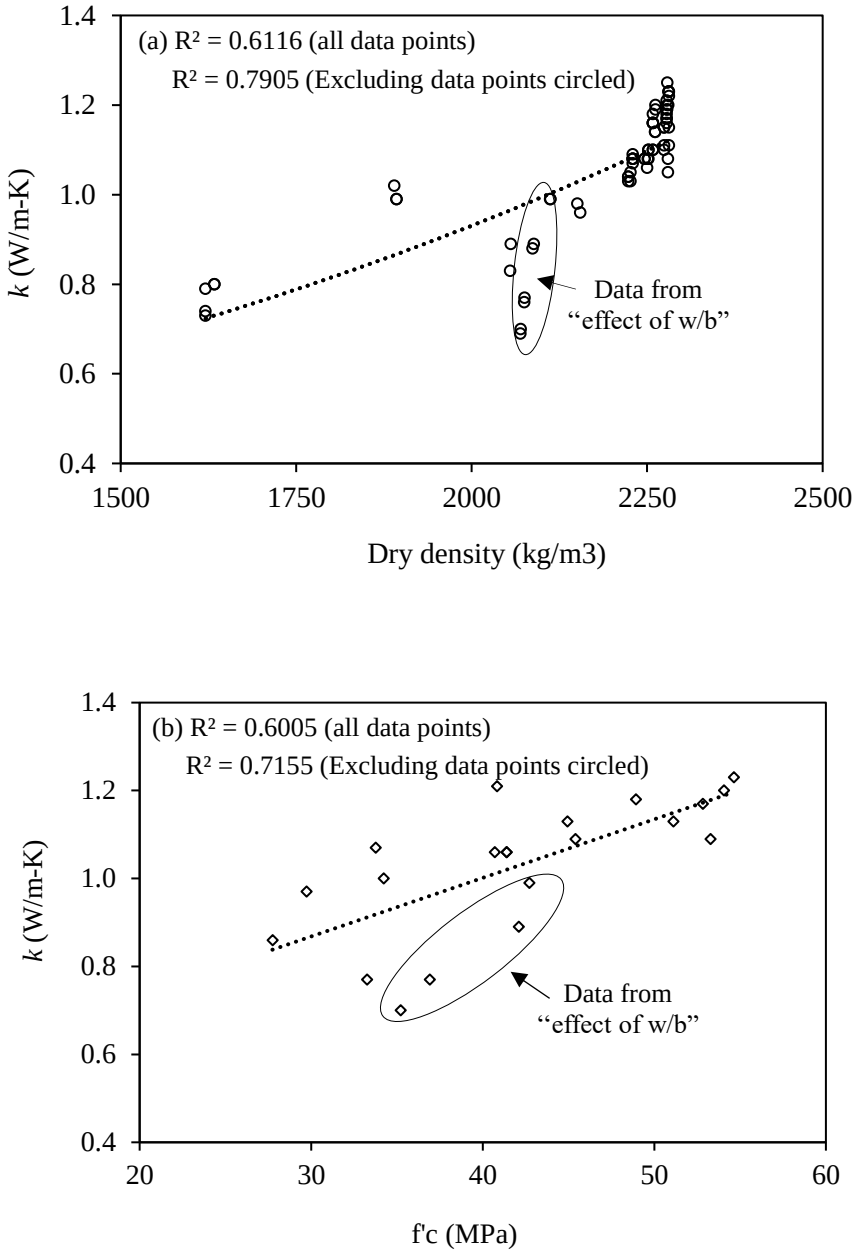

Fig. 12. Thermal conductivity relationships

(a) with dry density and (b) with compressive strength

Tables

Table 1. Chemical Composition, Blaine, and Specific Gravity of Tested Cementitious Materials

Oxide (%)	Cementitious material				
	I/II	IP (25)	IS (20)	C Fly ash	GGBFS
SiO_2	20.05	31.00	23.27	36.09	38.8
Al_2O_3	4.34	8.72	5.47	18.83	7.91
Fe_2O_3	3.05	3.92	2.76	5.85	0.49
CaO	63.18	46.2	59.44	25.85	38.37
MgO	2.24	2.68	3.80	5.76	10.64
SO_3	3.18	3.33	3.15	1.58	2.54
Na_2O	0.09	0.24	0.12	1.78	-
K_2O	0.68	0.84	0.62	0.48	0.43
Others	0.85	0.62	0.80	3.44	0.82
LOI	2.55	2.20	0.56	0.34	-
Blaine (m^2/kg)	376	503	389	483	597
Specific gravity	3.14	2.99	3.08	2.62	2.89

Table 2. Properties of Coarse Aggregates used

Type of aggregate	Nominal maximum size (in.)	SSD specific gravity	Absorption (%)
Normal weight	1	2.64	0.61
Normal weight	1/2	2.63	1.13
Lightweight	1/2	1.15	25.00
Recycled Concrete	3/4	2.12	7.06

Table 3. Concrete Mix Proportions by Volume Fraction of Constituents

Desired Effect of	Mix Designation	Water-binder ratio	Volume Fraction (%)							Particulars
			Water	Cement	Fly Ash	GGBFS	Coarse Aggregate	Fine Aggregate	Fiber	
	w/b-0.35	0.35	12	11	0	0	46	31	0	
Water-binder	w/b-0.45	0.45	16	11	0	0	44	29	0	Recycled coarse aggregate
	w/b-0.50	0.50	17	11	0	0	43	29	0	
Ratio	w/b-0.55	0.55	19	11	0	0	42	28	0	
	Control-SCM	0.43	15	12	0	0	34	34	0	
	20%FA	0.43	15	9	3	0	34	34	0	
SCMs and	45%FA	0.43	15	7	5	0	34	34	0	
Age	20%FA+20%Slag	0.43	15	7	3	2	34	34	0	
	20%FA+30%Slag	0.43	15	5	3	4	34	34	0	
	F0.00 (Control)	0.40	15.7	10	3	0	32	32	0	
	F0.25	0.40	15.7	10	3	0	32	32	0.25	
Fiber	F0.50	0.40	15.7	10	3	0	32	32	0.50	
	F1.00	0.40	15.7	10	3	0	32	32	1.00	
	F2.00	0.40	15.7	10	3	0	32	32	2.00	
	NW100	0.40	15.7	10	3	0	32	32	0	
Lightweight	LW100	0.40	15.7	10	3	0	32	32	0	
Aggregate	LW50+NW50	0.40	15.7	10	3	0	32*	32	0	*16%NW+16%LW
	RA0	0.45	16	11	0	0	36.5	36.5	0	
Recycled	RA30	0.45	16	11	0	0	36.5**	36.5	0	**25.5%NA+11%RA
Aggregate	RA50	0.45	16	11	0	0	36.5***	36.5	0	***18.25%NA+18.25%RA
	RA100	0.45	16	11	0	0	36.5	36.5	0	
	L0.7	0.43	15	9	3	0	34	34	0	
Absorption	L2.9	0.43	15	9	3	0	34	34	0	L: Limestone
of	L3.5	0.43	15	9	3	0	34	34	0	D: Dolomite
Aggregate	D4.1	0.43	15	9	3	0	34	34	0	
	D6.8	0.43	15	9	3	0	34	34	0	

Table 4. Fresh and Hardened Properties of Concrete Mixes

Mix Designation	Slump, mm (in.)	Air content (%)	Unit weight, kg/m^3 (lbs./ft^3)	28-day f'_c, MPa (psi)
w/b-0.35	38.1 (1.5)		2209 (137.8)	43 (6193)
w/b-0.45	50.8 (2.0)	NA	2183 (136.3)	42 (6106)
w/b-0.50	50.8 (2.0)		2198 (137.2)	37 (5352)
w/b-0.55	88.9 (3.5)		2204 (137.6)	35 (5105)
Control-SCM	50.8 (2)	5.5	2377 (148.4)	55 (7922)
20%FA	76.2 (3)	5.5	2359 (147.2)	54 (7839)
45%FA	63.5 (2.5)	6.0	2358 (147.2)	53 (7662)
20%FA+20%Slag	63.5 (2.5)	6.0	2345 (146.3)	51 (7411)
20%FA+30%Slag	63.5 (2.5)	6.5	2347 (146.5)	53 (7726)
Control-F	76.2 (3.0)	6.0	2319 (144.8)	41 (6002)
F0.25	44.4 (1.75)	6.8	2323 (145.0)	41 (5903)
F0.50	44.4 (1.75)	6.0	2316 (144.6)	45 (6584)
F1.00	38.1 (1.5)	7.2	2342 (146.2)	45 (6515)
F2.00	38.1 (1.5)	7.5	2352 (146.8)	49 (7095)
NW100	76.2 (3.0)	6.0	2319 (144.8)	41 (6002)
LW100	127 (5.0)	7.7	1573 (98.2)	33 (4822)
LW50+NW50	88.9 (3.5)	6.6	1690 (105.5)	34 (4964)
RA0	50.8 (2.0)		2393 (149.4)	41 (5921)
RA30	38.1 (1.5)	NA	2355 (147.0)	34 (4894)
RA50	38.1 (1.5)		2285 (142.6)	30 (4311)
RA100	38.1 (1.5)		2168 (135.3)	28 (4023)
L0.7	88.9 (3.5)	6.5	2380 (148.6)	41 (5963)
L2.9	88.9 (3.5)	7.2	2371 (148.0)	42 (6133)
L3.5	101.6 (4.0)	7.0	2331 (145.5)	44 (6403)
D4.1	88.9 (3.5)	7.2	2339 (146.0)	43 (6270)
D6.8	101.6 (4.0)	7.5	2342 (146.2)	40 (5810)

Note: NA indicates that the property was not measured.

Table 5. Conductivity of Concrete Containing Aggregates with Different Absorption

Type of aggregate	Absorption (%)	Measured mean 'k' (W/m-K)	95% CI for mean 'k' (W/m-K)
Limestone	0.7	0.86	(0.83,0.89)
	2.9	0.88	(0.82,0.94)
	3.5	0.87	(0.84,0.90)
Dolomite	4.1	1.20	(1.14,1.26)
	6.8	0.94	(0.92,0.96)

Table 6. Studied Parameters and Obtained *k* Values

Parameter	Unit	Range of parameter values	Range of concrete *k* (W/m-K)
Age	Day	3 – 7 - 28	0.70 – 0.60 - 1.20
SCM	Repl. %	0 - 50	1.23 - 1.09
NWA	Abs. %	0.7 - 4.1 - 6.8	0.86 – 1.20 – 0.94
Steel fiber	Vol. fraction	0 - 2	1.05 - 1.18
PP fiber	Vol. fraction	0 - 2	1.05 - 1.07
LWA	Repl. %	0 - 100	1.05 - 0.77
RCA	Repl. %	0 - 100	1.20 - 0.86
w/b	Ratio	0.35 - 0.55	0.99 - 0.70

CHAPTER 4. PREDICTING THERMAL CONDUCTIVITY OF CONCRETE USING MACHINE LEARNING ALGORITHMS

Modified from a manuscript submitted to *ACI Materials Journal*

Yogiraj Sargam[1], Kejin Wang[2], In Ho Cho[3]

Abstract

Thermal conductivity, *k*, is an important property of concrete and it influences the design and energy-efficiency of many concrete-based structures. Due to the requirement of sophisticated test procedures, experimental measurement of *k* of concrete for every such structure is impractical. In this context, a model for prediction of *k* is demanded. For this purpose, 217 data points of *k* measurements were collected, and nine machine learning (ML) algorithms of function, tree, and ensemble-learning based categories were evaluated in this study. The database for training these algorithms was developed from published articles. Manual, Naïve, and fractional hot-deck imputation (FHDI) methods for curing missing values were applied and compared. Various feature selection tools, such as the mean decrease in impurity (MDI) and principal component analysis (PCA), were evaluated, and the results revealed that the mineralogy of coarse and fine aggregate and the dry density of concrete are the two most influential parameters of concrete thermal conductivity. Out of the nine ML algorithms, the predictive performance of artificial neural network (ANN) was the best. The hyperparameters of ANN were further tuned to optimize the

[1] Graduate Research Assistant; Iowa State University; Department of Civil, Construction, and Environmental Engineering; 813 Bissell Road , Ames, IA, USA, 50011; email: ysargam@iastate.edu
[2] Professor (corresponding author); Iowa State University; Department of Civil, Construction, and Environmental Engineering; 813 Bissell Road , Ames, IA, USA, 50011; email: kejinw@iastate.edu
[3] Assistant Professor; Iowa State University; Department of Civil, Construction, and Environmental Engineering; 813 Bissell Road , Ames, IA, USA, 50011; email: icho@iastate.edu

prediction accuracy, and a 14-6-1 ANN architecture was developed. Combining the performance on training and test dataset, a good match in the actual and ANN model predicted values of thermal conductivity was obtained with R^2 of 0.9079 and MSE of 0.0027. The model also performed reasonably well on an independent test set developed from laboratory-measured thermal conductivity of 18 concrete mixes. Overall, the ANN model was found to be robust in its predictions of thermal conductivity of concrete and is proposed to be an adequate ML tool for this purpose.

Keywords: Concrete – Thermal Conductivity – Missing Data – Machine Learning – ANN

Introduction

Thermal conductivity, *k*, is one of the important thermal properties of concrete that governs heat transfer. It is defined as the constant of proportionality between the heat flux and temperature gradient. The factors affecting the thermal conductivity of concrete include mineralogical characteristics of aggregate, the weight of constituents, and the density, moisture, and age of concrete (Breugel 1998; Campbell-Allen and Thorne 1963; Khan 2002; Marshall 1972; Schindler 2002). Since approximately 50-70% volume of concrete is often occupied by aggregates, the mineralogy and volume of aggregates in a concrete mix have the most influence on its conductivity. The dry density of concrete also shows a dominant effect on *k*. A direct relationship between dry density and *k* of concrete has been suggested by many researchers, while some have shown an exponential relationship (ACI (American Concrete Institute) 2002; Tinker and Cabrera 1992; Valore 1980).

A wide range of *k* values of concrete can be found in literature largely because different researchers might have used different test methods and materials. Lee et al. (2012) and Cavalline et al. (2017) presented a summary of published *k* values ranging from 0.7 to 2.6 W/m-K. Default

k values used in the various design and temperature prediction software are also different. For example, AASHTOware PaveME (AASHTO 2013) has a default global value of 2.16 W/m-K for concrete pavements. On the other hand, the adiabatic temperature rise prediction computer program, ConcreteWorks (Folliard et al. 2017), uses a default value of 2.7 W/m-K. Based on dry density, several publications suggested *k* values for concrete used in various engineering applications. A few mathematical (Campbell-Allen and Thorne 1963) and Artificial Neural Network (ANN) (Lee et al. 2012) models have also been developed for predicting *k* of concrete. However, the set of data used by Lee et al. (2012) to train the ANN model was taken from previous studies by other researchers who did not use many materials used in concrete nowadays such as slag, lightweight aggregates, fibers, and others. That is, many published prediction models are not updated to modern concrete materials, which often contain various supplementary cementitious materials (SCMs), different types of aggregates, and additives (e. g., fibers).

Depending on the application, concrete with a low or high *k* value can be desired in various structures such as floors with embedded heaters, large foundations, dams, and others (Gui et al. 2007; Sargam et al. 2018; Schindler 2002). The *k* value of concrete is often required for the prediction of heat development in mass concrete structures, such as foundations and pavements. It has been shown in the literature that increasing *k* value can reduce the probability of early-age thermal cracking in a mass concrete element (Poole et al. 2006; Riding et al. 2013; Sargam et al. 2019). An accurate prediction of *k* in such cases becomes important in order to minimize the cracking and to improve the durability and serviceability of the structure.

In light of the above discussions, it can be said that there is a need to develop a prediction model for thermal conductivity of modern concrete. In recent years, the use of machine learning (ML) for predictive analytics has grown in many fields including civil engineering. ML techniques

have been used in many applications of concrete such as structural health monitoring and damage detection (Farrar and Worden 2013; Neves et al. 2017; William et al. 2015; Worden and Manson 2007), predictions of compressive strength (Atici 2011; Chithra et al. 2016; Chou et al. 2011; Deshpande et al. 2014; Duan et al. 2013b; Naderpour et al. 2018; Omran et al. 2016; Trocoli et al. 2013; Young et al. 2019), elastic modulus (Sadati et al. 2019), carbonation depth (Zewdu Taffese et al. 2015), chloride resistance (Marks et al. 2015), and durability assessment (Taffese and Sistonen 2017). The use of ML, however, has been limited for predictions of thermal properties of concrete. In this study, a database of *k* values was developed from published articles and various ML algorithms were evaluated for their *k* prediction performances. Different sets of input variables and tuning of hyperparameters of ML algorithms were tried to optimize the prediction accuracy. A robust ANN model was developed using the database, and the model was also validated on an independent/unseen test set.

In this article, a general outflow of various machine learning algorithms evaluated in this study is presented first. The development of databases for training and independent testing of algorithms is then discussed. A step-by-step procedure of the development of thermal conductivity prediction model is summarized thereafter. Next, the performance of various algorithms on different parameters is compared and the development of the best performing model by tuning of hyperparameters is presented.

Machine Learning Algorithms

Machine learning (ML) algorithms provide techniques to recognize patterns in a dataset and make predictions based on them. Their popularity in various fields is featured to the fact that even without a deep understanding of the algorithms, performance-based predictive models can be developed from empirical data (Kuhn and Johnson 2013; Young et al. 2019). ML is categorized

as supervised, unsupervised, semi-supervised, and reinforcement learning. Supervised and unsupervised learning are the most widely used types of ML techniques in many fields of application (Murphy 2018). The goal of a supervised learning algorithm is to achieve low bias and low variance errors. This algorithm works on a database that has input instances as well as the desired outputs and the learning is supervised by a "teacher" (Kuhn and Johnson 2013). On the other hand, the outputs are not available in the unsupervised algorithm. It devises and presents the patterns in the data on its own (Taffese and Sistonen 2017). In this study, supervised learning algorithms were evaluated and WEKA (Waikato Environment for Knowledge Analysis) computer program (Frank et al. 2016) was used for this purpose. The thermal conductivity value to be predicted was numerical and therefore only regression algorithms were considered. Three broad categories of regression algorithms, based on function, tree, and ensemble-learning, were evaluated. A brief overview of these categories of algorithms is presented in the following sub-sections.

Function-based

Function-based algorithms evaluated in this study were linear, Gaussian process, and nonlinear regression. Nonlinear regression algorithms consisted of ANN and support vector regression.

In simple terms, linear regression is a model that assumes a linear relationship between the response and explanatory variables. The general form of a multiple linear regression model is as follows [Eq. (1)]:

$$y = \beta_0 + \beta_1 x_1 + \beta_2 x_2 + \cdots + \beta_n x_n + \epsilon,\ \epsilon \sim N(0, \sigma^2) \quad (1)$$

Where y is a response/dependent variable, x's are explanatory/independent variables, β's are coefficients/unknown parameters, and ε is the error. The explanatory variables in the model can also have higher-order terms and/or interaction amongst them. The model optimizes the values of coefficients such that the sum of the squared errors (SSE) is minimized. A linear regression model makes several assumptions such as the normal distribution, constant variance, and independence of errors, linear relationship between the expected response and the explanatory variables and others. The acceptance of a model can only be valid if the assumptions hold true. Although the linear regression models are simple in interpretation and implementation, they furnish poor predictions if the relationship between response and explanatory variables cannot be approximated by a linear function (Rasmussen and Williams 2006). Unlike a linear regression model where the error variance and coefficients are estimated from the data, a Gaussian process regression (GPR) model explains the response by introducing latent variables from a Gaussian process and explicit basis functions. A Gaussian process is a collection of random variables, any finite number of which have a joint Gaussian distribution (Rasmussen and Williams 2006). More details about the GPR model can be found elsewhere (Dattagupta 2013; MacKay 1998; Omran et al. 2016; Rasmussen and Williams 2006; Seeger 2004; Witten et al. 2016).

ANN is a non-linear computing algorithm inspired by the structure and functioning of a biological neural network (Dasgupta et al. 2018; Grossi and Buscema 2007; Jain et al. 1996; Tino et al. 2015). An ANN model develops an input-output relationship via a series of connected neurons (I. et al. 2019a; b; Kuhn and Johnson 2013). A typical ANN is composed of three building blocks: (1) input neurons representing explanatory variables; (2) output neurons representing response variable(s); and (3) hidden layer(s) that connects the input and output neurons and also represents the connection weights. Schematic of a typical ANN architecture can be found in many

published resources (Chou et al. 2011; Dasgupta et al. 2018; Grossi and Buscema 2007; Jain et al. 1996; Tino et al. 2015; Young et al. 2019). Each neuron in an ANN architecture consists of inputs, weights, transfer/activation function, and output. Weight determines the influence of a feature on the output. The mathematical relationship between the input variables and each neuron in the hidden layer is commonly expressed as shown in Eq. (2) (John Lu 2010; Young et al. 2019).

$$h_i = \sigma\,(w_i^T x) \tag{2}$$

Where, $x = [x_1, x_2, \ldots, x_n]^T$ is the vector of n input variables (features), $w_i = [w_{i,1}, w_{i,2}, \ldots\ldots, w_{i,n}]^T$ are the weights for each feature, and σ is an activation function. A range of activation functions such as linear, sigmoid, hyperbolic tangent sigmoid and others, are used. The sigmoid function is the most commonly used in regression problems and since this study dealt with the prediction of the numerical value of thermal conductivity, the sigmoid function was used. The general form of the function is as presented in Eq. (3) (John Lu 2010; Young et al. 2019). The neurons in the output layer are also related to those in the hidden layer through a linear function.

$$\sigma\,(w_i^T x) = \frac{1}{1+e^{w_i^T x}} \tag{3}$$

Another major step involved in an ANN architecture is the training of the network which is done using algorithms that adjust the connection weights and minimizes the prediction error. Some of the commonly used training algorithms in ANN are Levenberg-Marquardt, gradient descent, gradient descent with momentum, gradient descent momentum and adaptive learning rate, and gradient descent with adaptive learning rate (Brownlee 2016). The parameters of an ANN architecture should be well-optimized to avoid overfitting as architectures that have a large number of hidden layers and/or hidden neurons in each layer are prone to over-fitting.

Support Vector Regression (SVR) is based on a kernel trick, that implicitly creates a high-dimensional feature space and models linear relationships in this space (Cristianini and Shawe-Taylor 2000; Witten et al. 2016). A kernel defines the similarity or distance between new data and the support vectors. The models are produced in terms of a few support vectors. Unlike linear regression that finds parameter estimates by minimizing SSE, SVR uses ε loss function (ε-insensitive function) that seeks to minimize the effect of outliers on the regression equations (Cristianini and Shawe-Taylor 2000; Kuhn and Johnson 2013). A cost parameter is introduced that penalizes large residuals and is set by the user. SVR aims to find a line of best fit that minimizes the error of the cost parameter. The SVR coefficients minimize the expression shown in Eq. (4) (Kuhn and Johnson 2013).

$$Cost \ \sum_{i=1}^{n} L_{\epsilon} \left(y_i - \hat{y}_i\right) + \ \sum_{j=1}^{P} \beta_j^2 \tag{4}$$

Where 'n' is the number of data points, 'P' is the number of features, y_i is the i^{th} observed value of the outcome (i = 1….n), $\hat{y}_i$ is the predicted outcome of the i^{th} data point (i = 1….n), β is the model coefficient, Lε (.) is the ε loss function and *Cost* is the parameter that penalizes large residuals. More detailed information on SVR can be found in the literature (Chou et al. 2011; Chou and Tsai 2012; Cristianini and Shawe-Taylor 2000; Kuhn and Johnson 2013; Omran et al. 2016; Witten et al. 2016).

Tree-based

Random forest, random tree, and reduced error pruning (REP) tree were tree-based algorithms evaluated on the dataset. Unlike function-based algorithms that use mathematical functions or relationships to identify the pattern in the dataset and develop prediction models, tree-based algorithms perform this task through a "divide-and-conquer" approach (Witten et al. 2016).

The tree identifies splits in the data and uses a simple function to develop a prediction model. Classification and Regression tree (CART) is one of the most commonly used methodologies for constructing regression trees (Breiman et al. 1984). Starting with the entire training dataset, CART algorithm searches every distinct value of every predictor to find the split value that divides the data into two groups thereby minimizing the overall SSE and developing a final random tree (Kuhn and Johnson 2013). Random forest constructs a number of trees at the training time and furnishes the mean prediction of all the trees. Compared to a single tree, the generalization error and overfitting are minimized in a Random forest (Breiman 2001). A REP tree algorithm works by dividing the training dataset into two parts- a growing set and a pruning set. The growing set is used to form a rule, then a test is deleted from the rule, and the effect is evaluated by trying the reduced rule on the pruning set (Frank et al. 2016; Witten et al. 2016). The generated regression tree is pruned back by using reduced error with back fitting methodology (Omran et al. 2016; Witten et al. 2016).

Ensemble Learning-based

Ensemble learning algorithms applied in this study were bagging and additive regression. These algorithms function by combining the output of several different models with an aim to improve predictive performance (Opitz and Maclin 1999). Bagging is one of the earliest ensemble learning algorithms that uses bootstrapping along with any regression model to develop an ensemble (Breiman 1996; Kuhn and Johnson 2013). The bootstrapping method employed in this algorithm reduces the variance and stability of the prediction (Kuhn and Johnson 2013; Witten et al. 2016). Additive regression is a gradient boosting technique that implements forward stagewise additive modeling. At first, a standard regression model is built on the original data set, and then the successive models are trained in such a way that these models correct for the residual errors

from the previous model (Erdal 2013; Omran et al. 2016; Witten et al. 2016). However, this algorithm is prone to overfitting.

Methodology

Development of Database

The predictive performance of an ML model depends on the training dataset up to a great extent. As discussed earlier, thermal conductivity of concrete is influenced by a number of factors which certainly needs to be considered in the model training dataset. In this study, a comprehensive literature review was carried out to develop a database of 217 data points from various relevant articles published from 1988 to 2018 [25,26,27–34,35–38]. Since the objective was to develop a model using *k* value of concrete containing modern constituent materials (e.g. – various SCMs, fiber, lightweight aggregates, and others), only past 30 years of data were collected. Also, for modeling purpose, it was required to minimize the number of missing values that led to the omission of some dataset. The developed database is shown in Table 1 (Note: w_x refers to the unit weight of ingredient 'x' in the concrete mix). A total of 18 factors (also called features for modeling purpose) were considered that affected *k* of concrete, out of which 14 features were numerical and rest 4 were categorical. Numerical features included (I) concrete: dry density, temperature, age, and compressive strength; (II) paste: water-to-binder ratio, and unit weights of cement, fly ash, slag, silica fume, other SCMs, and water; and (III) aggregates and additives: fine aggregate, coarse aggregate, and fiber. Categorical features consisted of moisture condition of concrete, and types of fiber, coarse, and fine aggregate in the concrete mix. The minimum, maximum, mean, and standard deviation of each of the numerical features are presented while the categorical features are shown with their corresponding variables (in Table 1). Thermal conductivity values lied in the range of 0.20 - 4.18 W/m-K with a standard deviation of 0.60 W/m-K. The temperature at which

k is measured is one of the most important features and therefore, temperature data collected in this study lied from 20 – 1000 °C that included usually encountered ambient as well as high and elevated temperatures. Another significant feature is the moisture condition of concrete in which *k* is measured. Dry and saturated conditions were considered in database development. Categories of fine aggregates (FA) evaluated were silica, quartz, lightweight, and recycled sand, and FA containing natural river sand as well as recycled concrete aggregates (RCA). Mineralogy of coarse aggregate (CA) is also known to greatly impact *k* of concrete. Limestone, carbonate, siliceous, crushed stone, granitic gneiss, gravel, basalt, siltstone, quartzite, lightweight, recycled, and CA containing virgin as well as RCA were the categories of coarse aggregates included in the dataset.

An independent dataset (called as a testing dataset) was used for evaluating the predictive performance of the ML model. The testing dataset, containing 60 points, was developed from an experimental study conducted on 18 concrete mixes to measure their *k* values (Sargam et al. 2019). A steady-state test method performed on dry cylindrical concrete specimens (proposed by Carlson et. al (2010)), was followed for *k* measurement. All measurements were done in a closed room where temperature and humidity variations were negligible. The temperature during the tests was 21-23 °C. The concrete mixes consisted of different water-binder ratios, cements of ASTM C150 Type I/II, Type IP (25), and Type IS (20), ASTM C618 Class C and F fly ashes, and grade 100 ground granulated blast furnace slag. The replacement dosage of SCMs (fly ash and slag) ranged from 20 to 50%. All mixes constituted siliceous river sand as fine aggregate whereas limestone, lightweight (expanded shale), and recycled aggregates were used as coarse aggregates in various mixes. Some of the mixes also consisted of steel fiber in the range of 0 to 2% volume fraction (0-18.16 kg/m^3 by weight). Similar to the data presented in Table 1, the features of the developed testing dataset and their minimum, maximum, mean, and standard deviation values are presented

in Table 2. As shown in Table 2, the water-binder ratio of concrete mixes ranged from 0.35 to 0.55, dry density lied in the range of 1621 to 2281 kg/m^3, and the range of compressive strength was from 29 to 55 MPa. This suggests that the dataset included concrete mixes of normal strength and normal weight as well as high strength and lightweight.

Development of *k* Prediction Model

The development of an ML algorithm-based prediction model involves a series of steps to be followed. A flow chart of the steps, applied in this study, is shown in Fig. 1 and the steps are also explained below.

Data pre-processing: For building a robust ML model, data visualization and pre-processing is the first and a very important step. Data pre-processing includes processing of missing data, data normalization, and data partitioning. The presence of missing values in a training dataset can influence the performance of the model and hence these need to be cured before training the model. A recent comparative study showed that inaccurate missing data-curing method may result in several fold larger error in the subsequent ML predictions (Song et al. 2019). As the training dataset in this study was developed from previously published articles (Table 1), some of the features of the dataset contained missing values. These features were dry density, temperature, and compressive strength containing 15.20, 9.67, and 8.75% missing values, respectively. Imputation is one of the commonly used methods of curing missing or incomplete data. In this study, three different approaches to data curing were evaluated. These approaches are discussed below:

(1) Manual curing – In this method, the missing values of dry density, temperature, and strength were imputed with their corresponding values from similar concrete mixes in the training dataset. This was based on the visualization of the trends in the values of the three features

with a change in thermal conductivity. One of the drawbacks of this method, however, can be the presence of artificially similar values that might adversely impact the predictive performance of a model.

(2) *Naïve method* – In the Naïve missing data curing method, missing values are deleted or replaced with some statistics of the observed data corresponding to a particular feature. When mean values are used, all missing values were replaced with a constant mean value. However, since the thermal conductivity of concrete is sensitive to changes in the values of the features (dry density, temperature, and compressive strength), applying this method might result in a non-representative training dataset, especially if the proportion of missing data is large.

(3) Fractional Hot-Deck Imputation (FHDI) – FHDI, established by Kim et al. (Kwang Kim and Fuller 2004), replaces the missing value (called recipient) with a set of imputed values based on observed responses from similar data points (called donors). Amongst several variants, the method used in this study is the two-phase sampling approach proposed by Im et al. (2015) capable of curing multivariate missing data with arbitrary missing patterns. The imputation is carried out in four steps: cell construction by discretization following the finite mixture model, estimating cell probabilities using the modified expectation maximization (EM) algorithm, constructing fractional weights and subsequent imputation, estimating variance using the Jackknife method (Im et al. 2018). In the first phase, each missing unit contains at least 5 possible donors. In the second phase, each recipient is assigned with a set of donors with the associated fractional weights (Im et al. 2018). The FHDI package in *R* [69] was used for this imputation procedure.

The dataset cured using the above-mentioned three procedures was used to train models corresponding to various ML algorithms. The procedure that furnished the highest prediction accuracy was then selected as the data curing method for further model improvement.

The training dataset (Table 1) included a few features that contained values in a wide different range. For example, the water-binder ratio lied in the range of 0.25 to 0.62 whereas the range of dry density was from 1434 to 2390 kg/m^3. Clearly, these two features were in very different ranges. Using the data as-it-is might have affected the weights and biases of features in an ML model (especially ANN). Therefore, the normalization technique was applied that puts all features on a common scale. All numeric values in the training dataset were normalized to be in the range [0, 1].

Some of the commonly used methods of data partitioning in ML are – (1) splitting the dataset into training (around 70-80%) and test set (around 20-30%); (2) holdout; and (3) k-fold cross-validation. For evaluating various ML algorithms, k-fold cross-validation method was used in this study. In this method, the data are divided into k subsets, one of which is used as the test/validation set while the remaining k-1 subsets are used as the training set. *k* trials of the process are performed, and the model performance is averaged over all trials thereby reducing the bias. From the studies by researchers, it is known that ten-fold cross-validation yields the optimal computational time and reliable variance (Chou et al. 2014; Chou and Tsai 2012; Kohavi 1995), and therefore, this method was applied.

Performance measures: In order to evaluate the predictive performance of the ML regression algorithms and to make comparisons amongst them, three statistical performance measures (R, MAE, and RMSE) were used. Their mathematical formulae are presented in Equations 5-7.

$$\text{Linear Correlation Coefficient (R)} = \frac{n\sum y.y' - (\sum y)(\sum y')}{\sqrt{n(\sum y^2) - (\sum y)^2}\sqrt{n\left(\sum y'^2\right) - (\sum y')^2}} \quad (5)$$

$$\text{Mean Absolute Error (MAE)} = \frac{1}{n}\sum_{i=1}^{n}|y\text{-}y'| \quad (6)$$

$$\text{Root Mean Squared Error (RMSE)} = \sqrt{\frac{1}{n}\sum_{i=1}^{n}(y - y')^2} \quad (7)$$

Where y is the actual value, y' is the predicted value, and n is the number of instances/data points. The linear correlation coefficient (R) is a measure of how well the model fits the actual data. Along with R, the coefficient of determination (R^2) is also used. It is a measure of what proportion of variability in the dependent/target variable is explained by the model. MAE indicates the relative goodness-of-fit. The RMSE indicates the average distance of a data point from the fitted line.

Evaluation of various ML algorithms: The three cured datasets (Manual, Naïve, and FHDI method) were used to train prediction models for thermal conductivity considering all 18 features (predictors/independent variables). 10-fold cross-validation was applied in all models. Function, tree, and ensemble learning-based ML models were trained, as discussed earlier in section 2. The parameters of each of the models were tuned to obtain the best possible performance. The final parameter settings used for the three categories of models are listed in Table 3.

In the linear regression model, Akaike Information Criteria (AIC) was applied to reduce overfitting. AIC introduces a penalty term for the number of parameters in the model and also provides a trade-off between the model complexity (the number of parameters needed to describe the model) and quality of the fit of the data (Dziak et al. 2019). As discussed earlier, some function and ensemble learning-based models require a kernel as their covariance matrix (Omran et al. 2016). Hence, in the cases of GPR, SVR, additive regression, and bagging algorithms, polykernel was selected. An 18-8-1 architecture (18 nodes in the input layer, 8 nodes in the hidden layer, and

1 node in the output layer) was selected for the ANN model at a learning rate of 0.3 and momentum of 0.2. For all three tree-based algorithms, the batch size was limited to 100, which is the preferred number of instances to be processed, while performing batch prediction. The depth of the tree in the case of the random tree was kept unlimited. In regression trees, the minimum proportion of variance needs to be specified for performing splitting at a node (Frank et al. 2016). This value was set to 0.0001 in random and REP tree.

Model selection and further development: The relative predictive performances of all the ML models presented above were evaluated based on three performance measures (R^2, MAE, and RMSE) as discussed earlier. The models that furnished high R^2 values and low values of the error statistics i.e. MAE and RMSE were then selected as the best-performing models on the given dataset. An in-depth tuning of the parameters of the selected models was then performed to further develop a robust ML model for the prediction of thermal conductivity. An optimization technique, called feature selection, was also applied to improve the robustness of the model.

Feature selection: Feature selection is a technique of selecting only those features that have a significant influence on the dependent/target variable. The irrelevant and redundant features are recognized through this technique, and then a decision is made on their removal. Keeping only influential features in an ML model improves its predictive performance by increasing the learning rate and reducing the effect of the curse of dimensionality (Marks et al. 2015; Song et al. 2018b; a; Witten et al. 2016). However, the features should not be removed solely on this basis. If a feature is physically important (i.e. based on domain expertise or physics principles) for the prediction of the dependent/target variable, it should be kept for future extension. Such an approach is called a physics-based ML approach that helps develop extensible and interpretable learning model (Cho

2019; Raissi et al. 2017a; b). In this study, various combinations of features were evaluated based on their relative influences on the prediction of thermal conductivity. The best-performing set of features were then chosen for the development of the model.

Model testing: An ML predictive model can be called robust if its predictive performance is high not only on the training dataset that has been used to train it but also on an unseen dataset. In order to evaluate this, an independent dataset (presented in Table 2) was tested on the models developed from the previous step.

Results and Discussions

Comparison of ML Algorithms

This section presents and evaluates the relative predictive performances of nine ML algorithms evaluated in this study. The values of R^2, MAE, and RMSE, obtained after training of each of the ML models, are presented in Table 4 and are also plotted in Fig. 2 for a comparison purpose. A high value of the coefficient of determination (R^2) and low values of error terms MAE and RMSE are desired for a robust predictive model. Considering these parameters, one can observe from Table 4 and Fig. 2(a) that in the function category of algorithms, the predictive performance of the ANN algorithm was the best on all three types of cured datasets. R^2 values of 0.8037, 0.8363, and 0.8560 were obtained in the case of manual, naïve, and FHDI cured data. On all three datasets, MAE and RMSE values lied below 0.18 and 0.27, respectively, when ANN was applied. In the category of tree-based algorithms, the algorithms were ranked in the order of predictive performance as Random forest > Random tree > REP tree in the case of manual and FHDI cured datasets. When applied on the FHDI dataset, the parameter setting of the Random forest algorithm (as shown in Table 3) furnished R^2, MAE, and RMSE values of 0.8422, 0.15, and 0.24, respectively. Compared with the random tree and REP tree, Random forest performed better.

In the ensemble – learning category, predictions by additive regression were closer to the actual value than those furnished by bagging. However, this was true only when the performances were compared in terms of R^2 values. The MAE and RMSE values obtained on all three datasets did not show a particular trend to reach on a definite conclusion in this category.

Comparing the predictive performance of all nine algorithms evaluated in this study, one can observe that ANN performed better than the rest of the algorithms on all three datasets. High R^2 values (> 0.80), as well as low values of error terms, were obtained. Among the three datasets, FHDI cured dataset improved the performance of ANN with respect to manual and naïve curing. R^2, MAE, and RMSE values of 0.8560, 0.14, and 0.23, respectively were obtained on FHDI dataset. Improved performance of the model on this dataset was due to the imputation procedure employed in FHDI, as discussed in section 3.2. The missing values were replaced on the basis of multivariate joint probability and EM algorithm, unlike the procedure followed in manual and naïve curing.

The predictions by ANN (based on the model parameter settings presented in Table 3) are plotted in Fig. 3. Fig. 3(a) show the actual and predicted values of thermal conductivity (k) for each instance of the validation dataset. It can be noticed here that the full dataset consisted of 217 points and since 10-fold cross-validation was applied, each validation dataset constituted approximately 22 data points. ANN predictions were similar and close to the actual k values except for a relatively large variation observed in instances 7 to 10. These instances corresponded to higher values of k (3.0-4.5) for which only a small number of data points was available. Fig. 3(b) shows the comparison between the actual (x-axis) and model-predicted (y-axis) values of k. Data points closer to the straight line (actual = predicted) suggest better prediction accuracy of the model. From Fig. 3(b) also, it can be observed that the deviations from the straight line were large

only at higher values of *k*. The errors obtained in the ANN predictions are plotted in Fig. 3(c). Most of the prediction errors lied in the range of -1 to 1, except for a few large errors (> -1) in instances 7 to 10. These results were consistent with those observed in Figs. 3(a) and 3(b). Based on the results from the comparisons of ML algorithms and data curing methods, ANN algorithm and FHDI cured dataset was chosen for further development in order to improve the predictive performance.

Feature Selection

The predictive performance of ANN can be improved further by removing redundant features and selecting only a set of important features. In this study, seven different sets of features were evaluated. Sets I-IV are discussed first and Sets V-VII will be discussed later.

Set I – This set consisted of all 18 features as presented in Table 1. Parameters corresponding to the concrete mix proportion as well as the measured properties were included in this set of features.

Set II – With an aim to predict the thermal conductivity of concrete using only the concrete mix proportion parameters, only such features were included in Set II. These features were w/b, w_{cement}, $w_{fly\ ash}$, w_{slag}, $w_{silica\ fume}$, $w_{other\ SCMs}$, w_{water}, w_{FA}, w_{CA}, w_{fiber}, type of fiber, type of FA, and type of CA. The total number of features in this set was 13.

Set III – This set contained a total of 6 features that corresponded to water-binder ratio and other non-mix proportion parameters. These features were w/b, dry density, temperature, age, compressive strength, and moisture condition of concrete.

Set IV – This set was developed by following a ranking procedure that works on a mean decrease in impurity (MDI). The measure on which the optimal condition of dataset split at a node in a random forest is chosen is called impurity (Kuhn and Johnson 2013). For a forest, the decrease in impurity from each feature is averaged and the features are ranked based on their measure. The

ranking of features of the FHDI cured dataset is shown in Fig. 4. It shows the relative importance of all 18 features on a scale of 0 to 100%. The sum of all values adds up to 100%.

It can be observed that out of the 18 features, the type of coarse aggregate (CA) and the type of fine aggregate (FA) showed the highest influence on the prediction of thermal conductivity. The relative importance of the type of CA and FA were 41% and 27.5%, respectively. This can be attributed to the fact that thermal conductivity of aggregates is determined by mineralogical characteristics of the aggregates, and these characteristics define the types of the aggregates. Since 60-70% volume of a concrete mix is occupied by coarse and fine aggregates, the types of the aggregates will have the most effect on the thermal conductivity of the concrete. Next five features in terms of relative importance were moisture condition, W_{FA}, w/b, W_w, and W_{CA} with their values around 3-4%. Dry density of concrete, which also indicates the porosity of the concrete, was the most important measured property of concrete (2.3%) from the perspective of *k* prediction. Since the air in concrete pores is not conductive, *k* values of concrete decreased with its increasing porosity or reducing dry density. Following dry density of concrete was another measured property, compressive strength (2%), which is also closely related to concrete porosity. However, the age of concrete and the weights of cementitious materials, such as fly ash, slag, silica fume, and others, were amongst the least influential features with their relative importance values below 0.6%. Therefore, these parameters were not considered separately. Instead, the weights of all SCMs were included in the weight of cementitious materials represented as $w_{cementitious}$. The relative importance of age, to *k* prediction, was also found to be very less (0.5%), however, previous studies have suggested a considerable change in the value of *k* of concrete with its age (Breugel 1998; Brown and Javaid 1970; Choktaweekarn 2009; Schindler 2002). Hence, age was also included as one of the features in this set. In total, set IV consisted of fourteen features,

namely, w/b, $w_{cementitious}$, w_{water}, w_{FA}, w_{CA}, w_{fiber}, dry density, temperature, age, strength, moisture condition, type of fiber, type of FA, and type of CA.

Regarding Sets V-VII, below are the descriptions and discussions:

Set V – This set was developed from correlation-based feature subset (CFS) selection. In this procedure, the features are evaluated based on their individual predictive ability as well as the degree of redundancy between them. Feature subsets that are highly correlated with the target variable and have low intercorrelation are preferred (Witten et al. 2016). A subset of seven features was selected using this method. These features were w/b, w_{FA}, w_{CA}, w_{fiber}, dry density, moisture condition, and type of CA.

Sets VI and VII – These sets of features were developed based on the principal component analysis (PCA). In this method, most of the variability in the data is explained with a smaller number of features than the original dataset. PCA furnishes a low-dimensional representation of the dataset where each dimension is a linear combination of features (Kuhn and Johnson 2013). There can be 'n' number of such dimensions (where 'n' is the total number of features in the original dataset) called as principal components (PCs). The first PC usually captures the most variability while the subsequent PCs capture the remaining variability while also being uncorrelated with all previous PCs. Mathematically, the *j*th PC, or PC_j, can be represented as shown in Eq. (5) (Kuhn and Johnson 2013).

$$PC_j = \left(a_{j1} \times feature\ 1\right) + \left(a_{j2}\, x\, feature\ 2\right) + \cdots + \left(a_{jn}\, x\, feature\ n\right) \quad (5)$$

Where, n is the number of features, and coefficients a_{j1}, a_{j2}..., a_{jn} are the weights of their corresponding components. Fig. 5 shows the percentage of variance explained by the PCs. PC 1 and PC 2 explains 28.46% and 15.45 % of the variance, respectively. Rest of the 16 PCs explain the remaining 56% of the variance. Fig. 6 summarizes a biplot obtained from PCA. Arrows in the

plot represent each feature of the dataset. The arrows closer to each other means that the corresponding features are highly correlated and vice-versa. The arrows to the right side of the origin on the x-axis suggest that the corresponding features are positively correlated to PC1 and vice-versa. Based on these observations from PCA biplot, feature sets VI and VII were developed containing features in the positive direction and negative direction, respectively. Set VI contained 12 features, namely, w/b, $w_{silica\ fume}$, $w_{other\ SCMs}$, w_{FA}, w_{CA}, w_{fiber}, dry density, temperature, age, strength, type of fiber, and type of FA. Set VII consisted of 6 features – w_{cement}, $w_{fly\ ash}$, w_{slag}, w_{water}, moisture condition, and type of CA.

The performance of ANN on FHDI cured dataset was evaluated considering above-mentioned seven sets of features. Table 5 presents the obtained R^2 values in the case of different feature sets. On all the sets, R^2 values in the range of 0.5684 to 0.8440 were obtained. The highest R^2 was furnished in the case of set IV (0.8440) that contained 14 important features selected based on MDI. This suggests that as compared to other sets of features, ANN developed using set IV features can best explain the variability in the data. Therefore, it was decided to use features of only set IV for further development of the ANN prediction model.

ANN Model Development

The comparison of various data on curing methods, ML algorithms, and sets of features revealed that an ANN model, developed using FHDI cured dataset and 14 input features, would perform the best in predicting *k* of concrete. The parameters of the ANN model were further tuned in this section to optimize the prediction accuracy.

Developing a neural network requires the division of the complete dataset into two sets: training and testing. The dataset of 217 points developed in this study (Table 1) was randomly divided into these two sets with 80% corresponding to the training set and 20% to the test set.

Training of the network is another important step in which the weights of the neurons are adjusted to optimize the prediction accuracy. Levenberg-Marquardt Backpropagation (LMBP) training algorithm was employed in this study as it is known to be effective (Hagan and Menhaj 1994). There are some issues associated with a neural network that needs to be taken into account during training. For example, increasing the number of hidden layers and/or number of neurons in the hidden layer can also make the network more prone to overfitting, thereby increasing generalization error (John Lu 2010; Kuhn and Johnson 2013). Therefore, the number of neurons in the hidden layer was varied from 2 to 14 to optimize the performance by minimizing the mean squared error, generalization error, and overfitting. Fig. shows the R^2 values obtained after training the network by varying the number of neurons in the hidden layer. It can be observed that increasing the number of neurons increased R^2 in the case of both the sets up to 6 neurons after which it reduced. The network containing 6 neurons furnished R^2 of 0.9730 and 0.8722 on the training and test dataset, respectively which were the highest values. Hence, the number of neurons in the hidden layer of the network were kept as 6. The developed final ANN architecture was 14-6-1 as shown in Fig. 8. This denotes the number of neurons in the input, hidden, and output layers as 14, 6, and 1, respectively. The inputs for the network were w/b, $w_{cementitious}$, w_{water}, w_{FA}, w_{CA}, w_{fiber}, dry density, temperature, age, strength, moisture condition, type of fiber, type of FA, and type of CA. To minimize overfitting, another method called early stopping was also employed. In this method, the model is trained only for a while and stops well before approaching the global minima (John Lu 2010). The input features were also normalized on a scale of 0 to 1, as discussed earlier in section 3.2 as well.

The performance of the developed 14-6-1 ANN model is presented in Fig. . The comparison of actual conductivity (*k*) and ANN model predicted conductivity for the training and

test set is shown in Fig. (a) and (b), respectively. Fig. (c) and (d) show the absolute prediction errors (predicted-actual) for the training and test set. The best fit lines for the training and test set furnished R^2 values of 0.9730 and 0.8429, respectively. The prediction errors in the case of both the sets lied in the range of [-0.6, 0.6] with a few large errors observed in the case of instances containing higher *k* values. Final mean squared error (MSE) values for the training and test set were 0.0010 and 0.0044, respectively. The MSE values of the two sets were not significantly different and it also means that the overfitting was minimized. Overall, it can be said that a reasonable match in the actual and ANN model predicted values of thermal conductivity was obtained with a combined R^2 of 0.9079 and MSE of 0.0027.

ANN Model Performance on an Independent Dataset

The predictive performance of the developed ANN model was shown to be satisfactory (in section 4.3) on the dataset used to train the model with an overall R^2 of 0.9079. However, the developed model can be said to be robust if it can make correct predictions on an unseen dataset as well. Unseen data here means a dataset that has values in the range similar to the training data; however, it has not been used to train the model. In this study, an independent testing dataset (presented in Table 2) was used to evaluate the robustness of the developed ANN model. The predictive performance on this test set is presented in Fig. . Fig. (a) shows the actual and predicted *k* values - for each instance of the test set, Fig. (b) shows the comparison between the actual and predicted *k* values for the complete test set, and Fig. (c) presents the error (predicted-actual) corresponding to each instance. A determination coefficient of 0.7676 was obtained [Fig. (b)], which suggests that 76% of the variability in the predicted *k* value can be explained by the model. It can be observed from Fig. (a) and (c) that a good match in the actual and predicted values was obtained with small deviations and errors, except for the instances 20-22 and 52-60. These

instances consisted of data from lightweight concrete mixes (containing expanded shale lightweight coarse aggregate) whose measured *k* values were less than 1 W/m-K. The training data did not constitute enough values in this range which might be the reason for a relatively larger deviation in the actual and predicted values. However, the errors were still less than ±0.20. Overall, it can be said that the developed 14-6-1 ANN model performed reasonably well on an unseen and independent test set and ANN is an adequate machine learning tool for the prediction of thermal conductivity of concrete.

Conclusions

A database of 217 data points, containing thermal conductivity (*k)* values of concrete and other parameters affecting these values (features), was developed from published articles. The 18 features consisted of concrete mix proportion parameters (e.g., water-binder ratio, the weight of constituents, type and mineralogy of aggregates, etc.), measured properties (e.g., concrete dry density, compressive strength, etc.), and thermal conductivity testing parameters (age, temperature and moisture condition). Various machine learning algorithms were evaluated on the dataset for the prediction of thermal conductivity. Based on the observations from this study, the following conclusions can be drawn:

- Compared to manual and Naïve methods of replacing missing values, Fractional Hot-Deck Imputation (FHDI) method improved the performance of ML models.
- Considering all 18 features, the predictive performance of function, tree, and ensemble-learning based ML algorithms on three differently cured datasets (Manual, Naïve, and FHDI) was compared. In the function-based category, the artificial neural network (ANN) performed the best on FHDI-cured dataset with R^2 of 0.8560, MAE value of 0.14, and RMSE value of 0.23. Random forest (RF) was the best performing algorithm in the tree-based category.

- Seven different sets of features were selected based on educated judgment, MDI, CFS, and PCA. In the MDI method, all the features were ranked (on a scale of 0 to 100%) on the basis of their relative influences on the prediction of *k*. In the category of mix proportion parameters, the types of coarse and fine aggregate were found to be the most dominant features with their relative importance values being 41% and 27.5%, respectively. The dry density of concrete was found to have the highest influence on the prediction of *k* value (2.3%) in the category of measured properties. The predictive performance of ANN, considering 14 important features selected from MDI, was the best amongst all sets of features. These features were water-to-binder ratio, weights of cementitious materials and water, weights and types of fine aggregate (FA), coarse aggregate (CA), and fiber, concrete dry density and strength, testing age, temperature, and moisture condition.
- An improved ANN model was developed with 14 neurons in the input layer, one hidden layer with 6 neurons, and one output layer. The performance of the developed model was satisfactory with R^2 of 0.9730 and 0.8429 for the training (80%) and testing dataset (20%), respectively. The robustness of the model was evaluated on an unseen/independent testing dataset. R^2 of 0.7676 was obtained and absolute errors (the difference between predicted and actual values) for all the instances were less than ±0.20 with a few relatively large errors observed in the case of lightweight concrete mixes.

Acknowledgments

The present work was derived from a literature review on thermal conductivity of concrete, which was a part of a research project on mass concrete sponsored by Iowa Highway Research Board (IHRB). The authors would like to acknowledge the sponsorship from IHRB.

References

AASHTO. (2013). *AASHTOWare Pavement ME Design*. Washington, D.C., USA.

ACI (American Concrete Institute). (2002). "Guide to Thermal Properties of Concrete and Masonry Systems." *ACI 122-02*, Farmington Hills, MI.

Atici, U. (2011). "Prediction of the strength of mineral admixture concrete using multivariable regression analysis and an artificial neural network." *Expert Systems with Applications*, 38, 9609–9618.

Breiman, L. (1996). "Bagging predictors." *Machine Learning*, 24(2), 123–140.

Breiman, L. (2001). "Random Forests." *Machine Learning*, 45(1), 5–32.

Breiman, L., Friedman, J. H., Olshen, R. A., and Stone, C. J. (1984). *Classification and regression trees*. *Chapman & Hall/CRC*, Taylor & Francis, Boka Raton, FL, USA.

Breugel, K. Van. (1998). "Prediction of Temperature in Hardening Concrete." *Prevention of Thermal Cracking in Concrete at Early Ages*, R. Springenschmid, ed., London, 51–74.

Brown, T. D., and Javaid, M. Y. (1970). "The thermal conductivity of fresh concrete." *Materials and Structures/Materiaux et Constructions*, 3(18), 411–416.

Brownlee, J. (2016). *Master Machine Learning Algorithm*. Ebook.

Campbell-Allen, D., and Thorne, C. P. (1963). "The thermal conductivity of concrete." *Magazine of Concrete Research*, 15(43).

Carlson, J. D., Bhardwaj, R., Phelan, P. E., Kaloush, K. E., and Golden, J. S. (2010). "Determining Thermal Conductivity of Paving Materials Using Cylindrical Sample Geometry." *Journal of Materials in Civil Engineering*, 22(2), 186–195.

Cavalline, T. L., Castrodale, R. W., Freeman, C., and Wall, J. (2017). "Impact of Lightweight Aggregate on Concrete Thermal Properties." *ACI Materials Journal*, 114, 945–956.

Chithra, S., Kumar, S. R. R. S., Chinnaraju, K., and Alfin Ashmita, F. (2016). "A comparative study on the compressive strength prediction models for High Performance Concrete containing nano silica and copper slag using regression analysis and Artificial Neural Networks." *Construction and Building Materials*, 114, 528–535.

Cho, I. H. (2019). "A Framework for Self-Evolving Computational Material Models Inspired by Deep Learning." *International Journal for Numerical Methods in Engineering*, In Press.

Choktaweekarn, P. (2009). “A model for predicting thermal conductivity of concrete.” *Magazine of Concrete Research*, 61(4), 271–280.

Chou, J.-S., Chien-Kuo, ;, Chiu, P. E., Farfoura, M., and Al-Taharwa, I. (2011). “Optimizing the Prediction Accuracy of Concrete Compressive Strength Based on a Comparison of Data-Mining Techniques.” *Journal of Computing in Civil Engineering*, 25(3), 242–253.

Chou, J.-S., and Tsai, C.-F. (2012). “Concrete compressive strength analysis using a combined classification and regression technique.” *Automation in Construction*, 24, 52–60.

Chou, J.-S., Tsai, C.-F., Pham, A.-D., and Lu, Y.-H. (2014). “Machine learning in concrete strength simulations: Multi-nation data analytics.” *Construction and Building Materials*, 73, 771–780.

Cristianini, N., and Shawe-Taylor, J. (2000). *An Introduction to Support Vector Machines and Other Kernel-based Learning Methods*. Cambridge University Press, Cambridge, UK.

Dasgupta, B., Liu, D., and Siegelmann, H. T. (2018). “Neural networks.” *Handbook of Approximation Algorithms and Metaheuristics*, T. Gonzalez, ed., Chapman & Hall/CRC, Boka Raton, FL, USA.

Dattagupta, S. (2013). “Gaussian Processes.” *Diffusion: Formulism and Applications*, Taylor & Francis, Boka Raton, FL, USA.

Demirbog˘, R. (2007). “Thermal conductivity and compressive strength of concrete incorporation with mineral admixtures.” *Building and Environment*, 42, 2467–2471.

Deshpande, N., Londhe, S., and Kulkarni, S. (2014). “Modeling compressive strength of recycled aggregate concrete by Artificial Neural Network, Model Tree and Non-linear Regression.” *International Journal of Sustainable Built Environment*, 3(2), 187–198.

Duan, Z. H., Kou, S. C., and Poon, C. S. (2013). “Prediction of compressive strength of recycled aggregate concrete using artificial neural networks.” *Construction and Building Materials*, 40, 1200–1206.

Dziak, J. J., Coffman, D. L., Lanza, S. T., Li, R., and Jermiin, L. S. (2019). “Sensitivity and Specificity of Information Criteria.” *bioRxiv*, 449751.

Erdal, H. I. (2013). “Two-level and hybrid ensembles of decision trees for high performance concrete compressive strength prediction.” *Engineering Applications of Artificial Intelligence*, 26, 1689–1697.

Farrar, C. R., and Worden, K. (2013). *Structural Health Monitoring: A Machine Learning Perspective*. John Wiley & Sons, Ltd (10.1111), Chichester, West Sussex, UK.

Folliard, K., Schindler, A., and Pesek, P. (2017). "ConcreteWorks V3 Training / User Manual ConcreteWorks Software (P2)." Concrete Durability Center, Texas, USA.

Frank, E., Hall, M. A., and Witten, I. H. (2016). *The WEKA Workbench: Online Appendix for "Data Mining: Practical Machine Learning Tools and Techniques."* Morgan Kaufmann.

Ganjian, E. (1990). "The Relationship between Porosity and Thermal Conductivity of concrete." *PhD Dissertation*, The University of Leeds.

Grossi, E., and Buscema, M. (2007). "Introduction to artificial neural networks." *European Journal of Gastroenterology and Hepatology*, 19(12), 1046–1054.

Gui, J., Phelan E., P., Kaloush, K. E., and Golden, J. S. (2007). "Impact of pavement thermophysical properties on surface temperatures." *Journal of Materials in Civil Engineering*, 19(8), 1–6.

Hagan, M. T., and Menhaj, M. B. (1994). "Training feedforward networks with the Marquardt algorithm." *IEEE Transactions on Neural Networks*, 5(6), 989–993.

Hossain, M. I., Gopisetti, L. S. P., and Miah, M. S. (2019a). "International Roughness Index Prediction of Flexible Pavements Using Neural Networks." *Journal of Transportation Engineering, Part B: Pavements*, American Society of Civil Engineers, 145(1), 4018058.

Hossain, M. I., Gopisetti, L. S. P., and Miah, M. S. (2019b). "Prediction of International Roughness Index of Flexible Pavements from Climate and Traffic Data Using Artificial Neural Network Modeling." *Airfield and Highway Pavements 2017*, Proceedings.

Im, J., Cho, I. H., and Kim, J. K. (2018). "FHDI: An R Package for Fractional Hot Deck Imputation." *The R Journal*, 10(1), 140–154.

Im, J., Kim, J.-K., and Fuller, W. A. (2015). "Two-phase sampling approach to fractional hot deck imputation." *Survey Research Methodology Section*, Seattle, WA, USA, 1030–1043.

Jain, A. K., Mao, J., and Mohiuddin, K. M. (1996). "Artificial neural networks: A tutorial." *Computer*, 29(3), 31–44.

John Lu, Z. Q. (2010). "The Elements of Statistical Learning: Data Mining, Inference, and Prediction." *Journal of the Royal Statistical Society: Series A (Statistics in Society)*, John Wiley & Sons, Ltd (10.1111), 173(3), 693–694.

Khan, A. A., Cook, W. D., and Mitchell, D. (1998). "Thermal properties and transient thermal analysis of structural members during hydration." *ACI Materials Journal*, 95(3), 293–303.

Khan, M. . (2002). "Factors affecting the thermal properties of concrete and applicability of its prediction models." *Building and Environment*, 37(6), 607–614.

Kim, K.-H., Jeon, S.-E., Kim, J.-K., and Yang, S. (2003). "An experimental study on thermal conductivity of concrete." *Cement and Concrete Research*, 33(3), 363–371.

Kodur, V. K. R., and Sultan, M. A. (2003). "Effect of Temperature on Thermal Properties of High-Strength Concrete." *Journal of Materials in Civil Engineering*, 15(2), 101–107.

Kohavi, R. (1995). "A Study of Cross-Validation and Bootstrap for Accuracy Estimation and Model Selection." *Proc. International Joint Conference on Artificial Intelligence*, Montreal, CA.

Kuhn, M., and Johnson, K. (2013). *Applied predictive modeling*. Springer, New York.

Kwang Kim, J., and Fuller, W. (2004). "Fractional hot deck imputation." *Biometrika*, 91(3), 559–578.

Lee, J.-H., Lee, J.-J., and Cho, B.-S. (2012). "Effective Prediction of Thermal Conductivity of Concrete Using Neural Network Method." *International Journal of Concrete Structures and Materials*, 6(3), 177–186.

Lie, T. T., and Kodur, V. K. R. (1996). "Thermal and mechanical properties of steel-fibre-reinforced concrete at elevated temperatures." *Canadian Journal of Civil Engineering*, 23(2), 511–517.

Liu, K., Lu, L., Wang, F., and Liang, W. (2017). "Theoretical and experimental study on multi-phase model of thermal conductivity for fiber reinforced concrete." *Construction and Building Materials*, 148, 465–475.

MacKay, D. J. C. (1998). "Introduction to Gaussian Processes." *NATO ASI Series F Computer and Systems Sciences*.

Majumder, M. (2015). "Artificial Neural Network."

Marks, M., Glinicki, M. A., and Gibas, K. (2015). "Prediction of the chloride resistance of concrete modified with high calcium fly ash using machine learning." *Materials*, 8(12), 8714–8727.

Marshall, A. L. (1972). "The Thermal Properties of Concrete." *Build. Sci*, Pergamon Press, 7, 167–174.

Morabito, P. (1989). "Measurement of the thermal properties of different concretes." *High Temperatures-High Pressures*, 21(1), 51–59.

Murphy, K. P. (2018). *Machine Learning: A Probabilistic Perspective, ; Adaptive Computation and Machine Learning Series*. The MIT Press: London, UK, Cambridge, MA.

Naderpour, H., Rafiean, A. H., and Fakharian, P. (2018). "Compressive strength prediction of environmentally friendly concrete using artificial neural networks." *Journal of Building Engineering*, 16, 213–219.

Neves, A. C., González, • I, Leander, • J, and Karoumi, • R. (2017). "Structural health monitoring of bridges: a model-free ANN-based approach to damage detection." *Journal of Civil Structural Health Monitoring*, 7(5), 689–702.

Omran, B. A., Chen, ; Qian, Asce, A. M., and Jin, R. (2016). "Comparison of Data Mining Techniques for Predicting Compressive Strength of Environmentally Friendly Concrete." *Journal of Computing in Civil Engineering*, 30(6), 04016029.

Opitz, D., and Maclin, R. (1999). "Popular Ensemble Methods: An Empirical Study." *Journal of Artificial Intelligence Research*, 11, 169–198.

Poole, J., Riding, K., Browne, R. A., and Schindler, A. (2006). "Temperature management of mass concrete structures." *Concrete Construction - World of Concrete*, Hanley Wood LLC, 51(11), 47–53.

Raissi, M., Perdikaris, P., and Karniadakis, G. E. (2017a). "Physics Informed Deep Learning (Part I): Data-driven Solutions of Nonlinear Partial Differential Equations." *Computing Research Repository*.

Raissi, M., Perdikaris, P., and Karniadakis, G. E. (2017b). "Physics Informed Deep Learning (Part II): Data-driven Discovery of Nonlinear Partial Differential Equations." *Computing Research Repository*.

Rasmussen, C. E., and Williams, C. K. I. (2006). *Gaussian Processes for Machine Learning*. the MIT Press.

Riding, K. A., Poole, J. L., Schindler, A. K., Juenger, M. C. G., and Folliard, K. J. (2013). "Statistical Determination of Cracking Probability for Mass Concrete." *Journal of Materials in Civil Engineering*, 26(9), 04014058.

Sadati, S., Enzo, L., Ii, D. C. W., and Khayat, K. H. (2019). "Artificial Intelligence to Investigate Modulus of Elasticity of Recycled Aggregate Concrete." *ACI Materials Journal*, (116), 51–62.

Sargam, Y., Wang, K., and Alleman, J. E. (2018). "Experimental Study on the Effect of Concrete Constituents on its Thermal Conductivity." *3rd R N Raikar Memorial International Conference on Science and Technology of Concrete*, Excel India Publishers, Mumbai, India, 917–925.

Sargam, Y., Wang, K., and Alleman, J. E. (2019). "Effect of Modern Concrete Materials on Thermal Conductivity." *Journal of Materials in Civil Engineering*, In Press.

Schindler, A. K. (2002). "Concrete Hydration, Temperature Development, and Setting at Early-Ages." *PhD Dissertation*, The University of Texas at Austin.

Seeger, M. (2004). "Gaussian processes for machine learning." *International journal of neural systems*, 14(2), 69–106.

Sengul, O., Azizi, S., Karaosmanoglu, F., and Tasdemir, A. (2011). "Effect of expanded perlite on the mechanical properties and thermal conductivity of lightweight concrete." *Energy & Buildings*, 43, 677–682.

Song, I., Cho, I. H., and Wong, R. K. W. (2018a). "An Advanced Statistical Approach to Data-Driven Earthquake Engineering." *Journal of Earthquake Engineering*, Taylor & Francis, 1–25.

Song, I., Cho, I., Tessitore, T., Gurcsik, T., and Ceylan, H. (2018b). "Data-Driven Prediction of Runway Incursions with Uncertainty Quantification." *Journal of Computing in Civil Engineering*, American Society of Civil Engineers, 32(2), 4018004.

Song, I., Yang, Y., Im, J., Tong, T., Ceylan, H., and Cho, I. (2019). "Impacts of Fractional Hot-Deck Imputation on Learning and Prediction of Engineering Data." *IEEE Transactions on Knowledge and Data Engineering*, 1.

Taffese, W. Z., and Sistonen, E. (2017). "Machine learning for durability and service-life assessment of reinforced concrete structures: Recent advances and future directions." *Automation in Construction*, 77, 1–14.

Tinker, L., and Cabrera, J. G. (1992). "Modeling the Thermal Conductivity of Concrete Based on Its Measured Density and Porosity." *Buildings V. Conference Proceedings*, 91–95.

Tino, P., Benuskova, L., and Sperduti, A. (2015). "Artificial neural network models." *Springer Handbook of Computational Intelligence*, Springer, 455–471.

Trocoli, A., Dantas, A., Leite, M. B., De, K., and Nagahama, J. (2013). "Prediction of compressive strength of concrete containing construction and demolition waste using artificial neural networks." *Construction and Building Materials*, 38, 717–722.

Valore, R. C. (1980). "Calculation of U-values of Hollow Concrete Masonary." *Concrete International*, 2(2), 40–63.

Vejmelková, E., Koňáková, D., Kulovaná, T., Hubáček, A., and Černý, R. (2014). "Mechanical and thermal properties of moderate-strength concrete with ceramic powder used as supplementary cementitious material." *Advanced Materials Research*, 1054, 194–198.

William, N., Kassahun, A., Gina, B., Albert, E., and Mannur, S. (2015). “A Study of Machine Learning Techniques for Detecting and Classifying Structural Damage.” *International Journal of Machine Learning and Computing*, 5(4), 313–318.

Witten, I. H., Frank, E., Hall, M. A., and Pal, C. J. (2016). *Data Mining: Practical machine learning tools and techniques*. Morgan Kaufmann, Cambridge, MA, USA.

Worden, K., and Manson, G. (2007). *The application of machine learning to structural health monitoring*. *Philosophical Transactions of the Royal Society A: Mathematical, Physical and Engineering Sciences*, The Royal Society Publishing, London, UK.

Young, B. A., Hall, A., Pilon, L., Gupta, P., and Sant, G. (2019). “Can the compressive strength of concrete be estimated from knowledge of the mixture proportions?: New insights from statistical analysis and machine learning methods.” *Cement and Concrete Research*, 115, 379–388.

Zewdu Taffese, W., Sistonen, E., and Puttonen, J. (2015). “CaPrM: Carbonation prediction model for reinforced concrete using machine learning methods.” *Construction and Building Materials*, 100, 70–82.

Zhu, L., Dai, J., Bai, G., and Zhang, F. (2015). “Study on thermal properties of recycled aggregate concrete and recycled concrete blocks.” *Construction and Building Materials*, 94, 620–628.

Figures

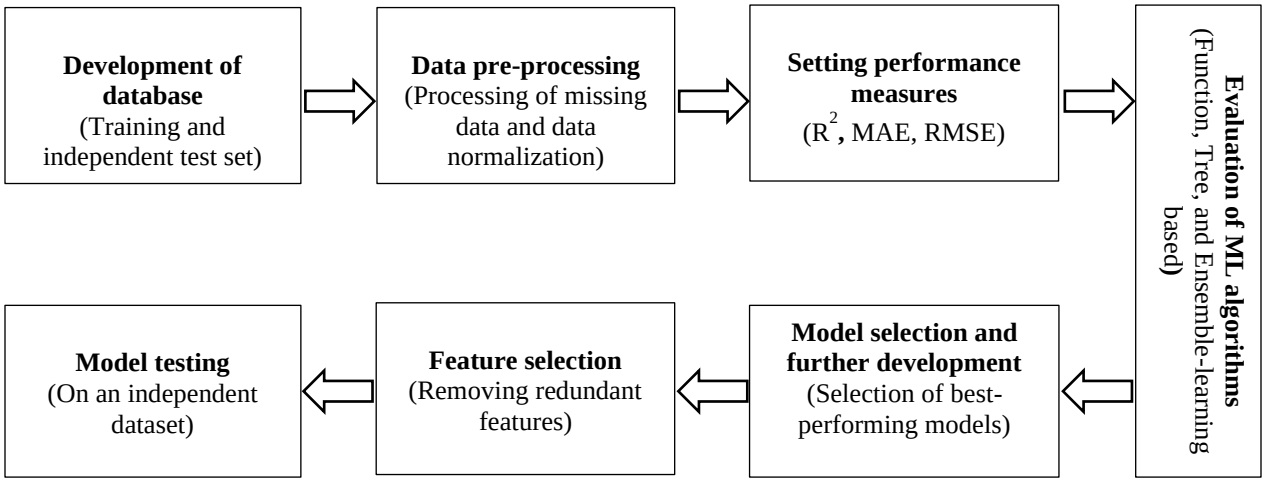

Fig. 1. Flow chart of model development for prediction of thermal conductivity

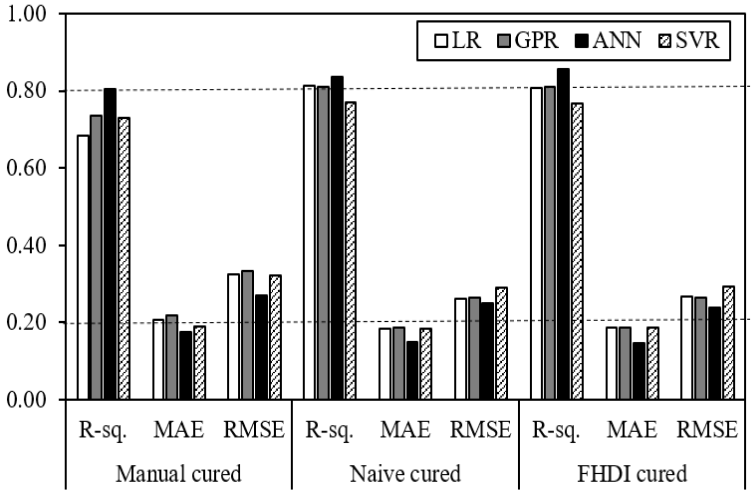

(a) Function-based

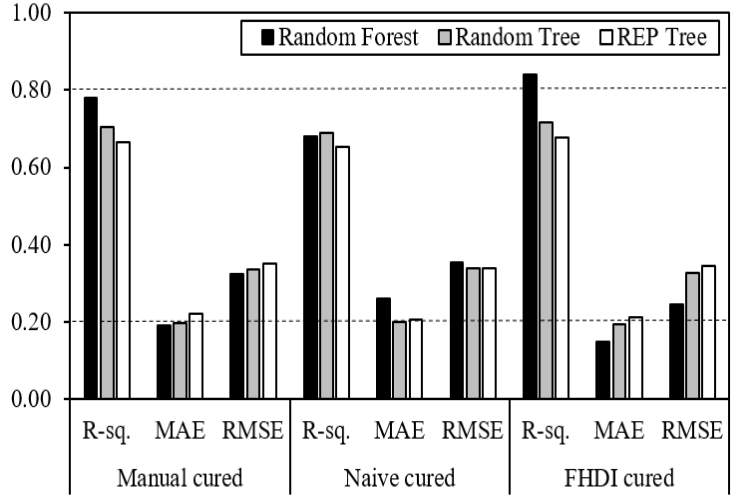

(b) Tree-based

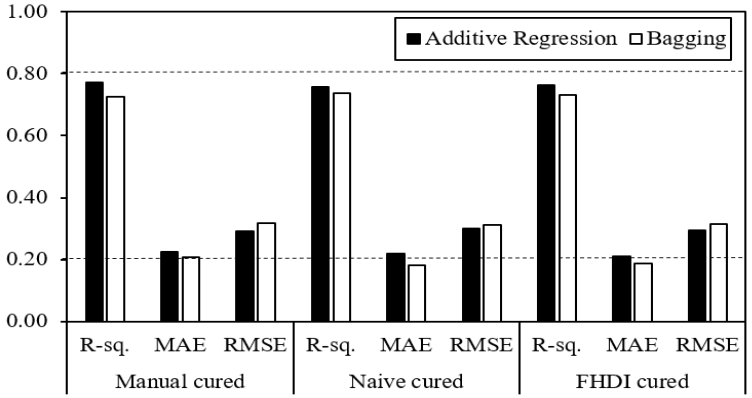

(c) Ensemble-based

Fig. 2. Predictive performance of ML algorithms

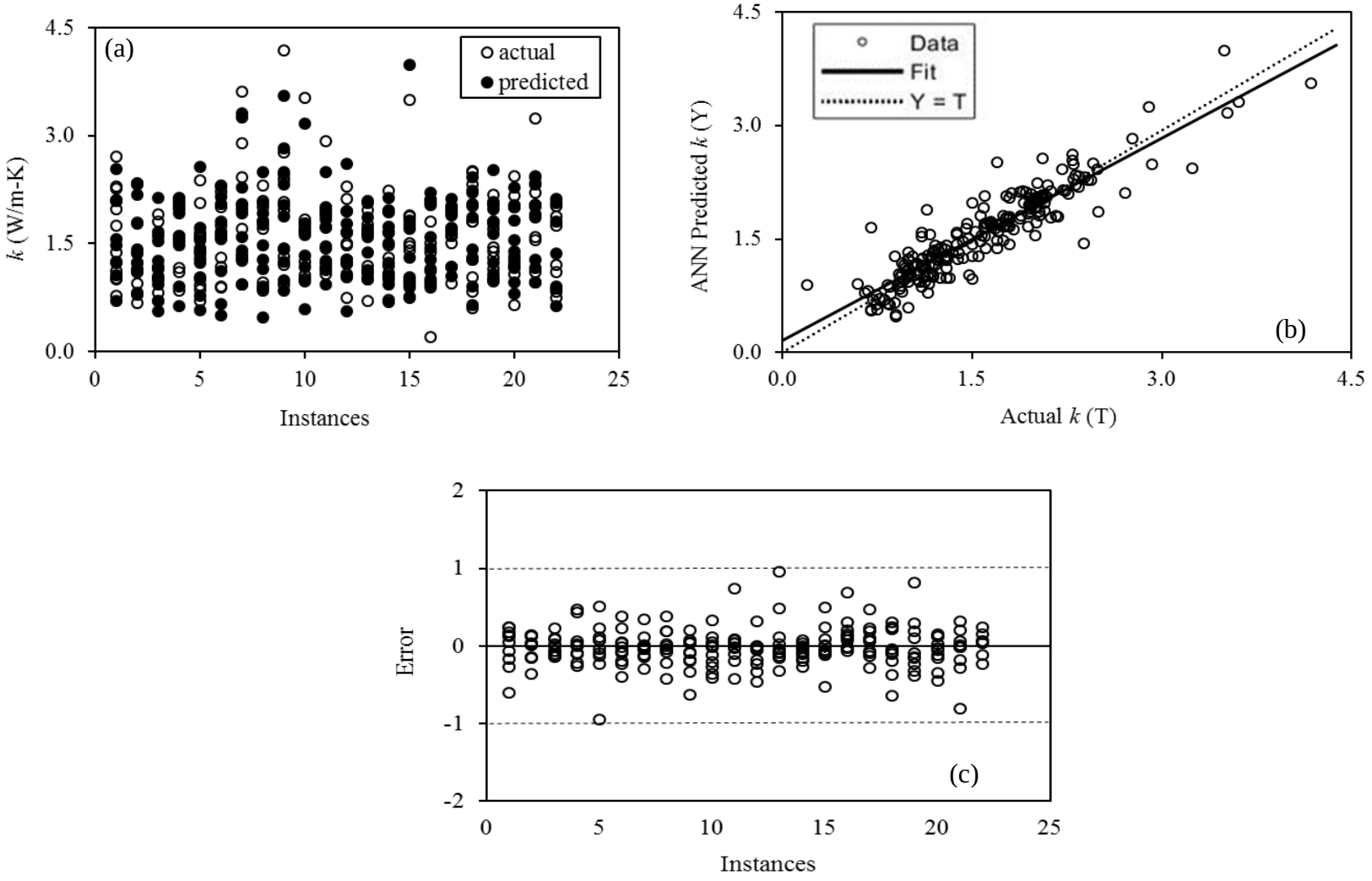

Fig. 3. ANN model performance with 18 input features; (a) actual and predicted values for all instances; (b) correlation coefficient between actual and predicted values; and (c) absolute errors for all instances

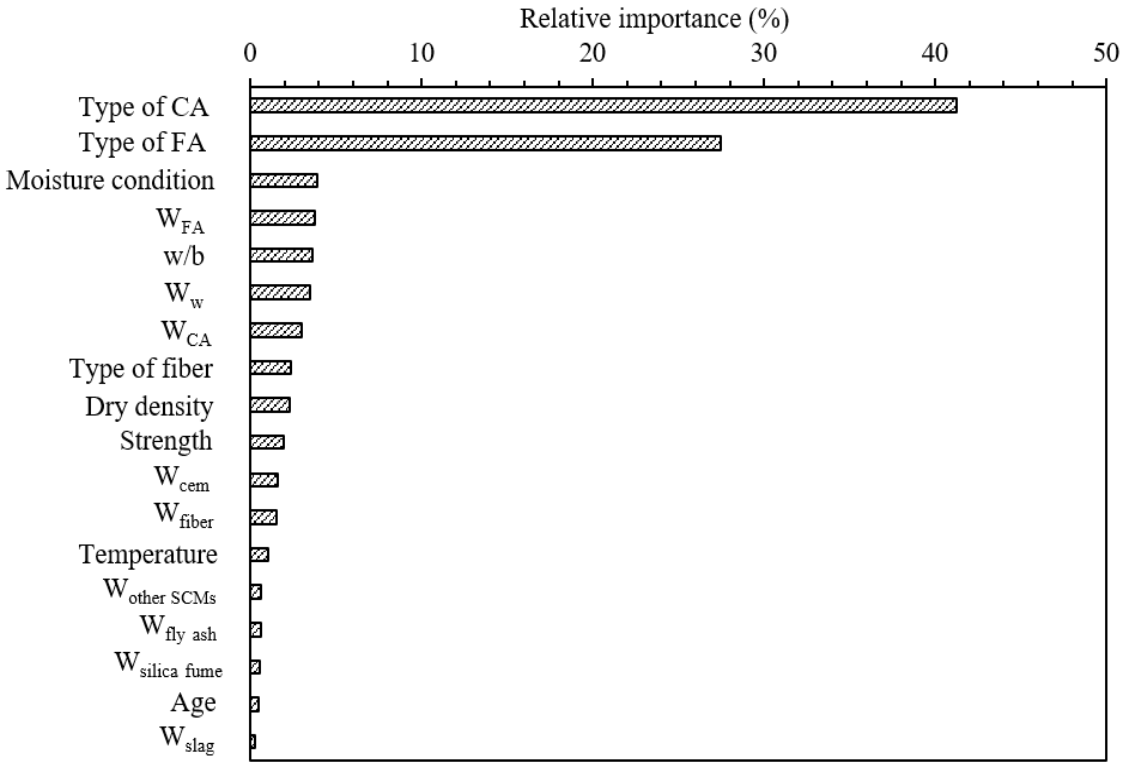

Fig. 4. MDI-based relative importance of input features on prediction of thermal conductivity

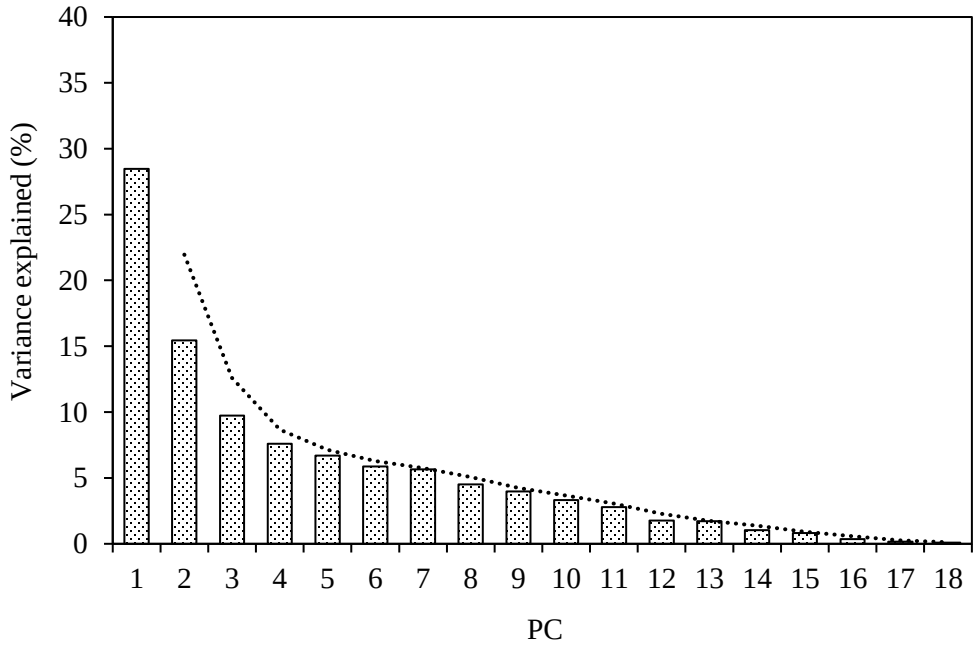

Fig. 5. Scree plot from PCA

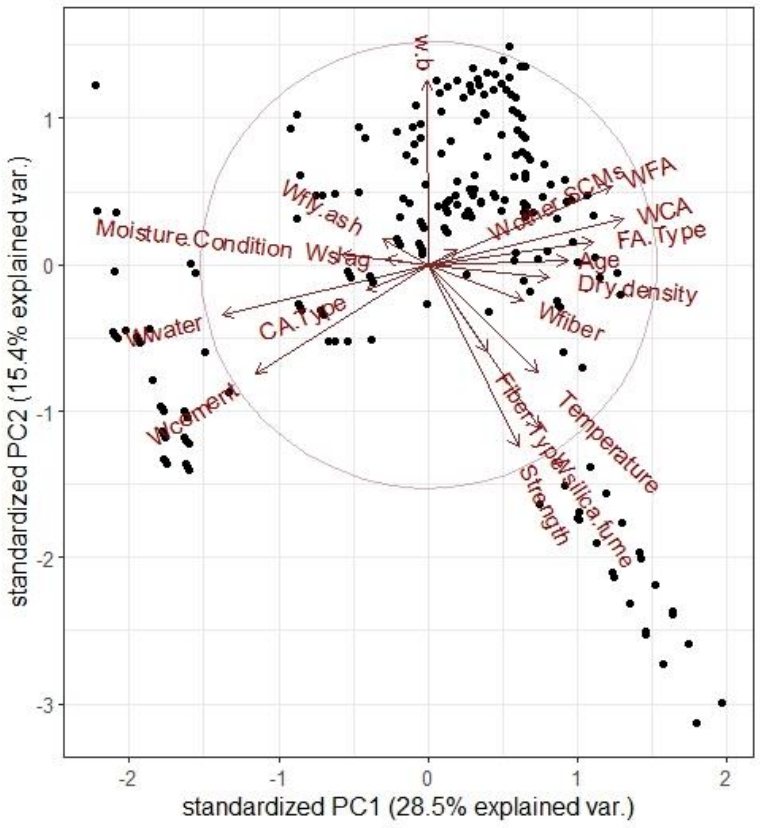

Fig. 6. Biplot from PCA

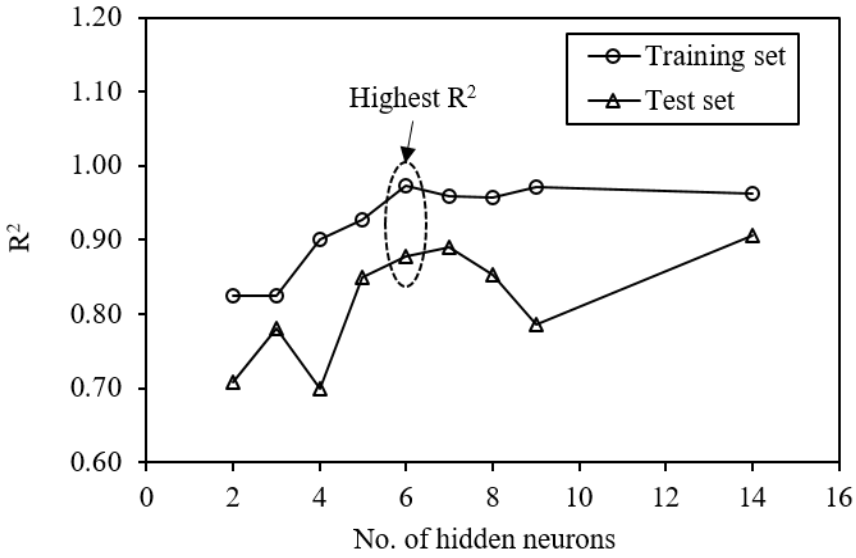

Fig. 7. Performance of ANN model by varying the number of neurons in hidden layer

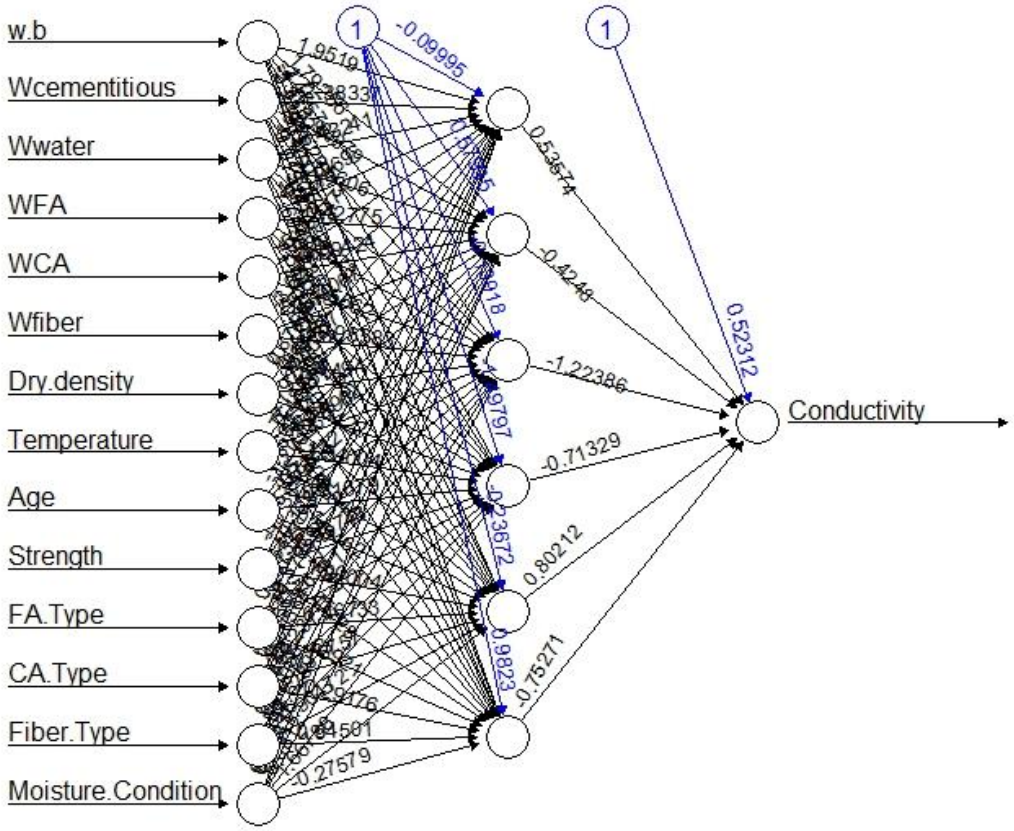

Fig. 8. 14-6-1 ANN architecture (Figures in black represent the weights and those in blue represent the biases of the network)

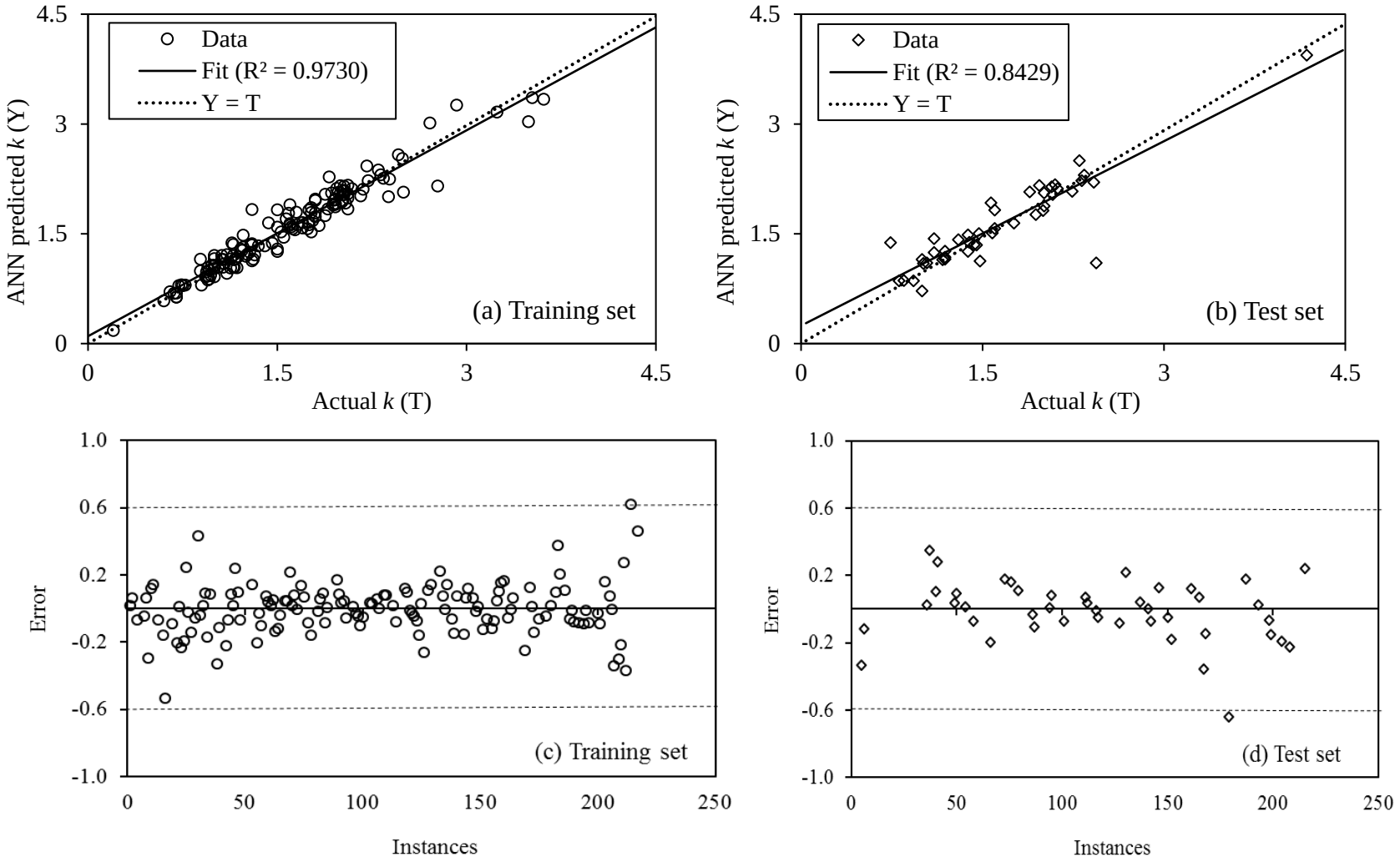

Fig. 9. 14-6-1 ANN model performance – actual and predicted values comparison on (a) training and (b) test dataset; and absolute prediction errors for all instances of (c) training and (d) test dataset

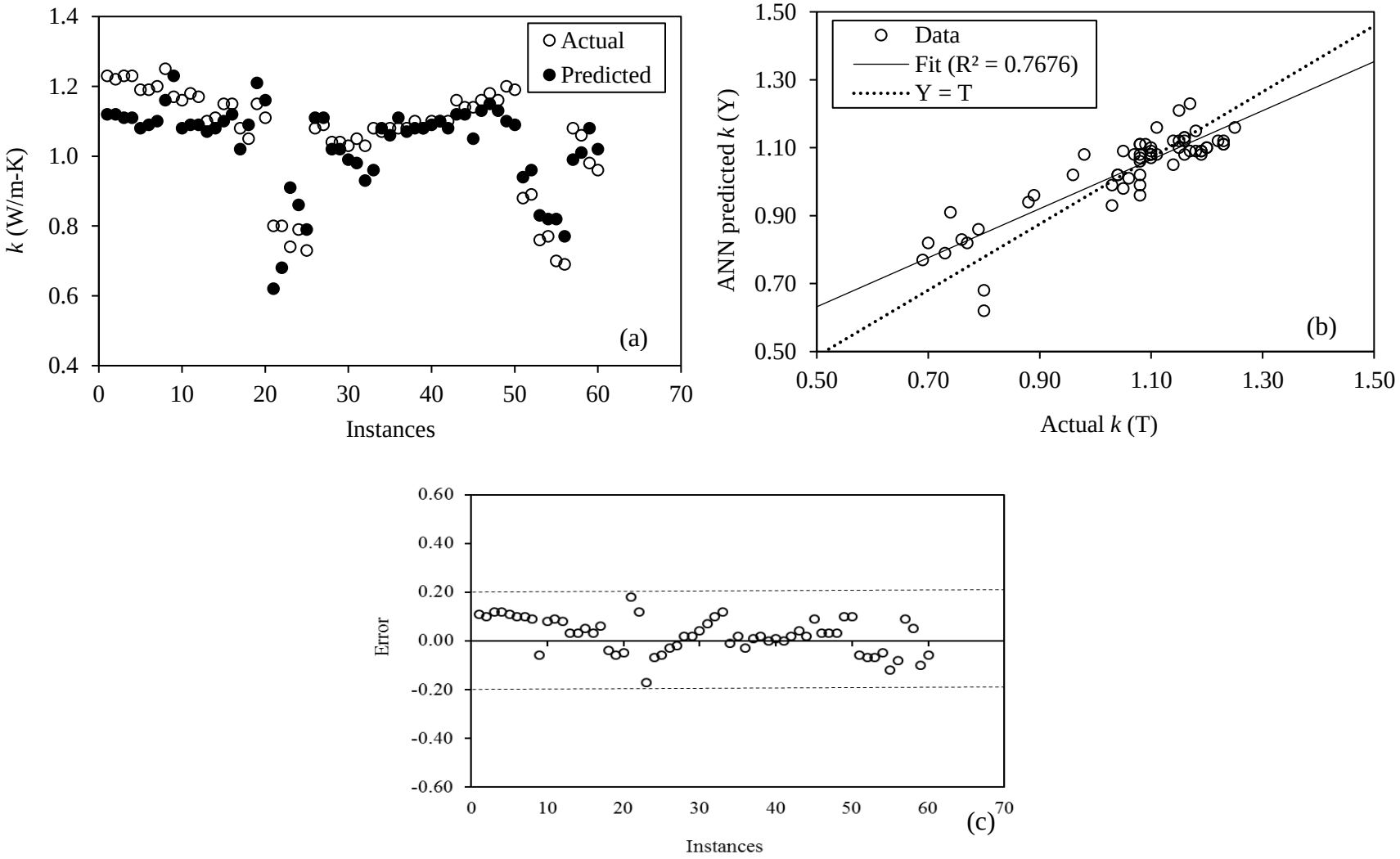

Fig. 10. 14-6-1 ANN model performance on independent test set; (a) actual and predicted values for all instances; (b) correlation coefficient between actual and predicted values; and (c) absolute errors for all instance

Tables

Table 1. Thermal conductivity database developed from published articles

No.	Feature	Unit	Min	Max	Mean	Std. deviation
1	Thermal conductivity (*k*)	W/m-K	0.2	4.18	1.58	0.60
2	w/b	ratio	0.25	0.62	0.40	0.09
3	Wt. of cement (w_{Cement})	kg/m^3	0	1762	609.11	420.31
4	Wt. of fly ash ($w_{Fly\ ash}$)	kg/m^3	0	973	12.05	75.89
5	Wt. of slag (w_{Slag})	kg/m^3	0	1282	9.95	97.42
6	Wt. of silica fume ($w_{Silica\ fume}$)	kg/m^3	0	52.5	5.85	15.77
7	Wt. of other SCMs ($w_{Other\ SCMs}$)	kg/m^3	0	231	4.60	27.58
8	Wt. of water (w_{Water})	kg/m^3	124	558	244.32	136.10
9	Wt. of fine agg. ($w_{Fine\ agg.}$)	kg/m^3	0	1559	556.39	308.74
10	Wt. of coarse agg. ($w_{Coarse\ agg.}$)	kg/m^3	0	1850	776.35	453.13
11	Wt. of fiber (w_{Fiber})	kg/m^3	0	117	7.93	21.60
12	Dry density	kg/m^3	1434	2390	2012.82	281.24
13	Temperature	°C	20	1000	96.69	191.18
14	Age	day	3	28	17.60	10.52
15	Compressive strength	MPa	18.7	99.2	54.01	24.04
16	Moisture condition	categorical	dry and saturated			
17	Type of fiber	categorical	steel and carbon			
18	Type of FA	categorical	silica sand, quartz sand, lightweight, recycled, and natural+recycled			
19	Type of CA	categorical	limestone, carbonate, siliceous, crushed stone, granitic gneiss, recycled, virgin+recycled, gravel, basalt, siltstone, quartzite, lightweight			

Table 2. Independent test set developed from 18 concrete mixes

No.	Feature	Unit	Min	Max	Mean	Std. deviation
1	Thermal conductivity (*k*)	W/m-K	0.69	1.25	1.05	0.15
2	w/b	ratio	0.35	0.55	0.42	0.03
3	w_{Cement}	kg/m^3	176	352	299.51	51.69
4	$w_{Fly\ ash}$	kg/m^3	0	141	60.58	39.46
5	w_{Slag}	kg/m^3	0	106	10.45	28.83
6	$w_{Silica\ fume}$	kg/m^3	0	0	0	0
7	$w_{Other\ SCMs}$	kg/m^3	0	0	0	0
8	w_{Water}	kg/m^3	122	192	155.13	9.98
9	$w_{Fine\ agg.}$	kg/m^3	747	980	847.64	53.15
10	$w_{Coarse\ agg.}$	kg/m^3	370	975	843.15	143.27
11	w_{Fiber}	kg/m^3	0	18.16	2.78	5.31
12	Dry density	kg/m^3	1621	2281	2182.60	177.51
13	Temperature	°C	21	23	22.00	1.00
14	Age	Day	28	28	28.00	0
15	Compressive strength	MPa	29	55	44.78	7.43
16	Moisture condition	categorical	dry			
17	Type of fiber	categorical	steel			
18	Type of FA	categorical	silica sand			
19	Type of CA	categorical	limestone, lightweight, recycled, virgin+recycled			

Table 3. Parameter settings of machine learning algorithms

Category	ML Algorithm	Parameters
Function	Linear Regression (LR)	Using Akaike Information Criteria (AIC)
	Gaussian Processes Regression (GPR)	Batch size = 100, noise = 1.0, exponent value = 3, polykernel
	Artificial Neural Network (ANN)	1 input, 1 hidden, 1 output layer, 8 neurons in hidden layer, learning rate = 0.3, momentum = 0.2
	Support Vector Regression (SVR)	Batch size = 100, complexity parameter = 1.0, exponent value = 3, polykernel
Tree	Random Forest	Batch size = 100, iteration = 100
	Random Tree	Batch size = 100, maximum depth of tree – unlimited, minimum proportion of variance = 0.001
	REP Tree	Batch size = 100, minimum proportion of variance = 0.001
Ensemble-learning	Additive Regression	Base classifier - GPR, iterations = 10, shrinkage rate = 1, exponent value = 3, polykernel
	Bagging	Base classifier - GPR, iterations = 80, exponent value = 3, polykernel

Table 4. Performance evaluation of ML algorithms

Category	ML Algorithm	Manual cured			Naive cured			FHDI cured		
		R^2	MAE	RMSE	R^2	MAE	RMSE	R^2	MAE	RMSE
Function	LR	0.6833	0.2081	0.3239	0.8134	0.1843	0.2622	0.8068	0.1868	0.2664
	GPR	0.7362	0.2196	0.3325	0.8120	0.1873	0.2650	0.8111	0.1877	0.2654
	ANN	**0.8037**	**0.1750**	**0.2694**	**0.8363**	**0.1496**	**0.2497**	**0.8560**	**0.1462**	**0.2382**
	SVR	0.7297	0.1895	0.3224	0.7700	0.1847	0.2916	0.7663	0.1867	0.2939
Trees	Random Forest	0.7795	0.1920	0.3236	0.6796	0.2613	0.3560	0.8422	0.1501	0.2458
	Random Tree	0.7054	0.1981	0.336	0.6892	0.2013	0.3402	0.7157	0.1944	0.3283
	REP Tree	0.6670	0.2204	0.3501	0.6540	0.2071	0.3409	0.6767	0.2116	0.3456
Ensemble	Additive Regression	0.7711	0.2253	0.2922	0.7578	0.2194	0.2989	0.7635	0.2110	0.2944
	Bagging	0.7244	0.2067	0.3188	0.7360	0.1821	0.3124	0.7302	0.1865	0.3158

Table 5. Comparison of performance of ANN on different sets of input features

Feature set	Features (No.)	Name of features	R^2
			ANN
I-all	All (18)	w/b, w_{cement}, $w_{fly\ ash}$, w_{slag}, $w_{silica\ fume}$, $w_{other\ SCMs}$, w_{water}, w_{FA}, w_{CA}, w_{fiber}, dry density, temperature, age, strength, moisture condition, type of fiber, type of FA, type of CA	0.7327
II-mix	Only mix proportion (13)	w/b, w_{cement}, $w_{fly\ ash}$, w_{slag}, $w_{silica\ fume}$, $w_{other\ SCMs}$, w_{water}, w_{FA}, w_{CA}, w_{fiber}, type of fiber, type of FA, type of CA	0.5121
III-non-mix	Non-mix proportion & w/b (6)	w/b, dry density, temperature, age, strength, moisture condition	0.6384
IV-MDI	Selected from MDI (14)	w/b, $w_{cementitious}$, w_{water}, w_{FA}, w_{CA}, w_{fiber}, dry density, temperature, age, strength, moisture condition, type of fiber, type of FA, type of CA	**0.8440**
V-CFS	Selected from CFS (7)	w/b, w_{FA}, w_{CA}, w_{fiber}, dry density, moisture condition, type of CA	0.6997
VI- PCA +ve	Positive direction from PCA (12)	w/b, $w_{silica\ fume}$, $w_{other\ SCMs}$, w_{FA}, w_{CA}, w_{fiber}, dry density, temperature, age, strength, type of fiber, type of FA	0.5684
VII-PCA -ve	Negative direction from PCA (6)	w_{cement}, $w_{fly\ ash}$, w_{slag}, w_{water}, moisture condition, type of CA	0.5849

CHAPTER 5. GENERAL CONCLUSIONS

Experimental measurement and predictive analysis of mass concrete parameters and concrete thermal conductivity were performed in this study. A computer program ConcreteWorks was used to predict the temperature development profile of the rectangular footing of a bridge. The predictions were validated with the measured data. Effect of various materials, used as an additive or replacement to concrete, on its thermal conductivity was also determined experimentally. For the purpose of prediction of thermal conductivity, machine learning algorithms of three different categories (Function, Tree, and Ensemble-learning) were evaluated and an ANN model was developed. Specific conclusions of this thesis are as follows:

- A sensitivity study on mass concrete parameters (using ConcreteWorks) revealed a considerable impact of concrete mix proportion, cement type, concrete thermal properties, placement temperature, insulation R-value, and foundation subbase on temperature development in the footing.
- ConcreteWorks predictions of absolute maximum temperature, maximum temperature differential, maturity, and compressive strength development for the rectangular footing were all very precise in their comparisons with the measured data. It can be said to be a useful tool for these predictions and for developing a thermal control plan.
- Thermal conductivity of concrete reduced with an increase in the water-binder ratio, SCM, lightweight aggregate, and recycled aggregate replacements whereas the addition of steel fiber resulted in an increase of conductivity.

- During the initial period of curing (from 3 to 7 days), conductivity reduced. However, it increased afterward as curing continued up to 28 days. After 28 days, little change in conductivity was observed.
- Machine learning algorithms of function, tree and ensemble-learning categories were evaluated for developing a prediction model for thermal conductivity of concrete. ANN performed the best and a 14-6-1 model architecture was finally adopted. The developed ANN model was robust in its predictions as it performed satisfactorily on an unseen/independent dataset furnishing R^2 of 0.7676 and absolute errors (for all instances of the dataset) less than ±0.20.